

STOCHASTIC AND SEMI-CLASSICAL APPROACHES TO THE QUANTUM VIRIAL EXPANSION

C. R. Shill

A dissertation submitted to the faculty at the University of North Carolina at Chapel Hill in partial fulfillment of the requirements for the degree of Doctor of Philosophy in the Department of Physics.

Chapel Hill  
2019

Approved by:

Joaquin Drut

Louise Dolan

Charles Evans

Alfred Kleinhammes

Amy Nicholson

© 2019  
C. R. Shill  
ALL RIGHTS RESERVED

## ABSTRACT

C. R. Shill: Stochastic and Semi-Classical Approaches to the Quantum Virial Expansion  
(Under the direction of Joaquin Drut)

Many-body quantum systems provide an interesting playground for experimentalists and theorists alike. In particular, ultracold atomic gases provide not only a realm of study for which experiments have a high degree of control, but also provides theorists with intriguing, yet challenging systems that may be accessed computationally. It is for these reasons that it is here where the majority of our work will focus. We discuss the necessary physics, thermodynamics, and computational methods for carrying out this work, and present several methods for computing coefficients of the quantum virial expansion across dimensions for Fermi gases with zero-range interactions. The techniques discussed are non-perturbative, and involve stochastic methods as well as a semi-classical lattice approximation. Through these algorithms, we have computed the interaction dependence (both attractive and repulsive where applicable) of the virial coefficients to a relatively high order as compared to current literature in one, two, and three spatial dimensions. Through one of said methods, we are able to provide a prediction for the radius of convergence of the virial expansion in one spatial dimension.

## TABLE OF CONTENTS

|   |            |
|---|------------|
| <b>LIST OF FIGURES</b> . . . . .  | <b>vii</b> |
| <b>LIST OF ABBREVIATIONS AND SYMBOLS</b> . . . . .                            | <b>ix</b>  |
| <b>1 Introduction</b> . . . . .   | <b>1</b>   |
| 1.1 Background Experiment and Motivation . . . . .                            | 1          |
| 1.1.1 Ultracold Atomic Gases . . . . .  | 2          |
| <b>2 Statistical Mechanics and Thermodynamics</b> . . . . .                   | <b>5</b>   |
| 2.1 Thermodynamics . . . . .  | 5          |
| 2.2 Classical Statistical Mechanics . . . . .                                 | 6          |
| 2.2.1 The Ideal Gas . . . . .   | 8          |
| 2.3 The Canonical Ensemble and $\mathcal{Z}$ as a Path Integral . . . . .     | 12         |
| 2.3.1 An alternative expression for the partition function . . . . .          | 14         |
| 2.4 The Grand Canonical Ensemble . . . . .                                    | 15         |
| 2.4.1 Quantum Statistics Derivation of the Grand Canonical Ensemble . . . . . | 16         |
| 2.4.2 The Quantum Ideal Gas . . . . .   | 22         |
| 2.4.3 Path Integral Representation of $\mathcal{Z}$ . . . . .                 | 24         |
| <b>3 Lattice Monte Carlo Methods</b> . . . . .                                | <b>26</b>  |
| 3.1 Lattice Monte Carlo Method . . . . .                                      | 26         |
| 3.1.1 Trotter-Suzuki Factorization . . . . .                                  | 28         |
| 3.1.2 The Hubbard-Stratonovich Transformation . . . . .                       | 28         |
| 3.1.3 Assembling the field integral representation . . . . .                  | 29         |
| 3.1.4 Doing the Integral with Monte Carlo Methods . . . . .                   | 30         |
| 3.1.5 The Metropolis Algorithm . . . . .                                      | 31         |

|          |   |           |
|----------|---|-----------|
| 3.2      | Hybrid Monte Carlo . . . . .                          | 32        |
| 3.3      | The Sign Problem . . . . .                            | 35        |
| 3.3.1    | Complex Langevin Method . . . . .                     | 36        |
| <b>4</b> | <b>Friedel Oscillations . . . . .</b>                 | <b>38</b> |
| 4.1      | Introduction . . . . .                                | 38        |
| 4.2      | Many-body method . . . . .                            | 41        |
| 4.2.1    | Hamiltonian and basic formalism . . . . .             | 41        |
| 4.2.2    | Expectation values of operators . . . . .             | 44        |
| 4.3      | Results . . . . .                                     | 45        |
| 4.3.1    | Ground-state energy . . . . .                         | 46        |
| 4.3.2    | Density profiles . . . . .                            | 46        |
| 4.3.3    | One-body density matrix . . . . .                     | 48        |
| 4.3.4    | Quasi-momentum distribution . . . . .                 | 48        |
| 4.3.5    | Tan's contact density and contact . . . . .           | 49        |
| 4.4      | Summary and Conclusions . . . . .                     | 50        |
| <b>5</b> | <b>Virial Projection in 1D and 2D . . . . .</b>       | <b>59</b> |
| 5.1      | Introduction . . . . .                                | 59        |
| 5.2      | Formalism . . . . .                                   | 61        |
| 5.2.1    | Stochastic Methods . . . . .                          | 61        |
| 5.2.2    | Semiclassical Lattice Approximation . . . . .         | 63        |
| 5.3      | Results . . . . .                                     | 64        |
| 5.3.1    | Virial coefficients in 1D . . . . .                   | 64        |
| 5.3.2    | Radius of convergence via projection method . . . . . | 65        |
| 5.3.3    | Virial coefficients in 2D . . . . .                   | 65        |
| 5.3.4    | Semiclassical lattice approximation . . . . .         | 66        |
| 5.3.5    | Systematic effects . . . . .                          | 67        |

|          |  |           |
|----------|--|-----------|
| 5.4      | Summary and Conclusions . . . . .                          | 68        |
| <b>6</b> | <b>Systems with Three-Body Forces . . . . .</b>            | <b>71</b> |
| 6.1      | Introduction . . . . .                                     | 71        |
| 6.2      | Hamiltonian and virial expansion . . . . .                 | 71        |
| 6.3      | The semiclassical approximation at leading order . . . . . | 73        |
| 6.4      | Results . . . . .  | 75        |
| 6.4.1    | Virial coefficients . . . . .                              | 75        |
| 6.4.2    | Thermodynamics and contact across dimensions . . . . .     | 76        |
| 6.5      | Summary and Conclusions . . . . .                          | 77        |
|          | <b>BIBLIOGRAPHY . . . . .</b>                              | <b>79</b> |

## LIST OF FIGURES

|     |  |    |
|-----|--|----|
| 1.1 | A representation for some of the possible systems of which we have access with the high degree of control of temperature ( $T/T_F$ ) and interaction strength ( $1/k_F a$ ) in 3D (13). We will discuss some of these regimes throughout this dissertation. . . . .  | 3  |
| 3.1 | Running average over Langevin time, $\tau$ , where $\tau_0$ is the total number of Langevin time steps, of the total particle numbers, $\langle \hat{n}_\uparrow \rangle$ and $\langle \hat{n}_\downarrow \rangle$ . Separate runs are seen to converge to the expected particle number for the 2 + 1 case (blue) and the 6 + 3 case (red). The data corresponds to $V = N_x^3$ , $N_x = 6$ , $\beta = 3.0$ , tuned to the unitary limit. . . . .  | 33 |
| 4.1 | Convergence of our energy estimator as a function of $\beta\varepsilon_F$ , for $N = 16$ particles in a 1D segment (discretized using $N_x = 80$ points), for couplings $\gamma = 0.0, 0.2, \dots, 4.0$ (top to bottom). . . . .   | 52 |
| 4.2 | The ground-energy of $N = 8, \dots, 24$ unpolarized fermions in a 1D segment (discretized using $N_x = 80$ points), in units of its non-interacting counterpart $E_{\text{FG}}$ , as a function of the dimensionless coupling $\gamma$ . . . . .   | 52 |
| 4.3 | Density profiles versus the scaled position $x/L$ for $N_x = 80$ at weak coupling ( $\gamma = 0.2$ , top panel) and strong coupling ( $\gamma = 3.0$ , bottom panel), for particle numbers $N = 8, 12, 16, 20, 24$ (from bottom to top). . . . .   | 53 |
| 4.4 | Hard-wall transform coefficients $B_k$ of Eq. (4.34), as a function of $Lp_k/\pi = k$ , for $N_x = 80$ and several values of the coupling $\gamma$ and particle number $N$ . Note the maximum at $k = 1$ is equal to unity to an accuracy better than 2% for all $\gamma$ and $N$ ; the minima, on the other hand, show clear variation with increasing $N = 8, \dots, 24$ (left to right) as well as increasing $\gamma$ (top to bottom; see inset). Inset: Value of the minimum as a function of the coupling $\gamma$ for $N = 8, \dots, 24$ (bottom to top). . . . . | 54 |
| 4.5 | Top: Hard-wall transform coefficients $B_{k,k'}$ of Eq. (4.36), as a function of $k = Lp_k/\pi$ and $k' = Lp_{k'}/\pi$ , for $N_x = 80$ , $\gamma = 4.0$ , and $N = 24$ . Bottom: Amplitude variation of the main peak $B_{\frac{N}{2}, \frac{N}{2}+1}$ as a function of $\gamma$ for several particle numbers. . . . .  | 55 |
| 4.6 | Quasi-momentum distribution $n(k)$ for $N = 16$ particles as a function of $\gamma = 0.2, 0.6, 1.0, \dots, 3.8$ (top to bottom around $k = 0$ ), for $N_x = 80$ . Inset: $\gamma$ -dependence of the discontinuity $\delta_N$ in $n(k)$ at the Fermi surface. While $\delta_N$ could depend on $N$ , our results for different $N$ agree within our statistical and systematic uncertainties. . . . .  | 56 |
| 4.7 | Contact density $\mathcal{C}(x/L)$ as a function of the scaled position $x/L$ for $N_x = 80$ at weak coupling ( $\gamma = 0.2$ , top panel) and strong coupling ( $\gamma = 3.0$ , bottom panel), for particle numbers $N = 8, 12, 16, 20, 24$ (top to bottom). . . . .  | 57 |
| 4.8 | Tan's contact of $N = 8, \dots, 24$ unpolarized fermions in a 1D segment (discretized using $N_x = 80$ points), in units of its non-interacting counterpart $E_{\text{FG}}$ , as a function of the dimensionless coupling $\gamma$ . . . . .   | 58 |
| 5.1 | Virial coefficients $b_n$ for $n = 1 - 6$ for the 1D Fermi gas, as a function of the dimensionless coupling $\lambda$ , as obtained with our projection method. Crosses on the $y$ axis denote the non-interacting values $b_n = (-1)^{n+1}n^{-3/2}$ . The leading order of the semiclassical lattice approximation (LO-SCLA) is shown with a dashed-dotted line for $\Delta b_3$ and with a dashed line for $\Delta b_4$ . Green and blue diamonds show the results obtained with our second stochastic method, for comparison. . . . .                                 | 64 |
| 5.2 | Estimate of the radius of convergence $\alpha_0$ of the virial expansion as a function of the coupling $\lambda$ . Inset: $b_n$ for $n = 1, 3, 5$ for $\lambda = -1$ . Constant behavior as a function of $\alpha$ is expected when the coefficient of the $n$ -th power of $z$ is extracted successfully. Deviation from such a constant as $\alpha$ is increased shows the appearance of roots of $\mathcal{Z}$ in the complex- $z$ plane, which yields the estimate $\alpha_0$ for the radius of convergence shown in the main plot. . . . .                          | 69 |

|     |  |    |
|-----|--|----|
| 5.3 | Interaction change of the virial coefficients $\Delta b_n$ for $n = 2 - 4$ for the 2D Fermi gas, as a function of the dimensionless coupling $\lambda_2$ . The solid red line connects the data for $\Delta b_2$ , the green shows $\Delta b_3$ , and the blue shows $\Delta b_4$ . The leading order of the semiclassical lattice approximation (LO-SCLA) is shown with a dashed-dotted line for $\Delta b_3$ and with a dashed line for $\Delta b_4$ . The solid black line shows the result for $\Delta b_3$ of Ref. (73). Note that the data for $\Delta b_2$ reproduces the exact result of Eq. (5.15) by virtue of the renormalization condition (see text). | 69 |
| 5.4 | Top: Illustration of the size of the finite- $N_x$ effects on $b_3$ and $b_4$ in 1D at $\lambda = 1$ . The errorbars show statistical effects. Bottom: Illustration of the size of the finite- $\tau$ effects on $\Delta b_3$ in 2D for varying $\lambda$ .  | 70 |
| 6.1 | Above are plots of the three body pressure (left) and density (right) equations of state to order five in the virial expansion in their dimensionless form in one two and three dimensions plotted against the log of the fugacity, $\ln z = \beta\mu$ . We have represented only one value of $\Delta b_3$ here as the values are directly proportional to this value.  | 78 |

## LIST OF ABBREVIATIONS AND SYMBOLS

|                 |  |
|-----------------|--|
| $S$             | - Action                               |
| BCS             | - Bardeen Cooper Schrieffer            |
| $g$             | - Bare Coupling                        |
| $k$             | - Boltzmann Constant                   |
| BEC             | - Bose-Einstein Condensate             |
| $\mu$           | - Chemical Potential                   |
| $\nu$           | - Correlation Length Critical Exponent |
| $a^k(t)$        | - Creation Operator                    |
| $a^{k*}(t)$     | - Annihilation Operator                |
| $T_c$           | - Critical Temperature                 |
| $U_t$           | - Fermion Matrix                       |
| F-R             | - Feshbach Resonance                   |
| $z$             | - Fugacity                             |
| $\mathcal{Z}$   | - Grand Canonical Partition Function   |
| $\Omega$        | - Grand Potential                      |
| $\mathcal{H}$   | - Hamiltonian                          |
| $\sigma$        | - Hubbard Stratonovich Auxiliary Field |
| HST             | - Hubbard-Stratonovich Transformation  |
| HMC             | - Hybrid Monte Carlo                   |
| $\beta$         | - Inverse Temperature                  |
| $\mathcal{L}$   | - Lagrangian                           |
| $\mathcal{Q}_N$ | - N-particle Partition Function        |

$N_\tau$  - Number of Time Lattice Points

$h$  - Planck's Constant

QCD - Quantum Chromo Dynamics

QMC - Quantum Monte Carlo

SCLA - Semi-Classical Lattice Approximation

$\lambda_T$  - Thermal Wavelength

$\delta_\tau$  - Time Lattice Spacing

$\mathcal{T}_t$  - Transfer Matrix

TSF - Trotter-Suzuki Factorization

## CHAPTER 1: Introduction

### Section 1.1: Background Experiment and Motivation

Throughout this dissertation, we will discuss the physics, methods, and results (computational as well as experimental) in the realm of many-body quantum systems. These systems provide an attractive playground for both experimentalists and theorists, and is one of the most rapidly advancing areas of physics today. Since the dawn of quantum mechanics it was understood that many-body quantum systems are as important as they are challenging: indeed, calculating the properties of even small nuclei, or small electronic systems, requires considerable computational resources. For that reason, quantum many-body systems have received significant attention, leading to many fundamental discoveries both in theory and experiment. These discoveries range from measuring and studying newly discovered phase transitions, to new states of quantum matter, to even observing macroscopic quantum effects. That is, microscopic quantum effects of few particles culminate to have large effects in matter on the scale that can be seen with the human eye.

There are many examples of these types of advancements throughout the past century. One popular example is that of the observation of superfluidity in liquid  $^4\text{He}$  in 1938 (4; 5), which is the phenomenon such that liquid can flow without resistance. The trouble with this state of matter, however, is that the interaction of the molecules is so strong that the underlying physics on the microscopic level is extremely difficult to understand and model theoretically. This brings us to a great counter example, which is what occurs to non-interacting bosons when brought to zero temperature. This curiosity was first theorized by Bose long before the measurement of superfluid helium. Bose was actually able to formulate this hypothesis before, even, the final formulation of quantum mechanics, by introducing a new way of counting microstates (6). Following this discovery, Einstein generalized the technique to include particle number conservation, leading to the development of the Bose-Einstein distribution, and even more importantly Bose-Einstein condensation (BEC). This is the phenomenon whereby, at some critical temperature,  $T_c$ , bosons condense and a large portion of the particles occupy the same single-particle quantum state. This remarkable phenomenon was theorized to be the underlying cause for superfluidity in Helium. The theories, however, are vastly different. A proper superfluid requires interactions, and the case of Helium atoms the interactions are actually strong, whereas the BEC described above is an ideal non-interacting boson gas. Thus, something about the theory needed to be modified in order to arrive at a proper description of the phenomenon (4).

Another good example of many-body experimental development was the discovery of superconductivity in 1911 (7). Similar to superfluidity, this is when electrons can flow through a conductor without resistance. Such a surprising phenomenon was studied extensively in a large amount of different metals, as this would be an exceptionally useful tool if able to adapt for a wide variety of uses. It was not for another 50 years, however, that a group of scientists (8) discovered that this effect was actually caused by BEC. Superconductivity occurs when the electrons in a metal (as a gas of fermions) form loosely bound pairs, known as Cooper pairs, effectively forming a gas of non-interacting bosons allowing for superfluidity of the gas within the metal. Another 20 years later in 1986 the discovery of high-temperature superconductors in ceramic materials was made (4). The microscopic physics behind this, however, remain an area of hot debate to this day.

Thus far, we have discussed several important experimental and theoretical discoveries within the field of many-body quantum systems. To further our understanding of the vast advancements in this field and to understand the realm in which the majority of this work focuses, however, we must enter a slightly more specific and more modern area of quantum matter: ultra-cold atomic quantum gases.

#### 1.1.1: Ultracold Atomic Gases

Ultracold atomic gases represent a relatively new area of study within many-body systems that came to the forefront of condensed matter research after several groups achieved BEC for the first time in a trapped dilute gas of bosonic alkali atoms in 1995 (9; 10; 11), over 70 years after its theoretical development. With this research came new techniques for studying and producing novel states of quantum matter. These techniques involve the use of 1) laser cooling, 2) trapping atoms in a magnetic trap, and finally 3) evaporative cooling (4). Those steps are essential for the observation of BEC for a few reasons. An atomic BEC first requires extremely low densities (between  $10^{12}$  and  $10^{15}$  atoms/cm<sup>3</sup>) in order to avoid crystallization of the atomic cloud; second (and directly related to the previous item), an atomic BEC requires extremely low temperatures (1 - 100 nK). Such extremely low temperatures and densities were never before achievable through experiment. The development of magnetic trapping solved several roadblocks hindering BEC research. To begin, trapping allows experimentalists to isolate the gas from external walls, and therefore from external heat reservoirs, and impurities. Moreover, it allowed for a simple way to perform evaporative cooling. By increasing or decreasing the depth of the trap, the higher energy particles are able to escape, and scientists are able to adjust the gas to precise temperatures.

As a result, these gases are not only isolated, but also very clean, i.e. they have no impurities (unless one wishes to add them), and are highly malleable. These systems are low in density and weakly interacting, meaning that we can handle these systems theoretically with approximate methods like perturbation theory.

What is even more interesting is that we can utilize various numerical methods as well as advanced field theory techniques to obtain accurate microscopic depictions of these ultracold atomic systems. We will return to those later.

Our understanding of, and access to, these systems has been furthered even more so by the implementation of Feshbach-resonance techniques, F-R (12), which refers to the idea of tuning of a magnetic field about a Feshbach resonance, allowing experimentalists to precisely control interaction strength between atoms. The scattering length, and therefore interaction strength, between two particles colliding is directly dependent on the energy difference between the internal levels of the atoms. That energy difference can be controlled by tuning a magnetic field about the F-R, as the magnetic field couples to the internal properties (namely the magnetic moment) of the otherwise neutral atoms. Using the above-mentioned suite of techniques, parameters such as temperature, density, and interaction strength are under precise experimental control, giving experimentalists access to a wide array of quantum many-body systems, from weakly to strongly coupled and from nearly zero to high temperature (see e.g. Fig.?? below).

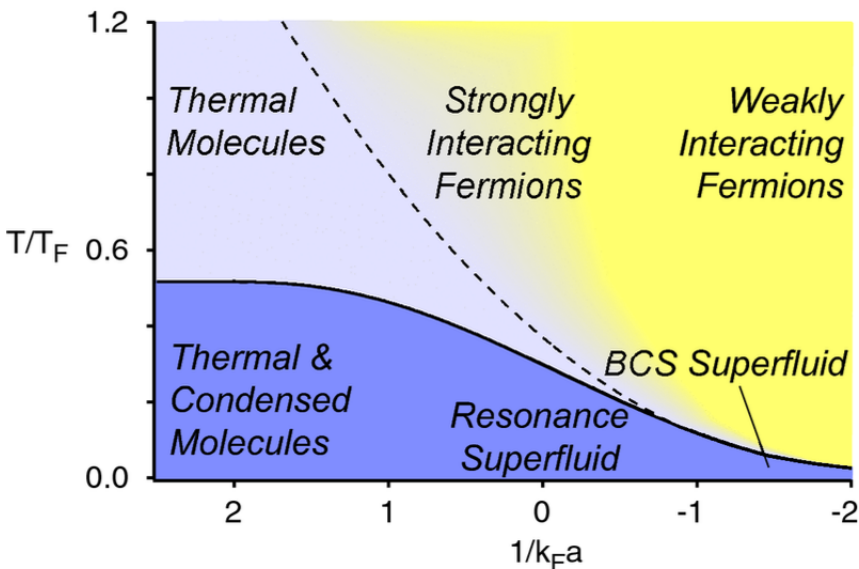


Figure 1.1: A representation for some of the possible systems of which we have access with the high degree of control of temperature ( $T/T_F$ ) and interaction strength ( $1/k_F a$ ) in 3D (13). We will discuss some of these regimes throughout this dissertation.

The ability to finely tune the interaction strength allowed for yet another huge development within this field. It allowed for the possibility of achieving superfluidity and BEC in fermions. Indeed, experimentalists were able to measure a BEC of Cooper pairs within an atomic Fermi gas (14; 15).

With that we can officially study two phases of incredible ultracold atomic matter, that is to say, we can fully study the physics of the infamous BCS-BEC crossover. By tuning about the F-R we can study large

positive scattering length (also known as detuning), no bound molecule, weakly attractive systems (BCS), to large negative detuning where we have bound molecules. As it so happens, this transition from BCS to BEC is completely smooth, i.e. the transition is continuous (4)!

The continuation and applicability of this research is nearly limitless. For instance, all of the afore mentioned experiments with fermions used spin 1/2 fermions (as required for poly exclusion) in an unpolarized case ( $n_{\uparrow} = n_{\downarrow}$ ). The question then is, what happens in a polarized case? A large amount of research has gone into this question that could shed light on the physics in neutron stars, where mixtures of quarks with attractive interactions exist, and could form something known as a color superconductor (4). Another outlet involves the use of lasers to form standing waves and create an optical lattice, which can be used to simulate ionic lattices, and therefore allow the study of solid state physics with the degree of control of ultracold atomic experiment. In addition, this method can even be used to provide insight into high temperature superconductors. Lastly, and directly relevant to the work in this dissertation, optical lattices can be used to create reduced dimensional systems of trapped gases. These lower dimensional systems often yield interesting or unexpected behaviors, such as strongly correlated effects. Crucially, when considering systems in one spatial dimension we often have the luxury of exact theoretical solutions for certain classes of systems (4).

The list of possible research directions goes on. The highly clean and controllable nature of ultracold atomic gases allows for the study of an extremely wide degree of systems, and as previously mentioned because of the nature of these systems (low density, small interaction strength) we have the capability of applying certain approximate methods to help study and explore them both theoretically and numerically on a microscopic level. This in turn allows for a high degree of collaboration between theorists and experimentalists, that is not usually seen in modern day physics.

Throughout this dissertation we will discuss the development of the statistics and thermodynamics behind these theories. Starting with the classical non-interacting ideal gases, and working our way through the grand canonical ensemble and the quantum ideal gas. We will also lay out the foundation for carrying out our numerical calculation through quantum Monte Carlo methods, and discuss some difficulties therein. We will conclude with the presentation of our methods that have been developed to help tackle some difficult problems such as the virial expansion, as well as results from these projects seen in references (1; 2; 3).

## CHAPTER 2: Statistical Mechanics and Thermodynamics

In this chapter we present some elementary consideration regarding thermodynamics and statistical mechanics. The goal is to introduce some of the essential quantities needed to understand the main results obtained in this thesis, which are discussed in later chapters. To that end, we begin with a review of thermodynamics in the context of classical (i.e. non-quantum) systems. We then discuss the classical ideal gas and introduce the partition function. Finally, and with a view to addressing the quantum many-body problem, we review second quantization and the quantum version of the grand-canonical ensemble.

### Section 2.1: Thermodynamics

Thermodynamics studies the equilibrium behavior of macroscopic systems (macrostates), such as work heat and entropy, based on the culmination of microscopic properties (microstates) of particles, such as kinetic and potential energies and interaction strength. At the microscopic level, the physics and behavior of these particles is relatively well known through varying theories of their interactions and dynamics. Assuming these microscopic descriptions are relatively complete, we should ideally be able to describe the overarching behavior of the system, i.e. the macroscopic properties. This is best achieved using the kinetic theory of gases.

The simplest system to study to better understand this theory, is the dilute (essentially ideal) gas. Given a volume of gas,  $V$ , kinetic theory attempts to describe the macroscopic properties of the system by considering the total energy and time evolution of the  $N$  microscopic particles occupying the system. Both the energy consideration and the time evolution can be studied using the Hamiltonian,  $\mathcal{H}$ , given the microstate of all  $N$  particles in terms of their position and momenta,  $q(t)$  and  $p(t)$  respectfully, at any time  $t$ . For this system of  $N$  particles the Hamiltonian is defined as,

$$\mathcal{H}(\mathbf{q}, \mathbf{p}) = \sum_{i=1}^N \frac{p_i^2}{2m} + U(\mathbf{q}) = \sum_i E_i n_i \quad (2.1)$$

which denotes the total energy of the system, with coordinates  $\mathbf{q} \equiv \{\vec{q}_1, \vec{q}_2, \dots, \vec{q}_N\}$  and momenta  $\mathbf{p} \equiv \{\vec{p}_1, \vec{p}_2, \dots, \vec{p}_N\}$ . Likewise, the  $E_i$  are the energy levels available to the microstates of the system, and  $n_i$  are the number of particles that occupy that energy state, such that  $\sum_i n_i = N$ . Also the number of microstates corresponding to a given energy state  $E_i$ , is denoted as  $\Omega(E_i)$ . The time evolution for this point

in the  $6N$  dimensional phase space (for 3D systems) is then governed by the canonical equations of motion,

$$\begin{aligned}\frac{\partial \vec{q}_i}{\partial t} &= \frac{\partial \mathcal{H}}{\partial \vec{p}_i} \\ \frac{\partial \vec{p}_i}{\partial t} &= -\frac{\partial \mathcal{H}}{\partial \vec{q}_i},\end{aligned}\tag{2.2}$$

These equations of motion are subject to *time reversal symmetry*, such that if the momenta are reversed, that is  $\mathbf{p} \rightarrow -\mathbf{p}$ , at  $t = 0$ , the particles follow their previous trajectory,  $\mathbf{q}(t) = \mathbf{q}(-t)$ . This comes from the invariance of  $\mathcal{H}$  under the transformation  $(\mathbf{p}, \mathbf{q}) \rightarrow (-\mathbf{p}, \mathbf{q})$ .

The *macrostates*  $M$ , of an ideal gas in equilibrium can be described by a small set of state functions like  $E$ ,  $T$ ,  $P$ , and  $N$ . The overall space spanned by  $M$  is much smaller than that of the space spanned by the *microstates*,  $\mu$ . This allows us to conclude that there must be a significant amount of microstates that correspond to a single macrostate. This is known as the *degeneracy* of the system, when there are multiple sets of microstates that yield the same macrostate, and each set of these degenerate states is known as an *equivalence class* (16).

Again, degeneracy is a set of microstates that corresponds to the same set state functions, and the microstates are well understood using classical physics. The question now is, how do we access the information of these macrostates? This is where statistical mechanics comes into play, which we will now discuss.

## Section 2.2: Classical Statistical Mechanics

In the previous section we discussed microstates and how we can describe the corresponding macrostates by a fixed number of particles  $N$ , fixed volume  $V$ , and a total energy  $\mathcal{H}$ , and our set of microstates will of course be a function of these,  $\Omega(N, V, E)$ . This gives us a direct connection between the kinetic theory of gases and its eventual successor ensemble theory. Which reduced the problem to the overarching statistics of the problem on the whole. So we migrated from a direct application of classical mechanics to the collective statistics of the system. So inevitably this new theory became known as *Statistical Mechanics*, go figure.

The idea behind the statistical nature of thermodynamics comes from the fact that we consider a macrostate with a larger number of microstate a more probable one. In fact the state in which the number of microstate,  $\Omega(E_0, E_i)$ , is maximized is considered the *most* probable one. This is due to the fact that the most probable state is the one that the system spends the vast majority of its time in, obviously, and

therefore can be identified as the *equilibrium state*. We may obtain this equilibrium state as,

$$\frac{\partial \Omega(E_i)}{\partial E_i} = 0, \quad (2.3)$$

and the corresponding energy associated with this state is denoted  $\bar{E}_i$ . Furthermore the equilibrium state can be defined by a parameter,  $\beta$ , which can be defined as follows,

$$\beta = \left( \frac{\partial \ln \Omega(N, V, E)}{\partial E} \right)_{N, V, E = \bar{E}}. \quad (2.4)$$

It can also be stated that if we have multiple systems in contact corresponding to a given  $N_i$ ,  $V_i$ , and  $E_i$ , then these systems are in equilibrium precisely when the  $\beta_i$  are equal. This is because at this point there must be no more net energy exchange between the systems (16). We can then conclude that this parameter,  $\beta$ , must be related the thermodynamic temperature of the system. Recall, from your introductory thermodynamics class, the following,

$$\left( \frac{\partial S}{\partial E} \right)_{N, V} = \frac{1}{T}, \quad (2.5)$$

such that  $S$  is the entropy of the system. From these two previous equations, we can then conclude that there is a relationship of these two of the form,

$$\frac{\Delta S}{\Delta \ln \Omega} = \frac{1}{\beta T} = C. \quad (2.6)$$

This was first determined by Boltzmann, and corresponds to a universal constant. Plank then followed this with a definition for entropy in terms of the number of microstates of a system,

$$S = k \ln \Omega, \quad (2.7)$$

and thus provided us with a statistical connection to the third law of Thermodynamics. This relationship allows us to further develop thermodynamics, and our understanding of universal constants. Namely,

$$\eta = \left( \frac{\partial \ln \Omega(N, V, E)}{\partial V} \right)_{N, V, E = \bar{V}}, \quad (2.8)$$

$$\zeta = \left( \frac{\partial \ln \Omega(N, V, E)}{\partial N} \right)_{N, V, E = \bar{N}}. \quad (2.9)$$

Again we can determine the physical meaning of these terms by using the thermodynamic equation of

state,

$$dE = TdS - PdV + \mu dN, \quad (2.10)$$

where  $P$  is the thermodynamic pressure, and  $\mu$  the chemical potential of the system. It follows that,

$$\eta = \beta P, \text{ and } \zeta = -\beta\mu, \quad (2.11)$$

such that  $\beta = 1/kT$  is the *inverse temperature*, and  $k$  the Boltzmann constant. The same equilibrium conditions as with  $\bar{E}$  apply here as well. Various other thermodynamic equations can be found in a standard Statistical mechanics book such as Pathria (16). To advance our understanding of the applications and implications of statistical mechanics, let us examine a specific system that in itself has many implications to other systems and much of our own work, the *ideal gas*.

### 2.2.1: The Ideal Gas

The ideal gas is a highly specialized system, but allows us to get a straightforward understanding of the Boltzmann constant and its relationship to other physical constants. Not only does this system provide insight into natural constants, but the classical ideal gas often provides parallels to other more complex systems, particularly real gases in extreme limits. For instance, taking the limit of high temperature, weak coupling, or dilute systems often brings us back to a similar behavior of the ideal gas.

In this system we are considering a set of classical, non-interacting particles, meaning that there is no spacial correlation between the location of the individual particles and the likelihood of a given particle to be in a specific location. That is to say that the location of these particles is independent of the location of the others. This implies that the total number of ways that the  $N$  particles may arrange themselves in the given volume,  $V$ , is equal to the product of the number of ways the particles may arrange themselves in the space independent of the others. With the total number of particles  $N$ , and the total energy  $E$  fixed, this number will be directly proportional to the volume of the system. It follows that the total number of microstates is thus proportional to the  $N$ th power of  $V$ :

$$\Omega(N, E, V) \propto V^N. \quad (2.12)$$

Combined with eq.(2.9) we can obtain

$$\frac{P}{T} = k \left( \frac{\partial \ln \Omega(N, V, E)}{\partial V} \right)_{N, E} = k \frac{N}{V}. \quad (2.13)$$

Which then leads to the very well known *ideal gas law*,

$$PV = kNT, \text{ or } PV = nRT, \quad (2.14)$$

where  $n$  is the number of moles of gas contained in the system, and  $R = kN_A$ ,  $N_A$  being the *Avogadro number*. This holds for any system of non-interacting particles, or can be employed as an approximation for *nearly* non-interacting systems (16).

To continue we will need to examine the relationship between the total energy and the energy of the various degrees of freedom for the system ( $\epsilon_r$ ). That is, how many ways can we satisfy the equation,

$$\sum_i^{3N} \epsilon_i = E. \quad (2.15)$$

The energy eigenvalues associated with a free system of particles confined in a three dimensional box of length  $L$ , such that the corresponding wave-functions,  $\psi(x)$ , vanish at the boundaries is given by

$$\epsilon(n_x, n_y, n_z) = \frac{h^2}{8mV^{2/3}}(n_x^2 + n_y^2 + n_z^2); \quad n_x, n_y, n_z = \{1, 2, 3, \dots, L\}. \quad (2.16)$$

Here  $h$  is Planck's constant, and  $m$  is the mass of the particles. It follows that the number of distinct microstates for a particle of a given energy  $\epsilon$  is the number of independent solutions of

$$(n_x^2 + n_y^2 + n_z^2) = \frac{8mV^{2/3}}{h^2} \epsilon = \epsilon'. \quad (2.17)$$

Let us represent this number by  $\Omega(1, \epsilon, V)$ . It then follows that the actual desired value of  $\Omega(N, E, V)$  is given by all the possible solutions of

$$\sum_r^{3N} n_r = \frac{8mV^{2/3}}{h^2} E = E'. \quad (2.18)$$

Now before we even are able to calculate  $\Omega(N, E, V)$  we can draw a very important conclusion from the above equation. That is that  $\Omega$  has a explicit  $V$  and  $E$  dependence of the form  $(EV^{2/3})$ . We can therefore make the reduction,

$$S(N, E, V) \equiv S(N, EV^{2/3}), \quad (2.19)$$

may conclude that through an *adiabatic process*, meaning that both  $S$  and  $N$  remain constant, that

$$EV^{2/3} = C, \quad (2.20)$$

$C$  being a constant. Taking this one step further using the well known thermodynamic equations,

$$P = \left( \frac{\partial S}{\partial V} \right)_{N,E} / \left( \frac{\partial S}{\partial E} \right)_{N,V} = - \left( \frac{\partial E}{\partial V} \right)_{N,S} = \frac{2}{3} \frac{E}{V}. \quad (2.21)$$

That is that the pressure of the ideal gas is exactly equal to two thirds of the overall energy density of the system. Interesting! What's more, combining the previous two equations we can see that,

$$PV^{5/3} = C. \quad (2.22)$$

Yielding the relationship between the pressure and volume in a *reversible adiabatic process* (16). It is safe to say that the above three equations should hold for both *Quantum* and *classical* statistics. Notice that we have not yet done a full calculation of  $\Omega$ , and yet we have been able attain a significant amount of information about the system! Lets do that now, however! Compute  $\Omega$  that is.

In this calculation we make the assumption of *distinguishable* particles (i.e. classical), meaning that if we were to exchange to particles in the system, then we would have a distinct countable microstate. It follows that the number  $\Omega(N, E, V)$  or better still  $\Omega_N(E')$  is exactly equal to the number of positive-integral lattice points on the surface of an  $3N$ -dimensional sphere with radius  $\sqrt{E'}$ . Now, this number can obviously be seen as an oddly behaving function of  $E'$ , considering that the close values of  $E'$  may yield extremely different numbers for  $\Omega_N(E')$ . So instead let us look at a different number,  $\Sigma_N(E')$ , which is similar to the above number but is defined as the number of positive-integral lattice points on and within the surface of an  $3N$ -dimensional sphere with radius  $\sqrt{E'}$ . So it is the number of microstates corresponding to all energy eigenvalues less-than-or-equal-to  $E'$ , or essentially the volume of the  $3N$ -dimensional sphere, not just the surface, also defined as  $\Sigma(N, E, V)$ . This is a much more well behaved number with respect to  $E'$ , given by

$$\Sigma(N, E, V) = \sum_{\mathcal{E} \leq E'} \Omega(N, \mathcal{E}, V) \quad (2.23)$$

or likewise,

$$\Sigma_N(E') = \sum_{\mathcal{E} \leq E'} \Omega_N(\mathcal{E}). \quad (2.24)$$

With this number, at least, we can expect a somewhat of an asymptotic behavior as  $E' \rightarrow \infty$ . Much more so than  $\Omega$  for sure. Both numbers, however, can give us information regarding the thermodynamics of the respective system. Again detailing the  $N$ -body problem of the ideal gas, the number  $\Sigma_N(E')$  should asymptotically approach the "volume" of the  $3N$ -dimensional sphere of radius  $\sqrt{E'}$ , giving

$$\Sigma_N(E') \approx \left(\frac{1}{2}\right)^{3N} \left[ \frac{\pi^{3N/2}}{(3N/2)!} E'^{3N/2} \right]. \quad (2.25)$$

Or in terms of  $N$ ,  $V$ , and  $E$ ,

$$\Sigma(N, V, E) \approx \left(\frac{V}{h}\right)^N \left[ \frac{(2\pi m E)^{3N/2}}{(3N/2)!} \right]. \quad (2.26)$$

Furthermore, by taking a logarithm and applying the approximation (Stirling's Formula),

$$\ln(n!) \approx n \ln n - n \quad (2.27)$$

we obtain

$$\ln \Sigma(N, V, E) \approx N \ln \left[ \frac{V}{h^3} \left( \frac{4\pi m E}{3N} \right)^{3/2} \right] + \frac{3}{2}N. \quad (2.28)$$

In order to derive the thermodynamics of a given system, we must find a way to fix the value of, or at least provide limits of the overall energy of the system. Given the erratic nature of the number  $\Omega(E)$ , specifying a precise energy value is not justifiable based on the physical nature of the system. In addition to this issue, we cannot make the assumption that a real world system has an exactly defined energy. This is highly idealized, and would be a rather naive assumption. Almost every real world system has some sort of contact with it's surroundings, however small, resulting in a non-exact energy value. Instead we consider an effective range of values for the energy, with bounds  $[E - \frac{\Delta}{2}, E + \frac{\Delta}{2}]$ , where  $\Delta$  is considered small relative to the mean value of the energy,  $\Delta \ll E$ . The resulting number of microstates,  $\Gamma$ , is then given by

$$\Gamma(N, V, E; \Delta) \simeq \frac{\partial \Sigma(N, V, E)}{\partial E} \Delta \approx \frac{3N}{2} \frac{\Delta}{E} \Sigma(N, V, E), \quad (2.29)$$

and thus

$$\ln \Gamma(N, V, E; \Delta) \approx N \ln \left[ \frac{V}{h^3} \left( \frac{4\pi m E}{3N} \right)^{3/2} \right] + \frac{3}{2}N + \left\{ \ln \left( \frac{3N}{2} \right) + \ln \left( \frac{\Delta}{E} \right) \right\}. \quad (2.30)$$

Now, for any system such that  $N \gg 1$  we know that  $\lim_{N \rightarrow \infty} (\ln N)/N = 0$ , so both terms inside the curly braces can essentially be considered negligible considering that  $\Delta/E \ll 1$  is also true for a reasonable system. Therefore, for most physical systems we have

$$\ln \Gamma \approx \ln \Sigma \approx N \ln \left[ \frac{V}{h^3} \left( \frac{4\pi m E}{3N} \right)^{3/2} \right] + \frac{3}{2}N. \quad (2.31)$$

We therefore arrive at the conclusion that, for most practical systems, the reasonable range allowed to the energy has little to no effect on the resulting thermodynamics of said system. Holy Cannoli! The reason behind this being that the number of microstates available increases with the energy, so even if we allow all possible energy states to be occupied, between 0 and  $E$ , it is only the small range around  $E$ ,  $[E - \frac{\Delta}{2}, E + \frac{\Delta}{2}]$ , that makes the most significant contribution to this number (16). Even more, since we are most concerned with the log of this value, the width  $\Delta$  can also be ignored, and the thermodynamics of the problem can be calculated in a relatively straightforward manor!

Hurray! Statistical mechanics works! Now, by holding certain quantities constant, like  $T$  and  $N$  for an *isothermal* change of state, or  $S$  and  $N$  for a *reversible adiabatic* process, many other thermodynamic properties can be derived using the same processes as above. Let's say we'll leave those as an exercise for the reader, or just go check out Pathria (16).

We have certainly demonstrated how the thermodynamics of a macroscopic system can be derived from considering the multiplicity or degeneracy of the microstates involved (i.e. with the numbers  $\Gamma$ ,  $\Sigma$ , and  $\Omega$ ). The whole understanding of any given system then relies on the asymptotic behavior of these numbers, which sadly is only realized in an extremely limited number of cases, like the ideal gas problem discussed above. So the question remains, how can we use these theories to discover the thermodynamic properties of any given system?

To that end, what we have essentially worked towards in the above section, without explicitly saying so, is the formulation of statistical mechanics in terms of the *canonical ensemble*, and what's more the representation of these systems in regards to *the grand partition function*,  $\mathcal{Z}$ . Which will be discussed next.

### Section 2.3: The Canonical Ensemble and $\mathcal{Z}$ as a Path Integral

As discussed in the previous section, with the asymptotic expressions for the numbers  $\Omega$ ,  $\Sigma$ , and  $\Gamma$  we may discuss the thermodynamics of any given system in a relatively straightforward way. For the vast majority of physical systems, however, computing these quantities is an extremely difficult calculation to carry out. We must then look to other methods in ensemble theory to make our lives easier.

First, lets point out that a fixed energy,  $E$ , for a real system just doesn't seem to quite fit reality. For one, it is nearly impossible to measure the total energy of a system of  $N$  particles, and furthermore that number is so apt to change that the measured value would very quickly become obsolete. A far more telling number to describe a system would appear to be the temperature,  $T$ . An easily measured, and more importantly *controllable* quantity. So let us transform our understanding of a given thermodynamic system from the variable  $N, V, E$  to that of  $N, V, T$ . This classification of an ensemble is known as the *canonical ensemble*.

In the canonical ensemble, the energy  $E$  is variable, and can take on values from zero to infinity. We may then ask the question: what is the probability that at a given time,  $t$ , that the system is found in a state that can be characterized by the energy  $E_i$ ? Let's call this probability  $P_i$ . Studying the statistics of the canonical ensemble in a similar manner as we did with the ideal gas, we can develop the thermodynamic understanding of these systems.

Using a number of statistical considerations detailing in Pathria (16), we can conclude the following,

$$P_i \propto \exp(-\beta E_i), \quad (2.32)$$

where  $\beta = 1/kT$  is the inverse temperature, and  $k$  the Boltzmann constant. Normalizing the above expression we can again conclude that,

$$P_i = \frac{\exp(-\beta E_i)}{\sum_i \exp(-\beta E_i)}, \quad (2.33)$$

where the sum in the denominator ranges over all possible energies available to our system in question. This is known as the *canonical distribution function* (16), and now allows us to start taking expectation values for our system. For instance the average energy,  $U$ ,

$$U = \frac{\sum_i E_i \exp(-\beta E_i)}{\sum_i \exp(-\beta E_i)} = -\frac{\partial}{\partial \beta} \ln \left\{ \sum_i \exp(-\beta E_i) \right\}. \quad (2.34)$$

Here  $U$  is related to the *Helmholtz free energy*,  $A = (U - TS)$ , such that

$$dA = dU - TdS - SdT = -SdT - PdV + \mu dN \quad (2.35)$$

$$S = -\left(\frac{\partial A}{\partial T}\right)_{N,V} \quad P = -\left(\frac{\partial A}{\partial V}\right)_{N,T} \quad \mu = \left(\frac{\partial A}{\partial N}\right)_{V,T} \quad (2.36)$$

We may further this by showing that there is a simple relationship between the statistical representation and the thermodynamic one given that  $\beta$  is the inverse temperature,

$$\beta A = -\ln \left\{ \sum_i \exp(-\beta E_i) \right\}, \quad \beta = -\frac{1}{kT}. \quad (2.37)$$

Equation 2.37 can be considered the most fundamental result of the canonical ensemble theory, as it is an extremely versatile representation that acts as a generating functional for many of the important thermodynamic quantities of a system. A much more commonly used expression for eq. 2.37 is,

$$A(N, V, T) = -kT \ln Q_N(V, T), \quad (2.38)$$

where

$$Q_N(V, T) = \sum_i \exp(-\beta E_i). \quad (2.39)$$

The quantity  $Q_N$  is an extremely important quantity in modern physics known as the *partition function*. There is a large amount of modern physics research devoted to finding both exact and approximate solutions to this very equation.

### 2.3.1: An alternative expression for the partition function

For the majority of physical systems, the energy levels,  $E_r$ , are degenerate, meaning that any given energy level can be occupied by a number of states,  $g_r$ . We may therefore write the expression for the partition function as,

$$Q_N(V, T) = \sum_i g_i \exp(-\beta E_i). \quad (2.40)$$

Yielding the following for the probability of a given state to have an energy value  $E_i$ ,

$$P_i = \frac{g_i \exp(-\beta E_i)}{\sum_i g_i \exp(-\beta E_i)}. \quad (2.41)$$

It is then obvious that the probability for a given state to have one of the defined energy levels is thus proportional to  $g_i$ , the *multiplicity*. Thus we can consider  $g_i$  to be the *weight* for the corresponding energy level. This, however, does not change our fundamental understanding of the basic relations laid out in the previous section (16).

To this point we have considered systems consisting of a discrete energy structure. In reality, however, when considering the overall size of our systems of interest, coupled with the remarkably large number of particles that we see in them (think Avogadro's number,  $\propto 10^{23}$ ), the energy structures are vary nearly continuous variables. Therefore we consider the probability for a certain energy as  $P(E)dE$ , instead of considering a range of energies within some finite range that will certainly contain a very large number energy states. Given the number of energy states within the given energy range,  $(E, E + dE)$ , as  $g(E)dE$ , where  $g(E)$  is known as the *density of states*, we define the normalized probability as,

$$P(E)dE = \frac{g(E) \exp(-\beta E)dE}{\int_0^\infty g(E) \exp(-\beta E)dE}. \quad (2.42)$$

We may now make the definition of the partition function in a continuous energy basis as,

$$Q_N(V, T) = \int_0^\infty g(E) \exp(-\beta E)dE, \quad (2.43)$$

as well as an expression for an expectation value,  $\langle f \rangle$ , for the same system as,

$$\langle f \rangle = \frac{\int_0^\infty f(E) e^{-\beta E} g(E) dE}{\int_0^\infty e^{-\beta E} g(E) dE}. \quad (2.44)$$

This derivation for the expectation value of a system is quite broadly applicable. In fact, it can be applied to both systems for which quantum effects are important, as well as for those that may be treated classically(16).

We are very nearly to the point where we may begin discussing the computation of these quantities using various integration methods, such as quantum and hybrid Monte Carlo techniques, but first we must take to canonical ensemble one step further, to the *grand canonical ensemble*. This is because the canonical ensembles limited capabilities becomes evident very quickly once you begin to look at broader, more general systems (16).

## Section 2.4: The Grand Canonical Ensemble

As mentioned, the limited usefulness of the canonical ensemble becomes quite clear as you begin to study broadly applicable systems. The need for a more generalized approach becomes necessary. This generalization comes from the idea that the energy *and* the particle number are essentially never directly fixed, but are observed quantities (i.e. outputs) instead. We may therefore consider both  $E$  and  $N$  as variables in our system.

In order to formulate the generalization, one can begin in a similar way to that of the canonical ensemble, that is by examining a system in equilibrium, and considering the system with any particle number. This, in fact, results in a summation over all particle numbers to obtain the grand canonical partition function,  $\mathcal{Z}$ ,

$$\mathcal{Z}(T, V, \mu) = \sum_{N=0}^{\infty} \frac{1}{N! h^{3N}} \int e^{-\beta(H(\omega) - \mu N)} d\omega. \quad (2.45)$$

Notice first that we have picked up an extra term in the exponent. This allows us to consider  $\mu$ , the chemical potential, for a given particle number. The expression may be reduced further by observing that  $\mu$

and  $N$  have no dependence on the phase space, so let's bring this factor outside of the integral by defining  $z = \exp(\beta\mu)$ , which is the fugacity of our system. Equation [2.45] then becomes,

$$\mathcal{Z}(T, V, z) = \sum_{N=0}^{\infty} \frac{1}{N!h^{3N}} \int z^N e^{-\beta H(\omega)} d\omega. \quad (2.46)$$

Now secondly notice that the expression inside of the integral looks exactly like our definition for the canonical partition function, which allows us to reduce even further,

$$\mathcal{Z}(T, V, z) = \sum_{N=0}^{\infty} z^N Q_N. \quad (2.47)$$

This is a very important definition that I will ask you to please keep stored away for future discussion, thank you.

The relationship between the grand canonical partition function to thermodynamics is not direct. We must first get at what we call the *grand potential*,  $\Omega$ , which relates to  $\mathcal{Z}$  as follows,

$$\mathcal{Z} = e^{-\beta\Omega} \rightarrow \beta\Omega = -\ln \mathcal{Z} = -\beta PV. \quad (2.48)$$

Therefore,

$$P(z, V, T) \equiv \frac{\beta}{V} \ln \mathcal{Z}(z, V, T) \quad (2.49)$$

We now have access to *exact* thermodynamic quantities in systems with an arbitrary particle number, a much more broadly applicable representation (16). Now lastly, before we begin our discussion of integration methods, let us examine the formulation using quantum statistics.

#### 2.4.1: Quantum Statistics Derivation of the Grand Canonical Ensemble

The previous sections involved general forms that allowed us to examine both classical and quantum systems consisting of *distinguishable* particles. Most physical quantum systems, however, involve *indistinguishable* particles such as bosons and fermions. This is an extremely important distinction to make. We therefore must write our above derivations in a form that allows for a more natural quantum mechanical definition. That is, we will rewrite in terms of *operators and wave functions*. So from here on out we take quantities such as the hamiltonian to the operator form,  $H \rightarrow \hat{H}$  (16).

To reiterate, the main point of the grand canonical ensemble is that the total particle number and total energy of the system are not necessarily constants. It is therefore important to work in a space that allows

for the fluctuation of both these quantities. We will thus introduce a quantum formalism that allows for exactly this, second quantization.

## Second Quantization

In order to work in a system where particle number is not fixed, we choose to work in a vector space comprised of the vacuum state,  $|0\rangle$ , all possible single particle states,  $\{|\alpha\rangle\}$ , all two particle states,  $\{|\alpha_1\alpha_2\rangle\}$ , all three particle states, and so on until we reach an infinite particle state. This set of all possible states of any particle number is known as the *Fock space*. We may represent the Fock space in terms of single particle quantum numbers as,

$$\sum_{N=0}^{\infty} \sum_{\alpha_1 \cdots \alpha_N} |\alpha_1\alpha_2 \cdots \alpha_N\rangle \langle \alpha_1\alpha_2 \cdots \alpha_N| = 1 \quad (2.50)$$

By definition, states of different particle number are orthogonal. The question then is, how do we transition from a state of one particle number to another? For fermions, we do this with the use of creation and annihilation operators, defined as follows,

$$a_{\alpha}^{\dagger} |\alpha_1\alpha_2 \cdots \alpha_N\rangle = |\alpha_{\alpha}\alpha_1\alpha_2 \cdots \alpha_N\rangle, \quad (2.51)$$

$$a_{\alpha} |\alpha_1\alpha_2 \cdots \alpha_{\alpha} \cdots \alpha_N\rangle = |\alpha_1\alpha_2 \cdots \alpha_N\rangle. \quad (2.52)$$

Where  $a_{\alpha}$  and  $a_{\alpha}^{\dagger}$  are the adjoint to each other such that  $(a_{\alpha}^{\dagger})^{\dagger} = a_{\alpha}$ . The creation and annihilation operators add and subtract fermions from the current  $N$  particle state respectively.  $a_{\alpha}^{\dagger}$ , the creation operator, adds a particle with the quantum number  $\alpha$  to the existing set of  $N$  single particle states, taking  $N \rightarrow N + 1$ . Since we are dealing with fermions, however, if the quantum state corresponding to  $\alpha$  is already occupied, then the result is zero due to Pauli exclusion. Furthermore, notice that applying these operators may affect the ordering of the states. Reordering them may introduce a minus sign, since fermions are antisymmetric when switching particles. Similarly,  $a_{\alpha}$ , the annihilation operator takes  $N \rightarrow N - 1$ , and, when acting on the vacuum state or a state where the quantum state corresponding to  $\alpha$  is unoccupied, the result is zero (17).

One extremely important feature to note of these operators is that of their anti-commutation relation,

$$\{a_\alpha, a_\beta^\dagger\} = a_\alpha a_\beta^\dagger + a_\beta^\dagger a_\alpha = \delta_{\alpha,\beta}, \quad (2.53)$$

$$\{a_\alpha, a_\beta\} = \{a_\alpha^\dagger, a_\beta^\dagger\} = 0. \quad (2.54)$$

These relationships can easily be shown given the properties previously discussed.

Now that we have developed the formalism for creation and annihilation operators, we can create anti-symmetric  $N$ -particle states in a straightforward manor. That is, we can apply the creation operator to the vacuum state,

$$\begin{aligned} |\alpha_1 \alpha_2 \alpha_3 \cdots \alpha_N\rangle &= a_{\alpha_1}^\dagger |\alpha_2 \alpha_3 \cdots \alpha_N\rangle = a_{\alpha_1}^\dagger a_{\alpha_2}^\dagger |\alpha_3 \cdots \alpha_N\rangle \cdots \\ &= a_{\alpha_1}^\dagger a_{\alpha_2}^\dagger \cdots a_{\alpha_N}^\dagger |0\rangle = \prod_i a_{\alpha_i}^\dagger |0\rangle. \end{aligned} \quad (2.55)$$

Equation 2.55 allows us to create ANY vector in the Fock space of  $N$ -particle fermion systems, and what's more, by definition this formulation adheres to the Pauli exclusion principal by the properties of the creation and annihilation operators (17).

A very similar formulation can be done for bosons as well, but without the need to enforce the Pauli principal. We mainly focus on fermions, however, so if one would like to get a better understanding of this formulation see such references as (16; 17).

To this point we have discussed how to develop the Fock space of quantum states using second quantization, but what about the other operators used to develop the various theories in the various systems that these particles are occupying? Let us now discuss the other operators that may be developed using second quantization.

There are two main types of operators that we focus on in this work. Those are one, and two-body operators. There are, of course, three, four, and five-body operators, but in this work we are largely using two-body interactions. Examples of one-body operators are the density operator  $\hat{n}$ , the particle number operator  $\hat{N}$ , and the kinetic energy operator  $\hat{T}$ . The density operator, which determines if the state corresponding to  $\alpha$  is occupied, is defined as,

$$\hat{n}(\alpha) = a_\alpha^\dagger a_\alpha, \quad (2.56)$$

such that,

$$\hat{n}(\alpha)|\alpha_1\alpha_2\cdots\alpha_N\rangle = a_\alpha^\dagger a_\alpha|\alpha_1\alpha_2\cdots\alpha_N\rangle \quad (2.57)$$

$$= \begin{cases} |\alpha_\alpha\alpha_1\alpha_2\cdots\alpha_N\rangle & \text{if } \alpha \text{ is occupied.} \\ 0 & \text{if } \alpha \text{ is not occupied.} \end{cases} \quad (2.58)$$

This is rather straightforward to see because  $a_\alpha$  acting on the given state vector will only return a vector if  $\alpha$  contains a particle, it returns zero otherwise.  $a_\alpha^\dagger$  will then repopulate  $\alpha$  with a particle, returning the original state possibly unordered.

We can now use the density operator to create another important one-body operator, the particle number operator,  $\hat{N}$ . Again, this is a straightforward definition based on the properties of  $a_\alpha^\dagger$  and  $a_\alpha$ ,

$$\hat{N} = \sum_\alpha \hat{n}(\alpha) = \sum_\alpha a_\alpha^\dagger a_\alpha, \quad (2.59)$$

such that,

$$\hat{N}|\alpha_1\alpha_2\cdots\alpha_N\rangle = \sum_\alpha a_\alpha^\dagger a_\alpha|\alpha_1\alpha_2\cdots\alpha_N\rangle = N|\alpha_1\alpha_2\cdots\alpha_N\rangle. \quad (2.60)$$

Once again, it is easy to see that this is true given the properties of the density operator above (17).

We have given a fairly plain definition of these operators, that is the only distinguisher between them is the quantum number  $\alpha$ . This is extremely limiting as we will be dealing with particles of multiple quantum numbers (like *alpha*, as well as spin, among others), as well as points in space-time. The use of second quantization, however, allows for this designation to be made quite easily,

$$a_\alpha \rightarrow a_\alpha^s(\mathbf{x}, t). \quad (2.61)$$

This allows for a much more comprehensive theory to be developed, while at the same time maintaining all the properties that we have previously mentioned.

Two-body operators, on the other hand, usual designate some sort of interaction. So before we move on, let's discuss a common interaction term that will be used in this work, the contact interaction. The contact interaction operator can be easily defined using the one-body operators above. For fermions interacting via the contact interaction, only interact if two fermions of different species occupy the same point in space-time. It therefore makes sense to use the density operator for varying species together to designate this operator. We may therefore define a two-body fermion (spin 1/2) contact interaction as,

$$\hat{V}_{contact} = \hat{n}_\alpha^\dagger(\mathbf{x}, t)\hat{n}_\beta^\dagger(\mathbf{x}', t'). \quad (2.62)$$

This makes sense because this will only return some non-zero when two particles of different flavor occupy the same quantum state at the same point in space-time. This is to say,

$$\hat{V}_{contact}|\Phi\rangle = \hat{n}_\alpha^\dagger(\mathbf{x}, t)\hat{n}_\beta^\dagger(\mathbf{x}', t')|\Phi\rangle \quad (2.63)$$

$$= \delta_{\alpha\beta}\delta(\mathbf{x} - \mathbf{x}')\delta(t - t'). \quad (2.64)$$

This type of interaction is very common in our work because, again, we are deal with ultracold atomic gases, which are extremely dilute systems dominated by short-range interaction. Short-range interactions are very well duplicated by contact interactions in this theory.

We are now at a point where we can officially develop the formalism for the grand-canonical partition function in the quantum realm using second quantization.

## Grand Canonical Ensemble in the Quantum Realm

Using the above development of second quantization, we can create the density operator of our entire system,  $\hat{\rho}$ , as,

$$\rho_{mn}(t) = \frac{1}{\mathcal{N}} \sum_{k=1}^{\mathcal{N}} \{a_m^k(t)a_n^{k*}(t)\}. \quad (2.65)$$

Such that  $\mathcal{N}$  is the total number of identical systems, and  $a_m^k(t)$  and  $a_n^{k*}(t)$  are creation and annihilation operators respectively. Note that the diagonal elements of this matrix,  $\rho_{nn}$ , represent the probability that a given system, at time  $t$ , is in the state  $\phi_n$ . Where  $\phi_n$  is a solution to the Schrodinger equation. So therefore we may assume,

$$\sum_n \rho_{nn} = 1 \text{ or } \text{tr } \rho = 1 \quad (2.66)$$

We may now define an expectation value in this system as,

$$\langle f \rangle = \frac{\text{tr}(\hat{\rho}f)}{\text{tr}(\hat{\rho})} \quad (2.67)$$

This looks very similar to our definition of the density of states above, and in fact can again be related

to the Hamiltonian as follows,

$$\begin{aligned}
\hat{\rho} &= \sum_n |\phi_n\rangle \frac{1}{\mathcal{Q}_N(\beta)} e^{-\beta E_n} \langle \phi_n| \\
&= \frac{1}{\mathcal{Q}_N(\beta)} e^{-\beta \hat{H}} \sum_n |\phi_n\rangle \langle \phi_n| \\
&= \frac{1}{\mathcal{Q}_N(\beta)} e^{-\beta \hat{H}} = \frac{e^{-\beta \hat{H}}}{\text{tr}(e^{-\beta \hat{H}})}
\end{aligned} \tag{2.68}$$

This looks very similar to that of the canonical density represented in the previous sections. That is because this coincides directly with the quantum canonical ensemble. In order to take things to the grand canonical ensemble, we again have to take into account the particle number and chemical potential,  $\mu$ , in the form of the fugacity,  $z$  (16; 17).

To be more clear, in the grand canonical ensemble the density operator  $\rho$  works on the *Hilbert space* of the system and has an undetermined number of particles. The density operator must therefore consider not only the Hamiltonian, but also the particle number operator,  $\hat{N}$ . We then define our density operator as,

$$\hat{\rho} = \frac{1}{\mathcal{Z}(\mu, V, T)} e^{-\beta(\hat{H} - \mu \hat{N})}, \tag{2.69}$$

such that

$$\mathcal{Z}(\mu, V, T) = \sum_{r,s} e^{\beta(E_r - \mu N_s)} = \text{tr} \left( e^{-\beta(\hat{H} - \mu \hat{N})} \right) = \sum_{N=0}^{\infty} z^N \mathcal{Q}_N \tag{2.70}$$

is of course the grand canonical partition function (16; 17).

To this point we have derived expressions for the canonical and grand canonical ensembles for classical and quantum systems, as well as for distinguishable and indistinguishable particles. Although these forms are easy to write and derive in theory, they can be *extremely* difficult to compute in practice when applied to physical systems. In particular the most applicable case, the one most previously mentioned (a quantum system of indistinguishable particles), is impossible to carry out exactly. So we need a method that can compute these values in an approximate, computational manor. That is, we would like to apply Monte Carlo methods, which will be discussed in the proceeding chapter, to our system. This requires us to put the indistinguishable particle form of  $\mathcal{Z}$  into an integrable form. In order to do this we require the use of field theory, and the path integral formulation of  $\mathcal{Z}$  (16). Before we discuss these ideas let's again return to the ideal gas to obtain a better understanding of quantum statistics as applied to an applicable system.

## 2.4.2: The Quantum Ideal Gas

As discussed in section 2.2.1, when examining a system of classical, non-interacting particles, the thermodynamics can be determined by considering the total number of ways in which  $N$  particles may arrange themselves in a system of volume,  $V$ , and fixed total energy,  $E$ . That is we can determine the thermodynamics by calculating the total number of microstates. The classical prescription, however, is quite limited when considering naturally occurring systems because the classical nature of particles breaks down in many instances, such as in low temperature and high density systems. This is due to the fact the the thermal wavelength of a given particle,  $\lambda_T$ , in these regimes becomes comparable to the intra-particle spacing (i.e. classical application only applies when the following inequality holds,  $\lambda_T \ll (V/N)^{1/3}$ , in 3D).

We mentioned in the introduction that this work mainly focuses on ultracold atomic gases, which is in fact very low temperature, meaning that a quantum prescription is needed. So let us again consider a system of volume  $V$ , and energy  $E$ , and again attempt to calculate the quantity  $\Omega(N, V, E)$ .

Let us begin using equation 2.70:

$$\mathcal{Z}(\mu, V, T) = \sum_{r,s} e^{\beta(E_r - \mu N_s)} = \text{tr} \left( e^{-\beta(\hat{H} - \mu \hat{N})} \right) = \sum_{N=0}^{\infty} z^N Q_N$$

As mentioned, however, this equation is essentially impossible to compute directly for indistinguishable particles. The expression in terms of the  $Q_N$  on the other hand may be calculated. So if we wish to compute  $\mathcal{Z}$  and therefore  $\Omega$  exactly, then we are tasked with calculating  $Q_N$  for all  $N$ .

Recalling equation 2.39,

$$Q_N(V, T) = \sum_r \exp(-\beta E_r),$$

such that  $r$  sums over all the possible energy eigenvalues of the  $N$  particle system,  $E_r$ , which may in fact be written in terms of the single particle energy eigenvalues found from the single particle Schrödinger equation of the system,  $\epsilon$ , such that

$$E_r = \sum_{\epsilon} n_{\epsilon} \epsilon. \tag{2.71}$$

Here,  $n_{\epsilon}$  denotes the degeneracy, the total number of particles occupying the single particle energy states, where  $\sum_{\epsilon} n_{\epsilon} = N$ . This allows us to rewrite equation 2.39 in terms of the density of states,  $g\{n_{\epsilon}\}$ ,

$$Q_N(V, T) = \sum_{\{n_{\epsilon}\}} g\{n_{\epsilon}\} e^{-\beta \sum_{\epsilon} n_{\epsilon} \epsilon}. \tag{2.72}$$

Here is where the quantum statistics truly comes into play. The sum is carried out over all possible distributions of  $N$  particles and possible energies of the system that follow the allowed occupation number for each quantum state as governed by the density of states. The allowed occupation numbers for each state are defined by various quantum particle statistics, namely *Bose-Einstein* statistics for bosons and *Fermi-Dirac* statistics for fermions which are the two types of particles that we generally see in nature. These statistics are,

$$g_b\{n_\epsilon\} = 1, \quad (2.73)$$

$$g_f\{n_\epsilon\} = \begin{cases} 1 & \text{if all } n_\epsilon = 0 \text{ or } 1 \\ 0 & \text{otherwise.} \end{cases} \quad (2.74)$$

What this means is that for Bose-Einstein statistics,  $g_b$ , all distributions are possible and any number of particles can occupy the same quantum state. Whereas for Fermi-Dirac statistics,  $g_f$ , only one particle is allowed per quantum state and therefore only distributions that follow this rule are allowed ( $g_f = 0$  for any distribution where  $\exists n_\epsilon$  such that  $n_\epsilon > 1$ ). Now to carry out the calculation of  $Q_N$  we consider the expressions for  $g_f$  and  $g_b$  into equation 2.72, and attempt to carry out the sum. This gives,

$$Q_N(V, T) = \sum_{\{n_\epsilon\}} e^{-\beta \sum_\epsilon n_\epsilon \epsilon}, \quad (2.75)$$

only inserting a 1 for bosons, and restricting the sum over  $\{n_\epsilon\}$  for fermions. The problem with this expression here is that we would be summing over all possible distributions of  $N$  particles for all possible energy levels of the given system, which is extremely difficult. Let us instead insert this expression into equation 2.71, for the  $\mathcal{Z}$ ,

$$\mathcal{Z}(z, V, T) = \sum_{N=0}^{\infty} \left[ z^N \sum_{n_\epsilon} e^{-\beta \sum_\epsilon n_\epsilon \epsilon} \right] \quad (2.76)$$

$$= \sum_{N=0}^{\infty} \left[ \sum_{n_\epsilon} \prod_{\epsilon} (z e^{-\beta \epsilon})^{n_\epsilon} \right]. \quad (2.77)$$

Notice now the sum over both  $N$  and  $\{n_\epsilon\}$  may be reduced. Considering that the sum over  $\{n_\epsilon\}$  is constrained by the sum over  $N$ , which is in turn summed to infinity (or). This allows us to rewrite the above expression as a product of summations over all possible values for each  $n_\epsilon$ ,

$$\mathcal{Z}(z, V, T) = \sum_{n_0, n_1, \dots} [(ze^{-\beta\epsilon_0})^{n_0} (ze^{-\beta\epsilon_1})^{n_1} \dots] \quad (2.78)$$

$$= \prod_{\epsilon} [(ze^{-\beta\epsilon})^{n_{\epsilon}}]. \quad (2.79)$$

Now this is something we can deal with! For bosons we sum each  $n_{\epsilon}$  from 0 to  $\infty$ , for fermions we need only sum over 0 to 1. We now the solutions to both of these summations,

$$\mathcal{Z} = \begin{cases} \prod_{\epsilon} \frac{1}{(1 - ze^{-\beta\epsilon})} & \text{for bosons} \\ \prod_{\epsilon} (1 + ze^{-\beta\epsilon}) & \text{for fermions.} \end{cases} \quad (2.80)$$

This, in turn would make the grand potential,  $\Omega$ ,

$$\Omega \equiv \ln \mathcal{Z} = \mp \sum_{\epsilon} \ln(1 \mp e^{-\beta\epsilon}). \quad (2.81)$$

This is a reasonable expression that can be easily handled. Given that we are dealing with a non-interacting gas, then we can sum over all possible kinetic energy states given by  $\frac{\hbar^2 k^2}{2m}$ , where we sum over all  $k$ . This sum can be easily carried out, and thermodynamic quantities can be easily computed by taking derivatives of  $\Omega$ .

Now that we have a firm understanding of the various ensembles as applied to quantum statistics, let us take the next step in the development of these theories. We have repeatedly mentioned that to actually make computations in meaningful systems then we need to be able to apply statistical integration techniques. This requires us to put these expressions into an integrable form. We will now discuss this topic.

### 2.4.3: Path Integral Representation of $\mathcal{Z}$

The idea of a path integral in quantum mechanics comes from the time evolution operator in quantum mechanics,  $U(x_a, x_b, t)$ , given by,

$$U(x_a, x_b, t) = \langle x_a | e^{-i\hat{H}t/\hbar} | x_b \rangle. \quad (2.82)$$

This allows us to calculate the probability that a particle will transition from state  $x_a$  to  $x_b$ , i.e. the probability that the particle will follow the path from  $x_a$  to  $x_b$  in a time,  $t$ . Adjusting this to path integral formalism, however, is quite different. In order to compute this quantity using the ideas of paths, we would have to consider all possible paths between points  $x_a$  and  $x_b$ ,

$$U(x_a, x_b, t) = \sum_{\text{all paths}} e^{i(\text{phase})} = \int \mathcal{D}x(t) e^{i(\text{phase})}, \quad (2.83)$$

where  $\int \mathcal{D}x(t)$  is a way two write "sum over all paths", or, say, integrate over all paths. A path integral! But what is this phase that we have mentioned? When considering the classical limit, there is only one idea of a path, and that is a path ( $x_c$ ) that follows the following condition,

$$\frac{\partial}{\partial x(t)} (S[x(t)])|_{cl} = 0, \quad (2.84)$$

where the action  $S$  is the time integral of the systems Lagrangian,  $S = \int \mathcal{L}dt$ . It would therefore make sense that the quantum realm would hold a similar parallel, and this is true up to a constant, that is as long as  $S \gg \hbar$ . We may therefore write the propagation probability as

$$U(x_a, x_b, t) = \langle x_a | e^{-i\hat{H}t/\hbar} | x_b \rangle = \int \mathcal{D}x(t) e^{iS[x(t)]/\hbar}. \quad (2.85)$$

The above was a discussion on how to formulate the time evolution operator (18), but a similar development can be used to show that this applies to the grand canonical ensemble as well. We can rewrite the trace formalism for the grand canonical partition function as,

$$\mathcal{Z} = \text{tr} \left( e^{-\beta(\hat{H} - \mu\hat{N})} \right) = \int \mathcal{D}x(t) e^{-\beta S(x)}, \quad (2.86)$$

where again  $S$  is the *action*, defined over the path  $x(t)$  of the Legrangian,  $\mathcal{L}$ , such that  $t \in \{t_i, t_f\}$ ,

$$S(x) = \int_{t_i}^{t_f} \mathcal{L}(x(t)) dt. \quad (2.87)$$

We are now, officially, at a point in our derivation of thermodynamics and statistical mechanics that we may attempt to calculate the macroscopic behavior of many physical systems. In many cases, however, these derivations run into serious difficulties that make these calculations extremely difficult, if not impossible to carry out analytically. It is for this reason that we must turn to computational approaches, such as quantum Monte Carlo. In the above path integral, this is needed due to the fact that we can cover all possible paths  $x(t)$  by implementing a random walk over the possible locations  $x$  at each given time  $t$ . For quantum many-body physics, however, a different formulation of the problem is required, which we discuss in the next chapter.

## CHAPTER 3: Lattice Monte Carlo Methods

In this chapter we discuss the details of the lattice Monte Carlo method which will be the main tool for the remainder of this thesis. The main components of the method are the Trotter-Suzuki factorization and the Hubbard-Stratonovich transformation, which are then combined to obtain a field-integral representation of the grand-canonical partition function. The calculation of such a field integral, however, requires sophisticated computational approaches. Here we discussed two such approaches (which are used in later chapters), namely: hybrid Monte Carlo and complex Langevin. The latter is in fact needed as some of the situations discussed in this thesis suffer from the so-called sign problem; we discuss the latter in this chapter as well.

### Section 3.1: Lattice Monte Carlo Method

As mentioned above, for the vast majority of physically interesting systems we cannot compute  $\mathcal{Z}$  or any useful observables through direct integration. In fact, beyond the ideal quantum gas (discussed above), the 1D Ising model, and the quantum harmonic oscillator we have very few exact solutions. We must therefore apply approximations like *perturbation theory* and *the virial expansion*, as well as statistical integration methods and various other numerical techniques in order to study and perform computation in the physically interesting systems. There are plenty of numerical methods that one may utilize, i.e. Green's function Monte Carlo, no-core shell-model, coupled cluster, density functional theory, the list goes on. Not all are created equal, however, as some may be more efficient, precise, or accurate than the others. We will focus on one numerical method in particular, lattice Monte Carlo methods.

The idea behind lattice Monte Carlo is that, one, computing on the continuum is, well, really freaking hard, and two, we need to be able to put these computations on a computer. Computers require discrete, defined steps in order to run, which is why we first discretize *space-time* so that it contains a finite number of degrees of freedom. This of course brings us away from a perfect understanding of continuous space-time, but computing in that regime was the trouble in the first place. Besides, one can increase their lattice to a point such that the continuum limit is achieved ( $N_\tau, N_x \rightarrow \infty$ ). Where here  $N_\tau$  and  $N_x$  are the number of time and space lattice points respectively. More specifically we want to get to a point where the thermal wavelength,  $\lambda_T = \sqrt{2\pi\beta}$ , is much smaller than the width of our lattice,  $1 \ll \lambda_T \ll N_x$ .

Remember that our goal in this is to compute observables,

$$\langle \hat{O} \rangle = \text{tr} [\hat{\rho} \hat{O}] = \frac{\text{tr} [e^{-\beta(\hat{H} - \mu \hat{N})} \hat{O}]}{\text{tr} [e^{-\beta(\hat{H} - \mu \hat{N})}]} \quad (3.1)$$

We can also think about this another way, by inserting a source.

$$\mathcal{Z} \rightarrow \mathcal{Z}[j(x)] = \text{tr} [e^{-\beta(\hat{H} - \mu \hat{N} - X[j(x)])}] \quad (3.2)$$

$$X[j(x)] = \int d^d x j(x) \hat{O}(x) \quad (3.3)$$

We can then write our expectation value as,

$$\langle \hat{O} \rangle = \frac{1}{\beta} \left. \frac{\delta \ln \mathcal{Z}[j(x)]}{\delta j(x)} \right|_{j \rightarrow 0} \quad (3.4)$$

Great, we have the formulation that we so painstakingly derived in the previous chapters. Now the question or problem is, how do we discretize this formalism? Given that  $\hat{H} = \hat{T} + \hat{V}$ , and

$$[\hat{H}, \hat{N}] = 0, \quad (3.5)$$

$$[\hat{T}, \hat{V}] \neq 0. \quad (3.6)$$

For the non-interacting case,  $\hat{V} \rightarrow 0$ , the Hamiltonian is trivial and diagonal in all N-particle subspaces. For an interacting system, however, each N must be diagonalized individually. So the dimension of the problem grows exponentially(19). We have to consider other ways of tackling this problem.

Given the commutators above, and taking a look at our equation for the expectation value for  $\hat{O}$ , eq.[3.1], we may notice that the meat of the problem lies in the exponential of the Hamiltonian. This is where the physics of our problem comes from. This is the portion of our formulation that we should focus our attention. Another way of putting this is that our focus should be on the *transfer matrix*,

$$\mathcal{T}_t = e^{-t\hat{H}}. \quad (3.7)$$

Again, all of our physics, and underlying problems are within this operator. Which immediately poses a bit of a challenge, how do we handle  $\exp(-\beta\hat{H})$ ? In order to tackle this problem we utilize *imaginary time*, and the *Trotter-Suzuki factorization* (TSF).

### 3.1.1: Trotter-Suzuki Factorization

We wish to discretize time into a number of  $N_\tau$  discrete points as follows,

$$e^{-\beta\hat{H}} = \left[ e^{-\tau\hat{H}} \right]^{N_\tau} = \mathcal{T}_t^{N_\tau}. \quad (3.8)$$

Such that  $\beta = \tau N_\tau$ . The TSF then says that we can factorize this further (20). The simplest approximation one can make would be

$$e^{-\tau\hat{H}} \simeq e^{-\tau\hat{T}} e^{-\tau\hat{V}} \quad (3.9)$$

But the right-hand side is not a *hermitian* operator, unlike the left-hand side. We then turn to a symmetric factorization, namely

$$e^{-\tau\hat{H}} \simeq e^{-\tau\hat{T}/2} e^{-\tau\hat{V}} e^{-\tau\hat{T}/2}. \quad (3.10)$$

This is now a hermitian operator that may be handled using quantum dynamics and the techniques detailed above (20). This, however, is still an extremely difficult problem to tackle as is. The potential energy factor of being where the difficulties lie. Removing this factor would obviously take us back to the non-interacting case, a trivial problem. The way to tackle a fully interacting case brings us to the *Hubbard-Stratonovich transformation*.

### 3.1.2: The Hubbard-Stratonovich Transformation

We have successfully put our expression for the transfer matrix into a more handleable form using the TSF, but now must find some way of handling the potential energy term specifically. Let's take a look at this problem using a specific example. For the majority of the work that we have done throughout this dissertation, we use a *zero-range interaction*. That is to say that two particles only interact if they occupy the same point in space-time. For spin 1/2 particles, this can be characterized as,

$$\hat{V} = -g \sum_j \hat{n}_{\uparrow,j} \hat{n}_{\downarrow,j}, \quad (3.11)$$

where  $\hat{n}_{s,j} = \psi_{s,j}^\dagger \psi_{s,j}$  is the density operator, and  $g$  the bare coupling that denotes the strength of the interaction. Then for each point in space-time we can expand the exponential to simplify the problem,

$$\begin{aligned}
e^{\tau g \hat{n}_{\uparrow,j} \hat{n}_{\downarrow,j}} &= 1 + C \hat{n}_{\uparrow,j} \hat{n}_{\downarrow,j} \\
&= \frac{1}{2} \sum_{\sigma=\pm 1} (1 + \sqrt{C} \hat{n}_{\uparrow,j} \sigma) (1 + \sqrt{C} \hat{n}_{\downarrow,j} \sigma).
\end{aligned} \tag{3.12}$$

With this we have taken an extremely difficult problem, and turned it into a manageable one, by decoupling the interaction (19).

There are several other ways of handling this transform as well, they are listed below (19),

$$\begin{aligned}
e^{\tau g \hat{n}_{\uparrow,j} \hat{n}_{\downarrow,j}} &= \frac{1}{2} \sum_{\sigma=\pm 1} (1 + \sqrt{C} \hat{n}_{\uparrow,j} \sigma) (1 + \sqrt{C} \hat{n}_{\downarrow,j} \sigma) \\
e^{\tau g \hat{n}_{\uparrow,j} \hat{n}_{\downarrow,j}} &= \frac{1}{2\pi} \int_{-\pi}^{\pi} d\sigma (1 + \sqrt{C} \hat{n}_{\uparrow,j} \sin \sigma) (1 + \sqrt{C} \hat{n}_{\downarrow,j} \sin \sigma) \\
e^{\tau g \hat{n}_{\uparrow,j} \hat{n}_{\downarrow,j}} &= \frac{1}{\sqrt{2\pi}} \int_{-\infty}^{\infty} d\sigma e^{-\sigma^2/2} e^{-\sigma \sqrt{C} (\hat{n}_{\uparrow,j} + \hat{n}_{\downarrow,j})}
\end{aligned}$$

### 3.1.3: Assembling the field integral representation

Taking both the TSF and the HST and applying them to equation [2.86] for the trace form of  $\mathcal{Z}$ , again using point-like interaction for spin 1/2 particles, we have

$$\begin{aligned}
\mathcal{Z} &\equiv \text{tr} \left[ e^{-\beta(\hat{H} - \mu \hat{N})} \right] \\
\mathcal{Z} &= \text{tr} \left[ \int \prod_i d\sigma_i \mathcal{T}[\sigma] \right] = \int \mathcal{D}\sigma \text{tr} \mathcal{T}[\sigma].
\end{aligned} \tag{3.13}$$

Where we define the following as,

$$\mathcal{D}\sigma \equiv \prod_i d\sigma_i \tag{3.14}$$

$$\mathcal{T}[\sigma] = \mathcal{T}_{\uparrow}[\sigma] \mathcal{T}_{\downarrow}[\sigma] \tag{3.15}$$

$$\mathcal{T}_s[\sigma] = U_1 U_2 U_3 \cdots U_{N_\tau} \tag{3.16}$$

$$U_t = e^{-\tau \hat{T}/2} \prod_j (1 + \sqrt{C} \hat{n}_{s,j} \sigma_{j,t}) e^{-\tau \hat{T}/2} \tag{3.17}$$

$\sigma$  being the auxiliary field that exists in all of space-time, and  $\mathcal{D}\sigma$  representing the path integral over all

possible paths for  $\sigma$ . Great! Now notice that we only must deal with one-body operators, so we can actually take the trace giving (19),

$$\text{tr } \mathcal{T}[\sigma] = \det M_{\uparrow} M_{\downarrow} \quad (3.18)$$

### 3.1.4: Doing the Integral with Monte Carlo Methods

For reference, let us go back to the expression for the expectation value of a given operator in terms of a path integral over the auxiliary field  $\sigma$ , eq. 3.4,

$$\langle \hat{O} \rangle = \frac{\delta \ln \mathcal{Z}[j]}{\delta j} \Big|_{j \rightarrow 0} = \frac{1}{\mathcal{Z}} \frac{\delta \mathcal{Z}[j]}{\delta j} \Big|_{j \rightarrow 0} = \frac{1}{\mathcal{Z}} \int \mathcal{D}\sigma \mathcal{P}[\sigma] \hat{O}[\sigma]. \quad (3.19)$$

Now, Monte Carlo integration is a stochastic method, i.e. it relies on random number generation in order to estimate a given quantity. Often this is done with true random number generation, for instance one can compute the value of pi,  $\pi$ , by generating two random  $x$  and  $y$  coordinates within a square and determining whether that set of coordinates lie within a circle of diameter equal to the side length of said square. Unfortunately, such an approach is not viable for the type of problems that appear in quantum many-body physics. Instead, we rely on the use of *Markov chains a probability measure* to guide this random number generation.

The above formalism allows us to sample our field,  $\sigma$ , in a region where the true expectation value of our operator, or *signal*, is likely to be. Leading to faster convergence to the “correct” value and more consistent results. Assigning a measure, however, is not as easy as it may seem. If the measure and the signal do not overlap in a significant way, then this method may result in largely inaccurate or even divergent results. This is a major issue that has plagued all fields of statistical computation since their inception, known as the *signal-to-noise problem* (19).

One may notice referring back to eq. [3.19], that  $\mathcal{P}[\sigma]$  would seem to be a good candidate for a probability measure. The question is, does it follow the rules of what a probability measure should be? That is, is it normalized and positive definite? This is where such problems as the signal-to-noise issue, and perhaps even more infamously the *sign problem* (a type of signal-to-noise problem, where the probability measure may diverge or become imaginary), which will be discussed in more detail shortly, arise. There are of course techniques and attempts to bypass these problems, we will discuss one such method that attempts to bypass the sign problem in detail in a subsequent section, but for example let us say we wanted to get around our measure possibly taking a negative value. That could be handled somewhat by adjusting the sign of the probability to the observable and taking the absolute value of our measure,

$$\mathcal{P}[\sigma]\hat{O}[\sigma] = |\mathcal{P}[\sigma]|[\text{sgn}(\mathcal{P}[\sigma])\hat{O}[\sigma]]. \quad (3.20)$$

We have thus shifted the the fluctuations in the measure to the observable, but have assured a positive definite probability. As for normalization, we can generally assume this true. By design we choose a measure that is normalized, but taking a look back at eq. [3.19] and eq. [3.13], we see that the definition of  $\mathcal{P}[\sigma]$ ,

$$\mathcal{P}[\sigma] \equiv \frac{\text{tr } \mathcal{T}[\sigma]}{\mathcal{Z}}, \quad (3.21)$$

is in fact already normalized by the normalization factor,  $N = \mathcal{Z}$ .

From here computing observables is a relatively straightforward process. Using various sampling techniques in regards to the *random walk*, and applying an accept/ reject step to move along our Markov chain, and hopefully begin to converge to the accepted expectation value of the given system. The accept/ reject step of the Markov chain usually comes in the form of the *Metropolis-Hastings*, or simply the *Metropolis algorithm*,

### 3.1.5: The Metropolis Algorithm

The Metropolis algorithm is main workhorse of Markov chain Monte Carlo methods, because one, it is both a simple and versatile algorithm, and two, it maintains ergodicity and is stationary relative to the probability distribution. That is to say, that the algorithm allows for the transition from one state to any other possible state, and that over a long period of time all possible states are equally likely to occur (ergodic hypothesis) (21). Needless to say, this is an hugely important part to all Monte Carlo techniques. The method is carried out as follows (22),

1. Start with some arbitrary initial configuration,  $\sigma_0$
2. Propose a new configuration,  $\sigma_1$
3. Accept or reject the new configuration using the probability,  $p = \min\{1, \mathcal{P}[\sigma_1]/\mathcal{P}[\sigma_0]\}$ 
  - If accepted,  $\sigma_1$  becomes the new configuration used
  - If rejected, continue using the previous configuration and test again with a new  $\sigma_2$

This transition preserved the stationary probability density,  $\rho(\sigma)$ , as long as the chain is ergodic. That is, again, as long as  $\sigma_i$  has the ability to transition to any possible point in the state space for the auxiliary field. The nature of this algorithm, however, does indeed assure this (21)!

Moving on, the running average then takes the form,

$$\langle \hat{O} \rangle = \frac{1}{N_\sigma} \sum_{\sigma} \hat{O}[\sigma], \quad (3.22)$$

and carries an uncertainty relative to the order,  $\mathcal{O}(1/\sqrt{N_\sigma})$ , and that should converge to the expected value over the given number of total samples,  $N_\tau$ . For instance, this convergence can be seen in fig. [??], which displays the running average for expected particle number of given systems of  $n_\uparrow + n_\downarrow$  particles, over Langevin time (similar to imaginary time, but will be discussed shortly).

The next logical question is, how do we propose a new configuration to the accept/ reject step?

In practice there are several ways of doing this. Namely these are,

1. Individually (one-by-one, random or ordered)
2. In clusters (spread out or compact)
3. Globally

Updating locally, i.e. individually or one-by-one, works in practice, but has terrible decorrelation properties. That is in the accept/ reject step, one may see a large number of rejections. Global updates, however, have excellent decorrelation. One should see acceptance at virtually all accept/ reject steps. That's great, but it is much more difficult to implement. This method of globally updating is known as *Hybrid Monte Carlo* (HMC).

### Section 3.2: Hybrid Monte Carlo

We want to be able to change our configuration,  $\sigma_i$ , as much as possible without obtaining some highly improbable configuration, while maintaining ergodicity. In order to do this we must introduce an auxiliary momentum,  $\pi$ , effectively transforming our n-dimensional phase space into a 2n-dimensional phase space. We then shift to the *canonical probability distribution*,

$$P[\sigma, \pi] = \frac{e^{-\mathcal{H}[\sigma, \pi]}}{\mathcal{Z}}. \quad (3.23)$$

Where  $\mathcal{Z}$  and  $\mathcal{H}$  are given by,

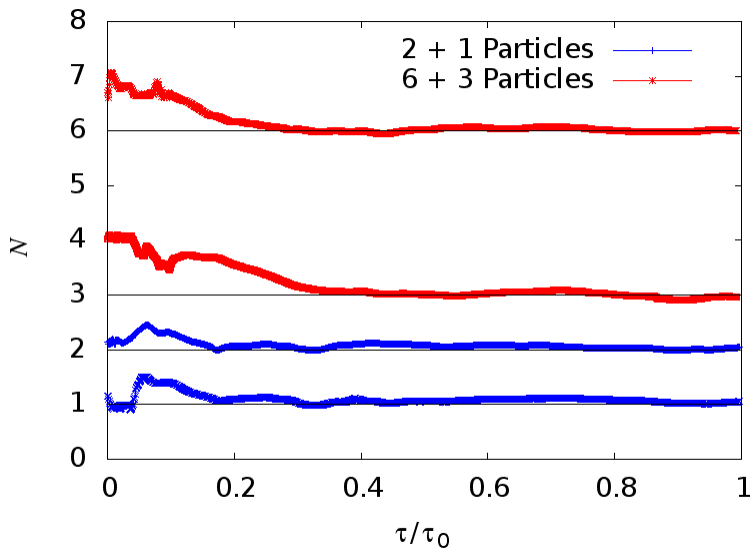


Figure 3.1: Running average over Langevin time,  $\tau$ , where  $\tau_0$  is the total number of Langevin time steps, of the total particle numbers,  $\langle \hat{n}_\uparrow \rangle$  and  $\langle \hat{n}_\downarrow \rangle$ . Separate runs are seen to converge to the expected particle number for the 2+1 case (blue) and the 6+3 case (red). The data corresponds to  $V = N_x^3$ ,  $N_x = 6$ ,  $\beta = 3.0$ , tuned to the unitary limit.

$$\mathcal{Z} = \int \mathcal{D}\sigma e^{-S_{eff}} \rightarrow \int \mathcal{D}\sigma \mathcal{D}\pi e^{-\mathcal{H}[\sigma, \pi]} \quad (3.24)$$

$$\mathcal{H}[\sigma, \pi] = \sum_{n, \tau} \pi_{n, \tau}^2 + S_{eff}[\sigma]. \quad (3.25)$$

We may then generate the desired vector field using *Hamilton's equations of motion*:

$$\dot{\sigma} = \frac{\delta \mathcal{H}}{\delta \pi} = \pi \quad (3.26)$$

$$\dot{\pi} = -\frac{\delta \mathcal{H}}{\delta \sigma} = F[\sigma, \phi]. \quad (3.27)$$

Notice that  $\pi$  is defined as a full derivative, so the physics of the problem remains unchanged as this addition does not affect the Hamiltonian. Also,  $\pi$  is defined as the gaussian momentum, so instead of randomly updating our field configuration, we are randomly updating the gaussian momentum. By doing so we are generating the gradient through the momentum instead of the field directly. We may then follow the vector field for some time,  $t$ , which will then produce trajectories that move quickly through phase space, while still maintaining ergodicity. This is largely due to the fact that that using Hamiltonian dynamics is a completely *reversible* process, which is to say that the mapping from one state at time  $t$ ,  $[\sigma(t), \pi(t)]$ , to a new state at time  $t + dt$ ,  $[\sigma(t + dt), \pi(t + dt)]$ , is one-to-one, and therefore has an inverse (23)! This also implies that these dynamics leaves the probability distribution invariant as well.

There are, in fact, several key factors that lead to this method being of great use in Monte Carlo algorithms. First was mentioned above, hamiltonian dynamics is a reversible process. Second, the process also conserves the Hamiltonian. This is important as the acceptance probability of the Metropolis step is one if the Hamiltonian is invariant! Third, Hamiltonian dynamics is also a *symplectic* process. In other words, total phase space volume is conserved, which again helps to ensure the extremely high acceptance rate of the Metropolis step (23).

To conclude, we are still utilizing the same Metropolis accept/ reject step as from QMC to ensure that we are moving in the correct direction and addressing the right problem. Furthermore, this is such a great method because we are using molecular dynamics to update our auxiliary field globally at all points, and furthermore energy and ergodicity is conserved, so the acceptance rate is extremely high, nearly 1 (19; 23).

Before we move on to our work, and the computations that we have carried out, we will discuss one of the most prominent issues in this field. The *sign problem*. We will also discuss a method that attempts to bypass the sign problem, giving us access to many physical systems that were previously out of reach.

### Section 3.3: The Sign Problem

The sign problem is actually a problem that can be described quite simply in a few lines, but the simply described problem has vast consequences when one attempts to perform calculations using probability distributions. This problem has been the root cause for many road blocks of computing in condensed matter physics, QCD and the like. It is because of this, in fact, that many physically interesting regimes have been completely unattainable (e.g. repulsive fermions). Likewise there have been a plethora of projects whose sole purpose has been to find a way to handle this exact problem, like the one we will discuss shortly, the Complex Langevin method.

So without further ado, what exactly is the sign problem? To answer this question let's examine eq. [3.20].

$$\mathcal{P}[\sigma]\hat{O}[\sigma] = |\mathcal{P}[\sigma]||\text{sgn}(\mathcal{P}[\sigma])\hat{O}[\sigma]|$$

We have briefly discussed the sign problem without directly mentioning it. That is, we asked the question, what happens if the measure is not positive definite? If the measure does carry some portion that is negative, then it cannot be considered a valid probability density. To handle this, we remove the overall sign of the measure, and carry it with the operator. The problem with this is that we have shifted the fluctuation in sign to the observable, which is good since we have assured a positive definite measure, but these fluctuations can be quite severe (19).

To examine this further, let's address an example regarding fermions. Considering the probability defined using the Grand Partition function, eq. [2.69]

$$\text{sgn}(\mathcal{P}[\sigma]) = \frac{\mathcal{P}[\sigma]}{|\mathcal{P}[\sigma]|} = \frac{e^{-\beta H[\sigma]}}{|e^{-\beta H[\sigma]}|} = \frac{e^{-\beta H[\sigma]}}{e^{-\beta H_B[\sigma]}} = e^{-\beta(H[\sigma]-H_B[\sigma])}. \quad (3.28)$$

Where  $H_B$  denotes the same type of Hamiltonian as  $H$  in the numerator (same kinetic, and interaction terms), but with the fermions replaced with Bosons. In the limit of low temperature ( $\beta \rightarrow \infty$ ) the average sign can become extremely small, meaning that the expectation of our observable,  $\langle O \rangle$ , is given by the ratio of two exponentially small numbers, determined stochastically. Furthermore, since the average sign is in fact the average of  $\pm 1$ , then the overall variance becomes quite large. Finally, when the error bars become proportional to the average sign, massive fluctuations in the computation of  $\langle O \rangle$  occur.

In this instance the sign problem was caused by fermion statistics, but in general this problem comes about in many scenarios for both QMC and HMC. For instance, in HMC, when the action becomes complex,  $S[\sigma, \pi] = S_R[\sigma, \pi] + iS_I[\sigma, \pi]$ , one immediately encounters a non-positive definite probability distribution,

and therefore a sign problem (19).

The next question would then be, how does one handle the sign problem? Sadly, the answer to that question is largely that one does not have a good handle on this problem. One would have to find some way of implementing a classical approximation, or avoid the problem all together. We have utilized a method, however, that attempts to handle the sign problem in regards to HMC. That is, it attempts to make use of the imaginary portion of the action directly. We will now discuss that method, *Complex Langevin*.

### 3.3.1: Complex Langevin Method

The idea of stochastic quantization is that a random process that obeys the Langevin equation,

$$\frac{\partial \sigma(\theta)}{\partial \theta} = -\frac{\delta S[\sigma]}{\delta \sigma(\theta)} + \eta, \quad (3.29)$$

will yield configurations  $\sigma$  that are distributed according to  $e^{-S[\sigma]}$ . Here,  $\theta$  is Langevin time and  $\eta$  is gaussian random noise. We generally assume that our Hubbard-Stratonovich field  $\sigma$  is real, but when  $S[\sigma]$  is complex, however, we have no way of dealing with the complex part of the action as eq [3.29] stands. Complex Langevin on the other hand is a means of stochastic quantization, using a complexified auxiliary field that helps to surpass the sign problem. We want to use the Langevin equation to update our field given a complex action. So what we do is convert the real auxiliary field into a real and imaginary component.

$$\sigma = \sigma^R + i\sigma^I \quad (3.30)$$

Thus, stochastic quantization requires complexified fields and the (spacetime local) Langevin equation now has both real and imaginary parts,

$$\sigma^R(n+1) = \sigma^R(n) + \epsilon K^R(n) + \sqrt{\epsilon} \eta(n), \quad (3.31)$$

$$\sigma^I(n+1) = \sigma^I(n) + \epsilon K^I(n), \quad (3.32)$$

where the Langevin time has been discretized as  $\theta = n\epsilon$ ,  $\epsilon$  is the time step, and  $K^R$  and  $K^I$  are the real and imaginary drift terms respectively. Again,  $\eta$ , is the real Gaussian noise such that  $\langle \eta(n) \rangle = 0$ . We may now

specify the drift terms as,

$$K_{a,x}^R = -\text{Re} \left[ \frac{\delta S}{\delta \sigma} \Big|_{\sigma \rightarrow \sigma^R + i\sigma^I} \right], \quad (3.33)$$

$$K_{a,x}^I = -\text{Im} \left[ \frac{\delta S}{\delta \sigma} \Big|_{\sigma \rightarrow \sigma^R + i\sigma^I} \right]. \quad (3.34)$$

These terms can be computed using various updating techniques such as the Euler and Runge Kutta methods.

Again this allows us to specifically treat the imaginary part of the action with its own force, and with the hope that the imaginary component will average to zero if you expect a real result.

## CHAPTER 4: Friedel Oscillations

Motivated by the realization of hard-wall boundary conditions in experiments with ultracold atoms, in this chapter we investigate the ground-state properties of spin-1/2 fermions with attractive interactions in a one-dimensional box. We use lattice Monte Carlo methods, namely hybrid Monte Carlo, explained in the previous chapter, to determine essential quantities like the energy, which we compute as a function of coupling strength and particle number in the regime from few to many particles. These many-fermion systems bound by hard walls display non-trivial density profiles characterized by so-called Friedel oscillations (which are similar to those observed in harmonic traps). In non-interacting systems, the characteristic length scale of the oscillations is set by  $(2k_F)^{-1}$ , where  $k_F$  is the Fermi momentum, while repulsive interactions tend to generate Wigner-crystal oscillations of period  $(4k_F)^{-1}$ . Based on the non-interacting result, we find a simple parametrization of the density profiles of the attractively interacting case, which we generalize to the one-body density matrix. In addition, we determine the spatially varying on-site density-density correlation, which in turn yields Tan's contact density.

### Section 4.1: Introduction

As is well-known, advances in trapping, cooling, and manipulation of ultracold atoms, single species and mixtures alike, have made it possible to realize controlled studies of quantum systems in strongly coupled few- and many-body regimes (24). The already large set of possibilities allowed by those experimental techniques continues to expand further and faster than ever. Understanding strongly coupled quantum matter in these atomic systems, in the wide variety of available scenarios, is of broad interest: strongly correlated matter is a challenging problem that pervades all energy scales, from quantum chromodynamics to condensed matter physics.

One of the most fruitful exchanges has actually been with the area of nuclear and neutron matter structure. In the latter, interactions are of limited range, and scattering lengths are comparatively large, a situation that bears strong similarities with ultracold atomic fermions close to a Feshbach resonance, differences notwithstanding (25). Similarly, the realization of periodic systems via optical lattices (26) and the creative approach to engineering topologically non-trivial phases using internal degrees of freedom (27) have recently strengthened the connections to condensed matter physics.

New experimental techniques allow for the implementation of (quasi-) hard-wall traps. This development is interesting because the “flat-bottom” of the trap simulates a uniform system (28). Close to the boundaries, or for low particle numbers, the edge effects result in the so-called Friedel oscillations, i.e. deviations from uniformity. The original work by Friedel actually considered the problem of the density variations due to the presence of an impurity (29) in an electronic system. Since then, other authors considered similar “impurity” problems (see e.g. (30; 31; 32)), and more recently the application of Friedel oscillations as probes for quasiparticles has been advocated (33).

In addition to the above, there are other motivations to understand Friedel oscillations in detail. For instance, it was shown by Zhang et al. in Ref. (34) that the presence of boundaries and interfaces in nanocomposites and heterostructures limits their mechanical strength precisely due to the appearance of Friedel oscillations. Clark et al. (35) showed that Friedel oscillations near a bilayer-monolayer graphene interface open a gap at the Fermi energy (for electrons with wave vectors normal to said interface), which consequently affects transport properties across the boundary. The interplay between the shape of the Fermi surface and Friedel oscillations (in particular for an oxygen impurity on the surface of a ferromagnetic thin film) was studied by Bouhassoune et al. (36), where “giant” directional effects were reported and shown to be tunable, with consequences for nanospintronics applications. Generally speaking, Friedel oscillations continue to be of interest to solid-state physics and materials science, even though their existence has been qualitatively understood for a while.

In this work, we do not consider impurities per se, but treat the problem of density oscillations resulting from “open” or “hard-wall” boundary conditions in a non-relativistic system of spin-1/2 fermions. Previous work studied this problem in the electronic case using bosonization (37; 38) or a variety of numerical methods (39; 40; 41; 42; 43). Using bosonization and density-matrix renormalization group (DMRG) techniques, Ref. (44) studied a related situation, namely the *repulsive* Hubbard model in 1D with hard-wall boundaries. It was then found that the repulsive interaction parametrizes a crossover between Friedel-type density oscillations (characterized by a  $2k_F$  wavelength) at weak coupling and Wigner-crystal-type oscillations (with  $4k_F$  wavelength) at strong coupling. In the latter regime, the repulsion forces particles of opposite spins to occupy higher momentum states, effectively doubling the Fermi momentum.

As mentioned above, here we quantitatively explore several properties of spin-1/2 fermions in 1D with *attractive* short-range interactions confined by hard-wall boundaries. We calculate density profiles and study the enhancement of Friedel oscillations with increasing interaction strength; determine the occupation of standing-wave orbitals; and find the ground-state energy. In addition, we present a detailed characterization of the one-body density matrix and the short-distance correlations by computing the so-called contact density (45), which in these systems is a spatially varying quantity. As is well known, the contact fully

characterizes the short-distance behavior of correlations and enters sum rules of transport coefficients (see e.g. (46)). We study all of the above in the few- to many-body range of  $N = 8, \dots, 24$  unpolarized particles and cover weakly to strongly coupled regimes, as measured by the conventional dimensionless coupling  $\gamma$  (see below).

Naturally, our work complements Ref. (44) mentioned above in that we study the regime of attractive interactions, but we also expand on that work by considering a range of particle numbers. In contrast to the repulsive case, strong pairing correlations induced by attractive interactions lead to two-body bound-state formation and an enhancement of the Friedel oscillations, with a characteristic coupling-dependent discontinuity in the momentum distribution. The effect on Friedel oscillations was also noted in Ref. (47), where a similar calculation was carried out in the presence of a harmonic trapping potential (see also Ref. (48)).

Our calculations are also a first step towards exploring the properties of analogue systems in higher dimensions. As outlined in Ref. (49), this is enabled by Fourier acceleration, which can be adapted to hard-wall boundaries without affecting the dominant scaling of computational cost with system size. The same methods can be applied to systems in optical lattices, in particular in cases of internal degeneracies  $N_f > 2$ .

Generally speaking, correlations tend to be stronger in 1D systems than in their 2D and 3D counterparts (50). For this reason, investigating and implementing non-perturbative methods [such as exact diagonalization, quantum Monte Carlo (QMC), density-matrix renormalization group (DMRG), Bethe ansatz (BA), bosonization, etc.] are essential. However, not all of these methods are universally applicable. For instance, quantum Monte Carlo can address problems in any number of spatial dimensions, but suffers from a sign problem at finite polarization and for repulsive interactions. The BA can solve the problem exactly for attractive or repulsive short-range interactions in 1D, and it has been widely applied for infinite systems (see e.g. Ref. (51)). The BA is not applicable in higher dimensions or in the presence of external trapping potentials, as translation invariance is broken, but it can and has been applied to 1D infinite square-well traps with repulsive interactions (52). The DMRG method has also been used to analyze that system (43). Finally, bosonization methods are often restricted to very low temperatures where the dispersion relation around the Fermi points can be well approximated as linear. As argued in Ref. (53), however, it has become clear in the last few years that considering non-linearities is important, as they account for characteristic behavior even at the level of broad, qualitative features, most noticeably so in the system's dynamic response functions (54). For these reasons, there have recently been a number of exact diagonalization (and similar) studies, with focus on pairing correlations in spin-polarized, harmonically trapped systems (see e.g. Refs. (55; 56; 57; 58)). The same reasons further motivate the present work.

## Section 4.2: Many-body method

### 4.2.1: Hamiltonian and basic formalism

In this work we will focus on a non-relativistic Hamiltonian  $\hat{H}$ , with short-range interactions, as a model relevant for matter in dilute regimes. Thus,

$$\hat{H} = \hat{T} + \hat{V}, \quad (4.1)$$

where

$$\hat{T} = \sum_{s=\uparrow,\downarrow} \int_0^L dx \hat{\psi}_s^\dagger(x) \left( -\frac{\hbar^2 \partial_x^2}{2m} \right) \hat{\psi}_s(x) \quad (4.2)$$

is the kinetic energy, and

$$\hat{V} = -g \int_0^L dx \hat{n}_\uparrow(x) \hat{n}_\downarrow(x), \quad (4.3)$$

is the two-body, zero-range interaction. Although we have written  $\hbar$  and  $m$  explicitly above, we will take them to unity from this point on and similarly for Boltzmann's constant  $k_B$ . While  $g$  is the bare coupling, it is physically meaningful in 1D:  $g = 2/a_0$ , where  $a_0$  is the scattering length. As conventional in studies of uniform systems, we define a dimensionless coupling

$$\gamma \equiv \frac{gL}{N}, \quad (4.4)$$

where  $L$  is the physical extent of the system and  $N$  is the total particle number, or similarly,

$$\lambda = \sqrt{\beta g}. \quad (4.5)$$

Now, at this point we must include a discussion of the units of this Hamiltonian, as when we attempt to make calculations on a lattice using Monte Carlo we require our effective action  $(-\beta\hat{H})$  to be completely dimensionless. First let us examine the scaling for each of the quantities in our effective action,

$$\begin{aligned}
[m] &= [\hbar] = 1 \\
[\beta] &\sim L^2 \\
[\hat{n}] &\sim \frac{1}{L} \\
[\psi] = [\psi^\dagger] &\sim \frac{1}{\sqrt{L}} \\
[x] &\sim L \\
[\nabla^2] &\sim \frac{1}{L^2} \\
[g] &\sim \frac{1}{L}
\end{aligned} \tag{4.6}$$

In order to assure that we are truly dimensionless, let's examine the kinetic and potential terms separately. We will first tackle the potential term,

$$\beta\hat{V} = -\beta g \int_0^L dx \hat{n}_\uparrow(x)\hat{n}_\downarrow(x). \tag{4.7}$$

We want the leading factor to be our unit-less coupling,  $\lambda$ . We can show this by distributing factors of  $g$ ,

$$\begin{aligned}
\beta\hat{V} &= -(\beta g^2) \int_0^L d(gx) \left( \frac{\hat{n}_\uparrow(x)}{g} \right) \left( \frac{\hat{n}_\downarrow(x)}{g} \right), \\
&= -\lambda^2 \int_0^L d(gx) \left( \frac{\hat{n}_\uparrow(x)}{g} \right) \left( \frac{\hat{n}_\downarrow(x)}{g} \right).
\end{aligned} \tag{4.8}$$

Notice that each term in parentheses can be considered dimensionless when considering the respective dimensionality defined above. We have shown that the interaction term can thus be written in a manifestly dimensionless form, and that the resulting dimensionless coupling is, as anticipated, governed completely by  $\lambda$ . Let us now do the same for the kinetic term,

$$\beta\hat{T} = \beta \sum_{s=\uparrow,\downarrow} \int_0^L dx \hat{\psi}_s^\dagger(x) \left( -\frac{\hbar^2 \partial_x^2}{2m} \right) \hat{\psi}_s(x). \tag{4.9}$$

We can again distribute factors of the bare coupling,  $g$ , in order to show that this term is dimensionless.

$$\beta\hat{T} = (\beta g^2) \sum_{s=\uparrow,\downarrow} \int_0^L d(gx) \left( \frac{\hat{\psi}_s^\dagger(x)}{\sqrt{g}} \right) \left[ \left( -\frac{\hbar^2 \partial_x^2}{2m} \right) \left( \frac{1}{g^2} \right) \right] \left( \frac{\hat{\psi}_s(x)}{\sqrt{g}} \right). \tag{4.10}$$

Notice again that all terms in parentheses and brackets are indeed dimensionless, while still maintaining

the original scaling for  $g$ , and therefore leaving the Hamiltonian unchanged. We have explicitly shown that our full effective action,  $\beta\hat{H}$ , is indeed dimensionless.

$$\beta\hat{H} = \lambda^2 \left( \sum_{s=\uparrow,\downarrow} \int_0^L d(gx) \left( \frac{\hat{\psi}_s^\dagger(x)}{\sqrt{g}} \right) \left[ \left( -\frac{\hbar^2 \partial_x^2}{2m} \right) \left( \frac{1}{g^2} \right) \right] \left( \frac{\hat{\psi}_s(x)}{\sqrt{g}} \right) - \int_0^L d(gx) \left( \frac{\hat{n}_\uparrow(x)}{g} \right) \left( \frac{\hat{n}_\downarrow(x)}{g} \right) \right) \quad (4.11)$$

Now that we have shown the Hamiltonian is dimensionless, we may approach the ground state of our many-body quantum system by imaginary-time evolution of a “guess” state  $|\psi_0\rangle$ , as in previous work (59),

$$|\psi\rangle_\beta = e^{-\beta\hat{H}} |\psi_0\rangle, \quad (4.12)$$

where  $\beta$  is the extent of the imaginary time evolution. This approach is feasible if the guess has a non-vanishing projection onto the true ground state. We take  $|\psi_0\rangle$  to be a Slater determinant of single-particle orbitals  $\{\varphi_k\}$  given by plane waves with hard-wall boundary conditions, i.e.

$$\varphi_k(x) = \sqrt{\frac{2}{L}} \sin\left(\frac{\pi k x}{L}\right), \quad (4.13)$$

where  $L$  is the size of the box, and  $k$  is a positive integer. More specifically, we take  $k = 1, 2, \dots, N_\uparrow$  with  $N_\uparrow = N_\downarrow = N/2$  being the number of fermions of each species. In this method, it is essential to have access to the operator

$$\hat{U}(t', t) \equiv \exp\left[-(t' - t)\hat{H}\right], \quad (4.14)$$

which is a complicated object in general, but which can be approximated using a Suzuki-Trotter decomposition

$$\hat{U}(t + \tau, t) = e^{-\tau\hat{T}/2} e^{-\tau\hat{V}} e^{-\tau\hat{T}/2} + O(\tau^3), \quad (4.15)$$

where  $\tau$  is our imaginary-time discretization parameter. This factorization allows us to use, at each time step  $t$ , an auxiliary-field Hubbard-Stratonovich transformation of the interaction, i.e. a representation of the two-body interaction via one-body potentials:

$$e^{-\tau\hat{V}} = \int \mathcal{D}\sigma(x) e^{-\tau\hat{V}_{\uparrow,\sigma}} e^{-\tau\hat{V}_{\downarrow,\sigma}}, \quad (4.16)$$

where the  $\hat{V}_{s,\sigma}$  are external-potential, one-body operators that depend on the auxiliary field  $\sigma(x)$ . The integral  $\int \mathcal{D}\sigma(x)$  is a sum over all possible configurations of  $\sigma$  at the specific time  $t$  [see Eq. (4.15)].

Combining the above steps, one finds

$$\hat{U}(\beta, 0) = \int \mathcal{D}\sigma(x, t) \prod_t \hat{U}_\sigma(t + \tau, t), \quad (4.17)$$

where the path integral is over all possible spacetime dependent fields  $\sigma(x, t)$  and the  $\sigma$ -specific evolution operator is

$$\hat{U}_\sigma(t + \tau, t) \equiv e^{-\tau\hat{T}/2} e^{-\tau\hat{V}_{\uparrow, \sigma}} e^{-\tau\hat{V}_{\downarrow, \sigma}} e^{-\tau\hat{T}/2}, \quad (4.18)$$

which is a product of exponentials of one-body operators.

Moreover, we identify a zero-temperature partition sum

$$\mathcal{Z} \equiv \langle \psi_0 | \hat{U}(\beta, 0) | \psi_0 \rangle = \int \mathcal{D}\sigma(x, t) P[\sigma], \quad (4.19)$$

where we defined

$$P[\sigma] \equiv \langle \psi_0 | \hat{U}_\sigma(\beta, 0) | \psi_0 \rangle. \quad (4.20)$$

Since  $\hat{U}_\sigma$  is composed of a string of exponentials of one-body operators, a well-known result of second-quantization formalism indicates that (assuming our guess state  $|\psi_0\rangle$  is a single Slater-determinant state, as specified above)

$$P[\sigma] = \langle \psi_0 | \hat{U}_\sigma(\beta, 0) | \psi_0 \rangle = \det^2 [M_\sigma(\beta)], \quad (4.21)$$

where the power of two results from our system having two distinguishable (but otherwise identical) fermion species. The matrix  $M_\sigma(\beta)$  is the one-particle representation of  $\hat{U}_\sigma(\beta, 0)$ , restricted to the Hilbert space of the occupied orbitals, i.e.,

$$[M_\sigma(\beta)]_{ab} = \langle a | \hat{U}_\sigma(\beta, 0) | b \rangle, \quad (4.22)$$

where  $a, b = 1, 2, \dots, N_\uparrow$ . Using this auxiliary field formalism, one may sample  $\sigma$  according to  $P[\sigma]$  using well-known methods. For the calculations carried out in this work, we used the lattice hybrid Monte Carlo algorithm (60; 62).

#### 4.2.2: Expectation values of operators

The above formalism enables the non-perturbative evaluation of arbitrary observables, as long as  $P[\sigma]$  is non-negative (which in our case it is, as mentioned above), as we shall see next. The ground-state expectation value of an operator  $\hat{O}$  is

$$\langle \hat{O} \rangle = \lim_{\beta \rightarrow \infty} O_\beta, \quad (4.23)$$

where

$$O_\beta \equiv \frac{\langle \psi_0 | \hat{U}(\beta, \beta/2) \hat{O} \hat{U}(\beta/2, 0) | \psi_0 \rangle}{\langle \psi_0 | \hat{U}(\beta, 0) | \psi_0 \rangle}. \quad (4.24)$$

Once the time-evolution operators  $\hat{U}$  are written in field-integral form, as shown in the previous section, Eq. (4.24) becomes

$$O_\beta = \frac{1}{\mathcal{Z}} \int \mathcal{D}\sigma P[\sigma] O[\sigma], \quad (4.25)$$

where

$$O[\sigma] \equiv \frac{\langle \psi_0 | \hat{U}_\sigma(\beta, \beta/2) \hat{O} \hat{U}_\sigma(\beta/2, 0) | \psi_0 \rangle}{\langle \psi_0 | \hat{U}_\sigma(\beta, 0) | \psi_0 \rangle}. \quad (4.26)$$

This path integral form Eq. 4.25 is a function of the imaginary time  $\beta$ , which should approach the ground-state answer when extrapolated to large  $\beta$  (see Fig. 4.1).

In practice, the calculation of  $O[\sigma]$  above, for a given configuration of the field  $\sigma$ , can be easily carried out when  $\hat{O}$  is generic one-body operator, in the following fashion. Going back to Eqs. (4.19)-(4.22), we insert a source factor  $\exp\{(\lambda \hat{O})\}$  as follows; we take

$$\langle \psi_0 | \hat{U}_\sigma(\beta, 0) | \psi_0 \rangle \rightarrow \langle \psi_0 | \hat{U}_\sigma(\beta, \beta/2) e^{\lambda \hat{O}} \hat{U}_\sigma(\beta/2, 0) | \psi_0 \rangle \quad (4.27)$$

Since the source factor is the exponential of a one-body operator, it modifies the form of  $M_\sigma$  defined above in a predictable way. Inserting the resulting expression in Eq. (4.19) (or rather its natural logarithm), differentiating with respect to  $\lambda$ , and taking  $\lambda = 0$ , it is easy to identify

$$O[\sigma] = \text{tr}[M_\sigma^{-1} U_\sigma(\beta, \beta/2) O U_\sigma(\beta/2, 0)], \quad (4.28)$$

where the trace is over the space of occupied orbitals, and  $U_\sigma(t, t')$  and  $O$  are the single-particle matrix representations of  $\hat{U}_\sigma(t, t')$  and  $\hat{O}$ , respectively. Note, in particular, that the matrix product of  $U_\sigma$  and  $O$  above is over the full single-particle space, not just the occupied orbitals.

### Section 4.3: Results

Using the formalism presented above, we carried out lattice calculations in fixed system sizes of length  $L = (N_x + 1)\ell$ , discretized by setting  $N_x = 20, 30, 40, 60, 80$  and maintaining  $L$  constant. Below we present plots for several quantities for  $N_x = 80$ , and discuss finite-size effects in a later section. The extent of the time direction, as measured by the dimensionless parameter  $\beta\varepsilon_F$ , was varied so as to allow for a meaningful extrapolation to the ground state, as explained below. Here,  $\varepsilon_F = k_F^2/2$ , and  $k_F = \pi N/(2L)$ , where  $N$  is

the total particle number. In such lattices, we studied systems of  $N = 8, 12, \dots, 24$  particles by taking  $10^4$  samples of the auxiliary field, which yields statistical uncertainties on the order of 1%. Finally, we varied the strength of the interaction between  $\gamma = 0$  and  $\gamma = 4.0$ .

#### 4.3.1: Ground-state energy

In order to determine the ground-state energy we used the formalism presented in the previous section, but used a shortcut: the  $\beta$  derivative of the path-integral form of  $\ln \mathcal{Z}$  produces the desired expression, up to a constant. It is not difficult to show (see Ref. (60)) that the resulting estimator  $E_\beta$  approaches the ground-state result  $E_{\text{GS}}$  exponentially, i.e.

$$E_\beta \equiv -\frac{\partial \ln \mathcal{Z}}{\partial \beta} \rightarrow E_{\text{GS}} + K e^{-\beta \Delta}, \quad (4.29)$$

where  $K$  is a constant and  $\Delta$  is the difference between the energy of the first excited state and the ground state. In Fig. 4.1 we show the above exponential fits to Monte Carlo data for a representative case ( $N_x = 80$ ,  $N = 16$ ) for several couplings.

In Fig. 4.2, we show our results for the ground-state energy  $E_{\text{GS}}$  in units of the energy of the non-interacting case

$$E_{\text{FG}} = \frac{\pi^2}{L^2} \sum_{k=1}^{N/2} k^2 = \frac{\pi^2}{24L^2} N(N+1)(N+2). \quad (4.30)$$

As is evident from the figure, for all the couplings we studied, the ground-state energy appears to approach the large- $N$  limit very quickly.

#### 4.3.2: Density profiles

To calculate the density profiles we used the expression of Eq. (4.28), where  $\hat{O} = \hat{n}(x)$ , which indicates that

$$n(x) = \langle \hat{n}(x) \rangle = \frac{1}{\mathcal{Z}} \int \mathcal{D}\sigma P[\sigma] n[\sigma, x], \quad (4.31)$$

where

$$n[\sigma, x] \equiv \sum_{a,b,c}^{N/2} [M_\sigma^{-1}]_{ab} [U_\sigma(\beta, \beta/2)]_{bx} [U_\sigma(\beta/2, 0)]_{xa}. \quad (4.32)$$

To derive the previous expression, we have used that the single-particle representation of  $\hat{O} = \hat{n}(x)$  is simply  $O_{y,y'} = \langle y|\hat{n}(x)|y'\rangle = \delta(y,y')\delta(x,y)$ , where  $|y\rangle$  is a coordinate eigenstate.

In Fig. 4.3 we show the density profiles for two different values of the attractive coupling  $\gamma$  as a function of particle number  $N$ . As is evident from the figure, the main effect of attractive interactions is to enhance the amplitude of the Friedel oscillations while their frequencies are maintained. In order to analyze the oscillations in more detail, we recall that the density profile of the noninteracting case can be easily obtained by summing the contributions of the  $N/2$  occupied single-particle states, namely

$$\begin{aligned} n(x/L) &= \frac{2}{L} \sum_{k=1}^{N/2} \sin^2\left(\frac{\pi kx}{L}\right) \\ &= \frac{N+1}{L} - \frac{1}{L} \frac{\sin\left(\frac{\pi(N+1)x}{L}\right)}{\sin\left(\frac{\pi x}{L}\right)}, \end{aligned} \quad (4.33)$$

where  $L$  is the physical size of the box. To analyze the interacting density profiles, we rewrite the above as

$$\begin{aligned} \frac{L}{N+1} n(x/L) \sin\left(\frac{\pi x}{L}\right) &= \sin\left(\frac{\pi x}{L}\right) - \frac{1}{N+1} \sin\left(\frac{\pi(N+1)x}{L}\right) \\ &= \sum_{k=1}^{N_x} B_k \sin\left(\frac{\pi kx}{L}\right) \equiv \tilde{n}(x/L), \end{aligned} \quad (4.34)$$

where we have used a general Fourier expression obeying hard-wall boundary conditions in the last equality. Obviously, the noninteracting system satisfies  $B_k = 0$  for all  $k$  except the cases of  $B_1 = 1$  and  $B_{N+1} = -1/(N+1)$ . Note that the multiplication by  $\sin(\frac{\pi x}{L})$  necessarily obliterates any information at  $x = 0$ , but we already know that the density vanishes at that point.

In Fig. 4.4 we show the coefficients  $B_k$  as a function of  $k$  and the coupling strength, for a representative case. The dominant contributions are always at  $k = 1$  and  $k = N + 1$ , regardless of the strength of the coupling. This is a remarkably clean signal that can be experimentally verified and which is especially surprising in light of bosonization analyses. The latter indicate that the denominator  $\sin(\pi x/L)$  should appear elevated to a non-trivial power (i.e. different from unity) that is directly related to the parameters of the low-energy effective theory (see e.g. Ref. (44)).

The physical origin of the  $k = 1$  and  $k = N + 1$  peaks can be gleaned from the non-interacting result Eq. (4.33). The former provides the “overall” or “average” density in the bulk and is responsible for (all but one of) the particle number count; it therefore survives in the thermodynamic limit. The second term (and presumably every other non-vanishing term in the interacting case) is associated with the physics at the Fermi surface.

### 4.3.3: One-body density matrix

In order to characterize the one-body density matrix in an efficient way, we perform a more general version of the spectral analysis previously applied to the density profile. The non-interacting one-body density matrix may be computed trivially by collecting contributions from the  $N/2$  occupied orbitals:

$$\begin{aligned} G_1(x, x') &= \frac{2}{L} \sum_{k=1}^{N/2} \sin\left(\frac{\pi kx}{L}\right) \sin\left(\frac{\pi kx'}{L}\right) \\ &= \frac{1}{2L} \left[ \frac{\sin\left(\frac{\pi(N+1)(x-x')}{2L}\right)}{\sin\left(\frac{\pi(x-x')}{2L}\right)} - \frac{\sin\left(\frac{\pi(N+1)(x+x')}{2L}\right)}{\sin\left(\frac{\pi(x+x')}{2L}\right)} \right]. \end{aligned} \quad (4.35)$$

Again, we rewrite the above as (for  $x \neq x'$ )

$$\begin{aligned} &2LG_1(x, x') \sin\left(\frac{\pi(x-x')}{2L}\right) \sin\left(\frac{\pi(x+x')}{2L}\right) \\ &= \sin\left(\frac{\pi Nx}{2L}\right) \sin\left(\frac{\pi(N/2+1)x'}{L}\right) - \sin\left(\frac{\pi(N/2+1)x}{L}\right) \sin\left(\frac{\pi Nx'}{2L}\right) \\ &= \sum_{k=1}^{N_x} \sum_{k'=1}^{N_x} B_{kk'} \sin\left(\frac{\pi kx}{L}\right) \sin\left(\frac{\pi k'x'}{L}\right) \\ &\equiv \tilde{G}_1(x, x'), \end{aligned} \quad (4.36)$$

where we see that  $B_{kk'} = 0$  for all  $k, k'$  except for the cases of  $B_{\frac{N}{2}, \frac{N}{2}+1} = -B_{\frac{N}{2}+1, \frac{N}{2}} = 1$ , corresponding to  $k_F$  and the first excited state above the Fermi level. Note that the antisymmetry in the coefficients was introduced in Eq. (4.36) via the antisymmetry in  $x$  and  $x'$ .

Interestingly, the non-zero  $B_{kk'}$  in the non-interacting case display the property that  $|k - k'| = 1$  and  $k + k' = N + 1$ , reflecting the same wavelengths observed in the spatial density profile,  $n(x)$ . As seen in Fig. 4.5 (top), in the presence of attractive interactions, amplitude from  $B_{\frac{N}{2}, \frac{N}{2}+1}$  and its antisymmetric partner appears to shift to neighboring modes, which continue to obey the same relations for  $|k - k'|$  and  $k + k'$ . This decay of the main peak is enhanced as  $\gamma$  is increased, as Fig. 4.5 (bottom) demonstrates.

### 4.3.4: Quasi-momentum distribution

In translationally invariant systems, the shape of the momentum distribution can reveal several aspects of a many-body system, ranging from condensation to short-range correlations and spatial structure. In the present case, the hard-wall boundaries break translation invariance, such that the eigenstates of the system in the absence of interactions are given by the usual standing waves with quantized momentum  $p_k = k\pi/L$ , as mentioned above. In this section we present the occupation distribution in the single-particle space of

those standing waves; we will refer to that distribution as the quasi-momentum distribution  $n(k)$ .

Figure 4.6 shows  $n(k)$  per spin for a representative particle number  $N = 16$ , and for several couplings. For non-interacting systems, the ground-state distribution is the expected step function, with a unit discontinuity at the Fermi surface. As attractive interactions are turned on, pairing correlations begin to dominate, and the system progressively becomes more bosonic. This is clearly seen in the variation of the discontinuity  $\delta_N$  in  $n(k)$  as a function of  $\gamma$ :  $\delta_N$  decreases monotonically as  $\gamma$  is increased. The inset of Fig. 4.6 shows  $\delta_N(\gamma)$  for  $N = 16$  particles. For the couplings studied here, it appears that  $\delta_N(\gamma)$  decreases without a bound. However, it seems difficult to imagine a situation in which  $\delta_N(\gamma) < 0$  and the energy is minimized. Under the assumption that that does not happen, we expect that  $\delta_N(\gamma)$  approaches a non-negative constant asymptotically at large  $\gamma$ , i.e. the curve described by the data in the inset of Fig. 4.6 should eventually change convexity as it approaches a constant from above. To determine whether this conjecture holds, however, calculations in the strong-coupling, hard-core boson limit are needed (63).

#### 4.3.5: Tan's contact density and contact

Short-range interactions, like the one studied here, induce correlations whose short-distance (high-momentum) form is encoded in Tan's contact (45). Indeed, the short-distance dynamics is governed by the shape of the relative-coordinate wavefunction of the two-body problem, up to an overall factor that encapsulates many-body effects as well as effects due to external trapping potentials. The latter is the so-called contact  $C$ . One of the many ways to define the contact is through the Feynman-Hellmann theorem as applied to the variation of the ground-state energy with respect to the scattering length, which yields

$$C = -g\langle\hat{V}\rangle, \tag{4.37}$$

where  $\langle\hat{V}\rangle$  is the ground-state expectation value of the interaction energy. Equation (4.3) indicates that  $C$  is given by an integral over the on-site correlation function among different spins, which for brevity we will call "contact density". In our case, the presence of hard walls yields a spatially varying contact density  $\mathcal{C}(x/L)$ . Note that since  $g$  has units of inverse length (i.e. momentum),  $C$  has dimensions of inverse length cubed. Moreover,  $C$  is an extensive quantity. Therefore, below we use the intensive dimensionless form  $C/(Nk_F^3)$ ; for the contact density we use  $\mathcal{C}(x/L)/k_F^4$ .

In Fig. 4.7 we show  $\mathcal{C}(x/L)$  as a function of the scaled position  $x/L$  and in units of  $k_F^4$  at two different couplings (top and bottom). In terms of number of peaks and valleys, the oscillations in  $\mathcal{C}(x/L)$  follow the same pattern as those of the density  $n(x/L)$ . The amplitude variations are such that the minima are at roughly one half of the value of the maxima, regardless of coupling or particle number. While that trend

remains as  $N$  is varied, the average value of  $\mathcal{C}(x/L)/k_F^4$  away from the boundaries does seem to quickly approach a limit as  $N$  is increased, and the overall amplitude of the oscillations also decreases markedly. The integrated contact  $C/(Nk_F^3)$ , shown in Fig. 4.8, also seems to approach the thermodynamic limit very quickly. This finding is in line with the observations of Ref. (59), which studied the few- to many-body progression of one-dimensional fermions with periodic boundary conditions.

#### Section 4.4: Summary and Conclusions

Studying systems with hard-wall boundaries via ultracold atoms is a way to access the behavior of the uniform-space limit, but when the boundaries are explicitly accounted for, it is also a different way to probe strongly coupled matter. In this work, we set out to characterize an elementary yet non-trivial many-body problem in that situation: spin-1/2 fermions with a zero-range interaction in a one-dimensional hard-wall box. We computed, in a fully ab initio fashion, the ground-state energy, density profiles, momentum distribution, and Tan’s contact density. Together, these quantities provide a basic yet comprehensive understanding of the effects of the boundaries and how they disappear in the thermodynamic limit. In short, we find that, upon scaling the density and the contact density by appropriate powers of  $k_F$ , the large- $N$  limit is approached surprisingly quickly, as the largest changes happen in the regime we studied, where  $N = 8 - 24$ .

The hard-wall boundaries lead to oscillating density profiles; such Friedel oscillations are characteristic not only of systems with interfaces but also of situations where an impurity is present. Our work clarifies the quantitative changes in the oscillation pattern due to short-range attractive interactions, which induce pairing correlations. We find that those effects are captured by a parametrization of the density which, while based on the noninteracting result, provides a remarkably clean way to understand the behavior of the density even in strongly coupled situations. We extended that analysis to the one-body density matrix, and further complemented it by computing the quasi-momentum distribution. The latter shows clear interaction effects as a change in the discontinuity at the Fermi surface.

Aside from the above, we calculated the ground-state energy (which we provide as a benchmark for other approaches and future studies) and the Tan contact density (i.e. on-site pairing correlations) which encode all of the short-distance behavior of response functions via the operator product expansion.

We carried out this work by discretizing space and (imaginary) time and using the auxiliary-field path-integral representation of the many-body problem. We estimated that path integral using stochastic methods, namely the hybrid Monte Carlo algorithm. Our study used lattices of up to  $N_x = 80$  points and covered weakly to strongly interacting regimes in systems of up to  $N = 24$  particles. This Monte Carlo approach is one of the few tools that, in one dimension, can provide fully non-perturbative and well-controlled access to

the physics of strongly coupled matter.

Our work is a first step towards: a) exploring the detailed structure of two-body correlations, b) studying finite-temperature effects, and c) higher dimensions, including mixed-dimensions. Point b) is particularly important because finite-T effects are only cleanly accessible with exact diagonalization or with QMC, as the Bethe ansatz does not provide a controlled approximation in that case (at least not for all temperatures).

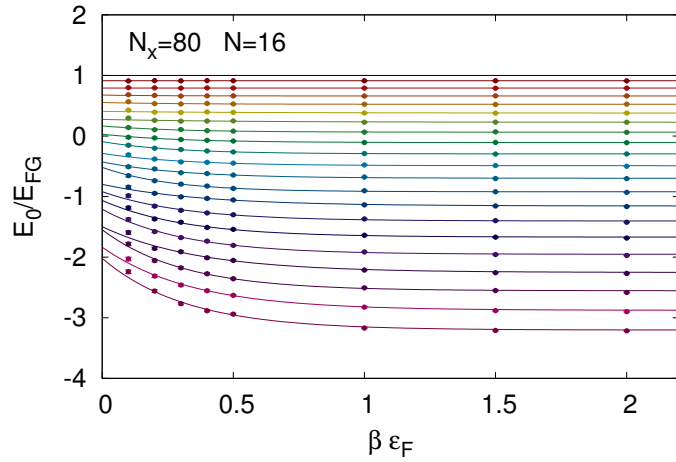


Figure 4.1: Convergence of our energy estimator as a function of  $\beta\epsilon_F$ , for  $N = 16$  particles in a 1D segment (discretized using  $N_x = 80$  points), for couplings  $\gamma = 0.0, 0.2, \dots, 4.0$  (top to bottom).

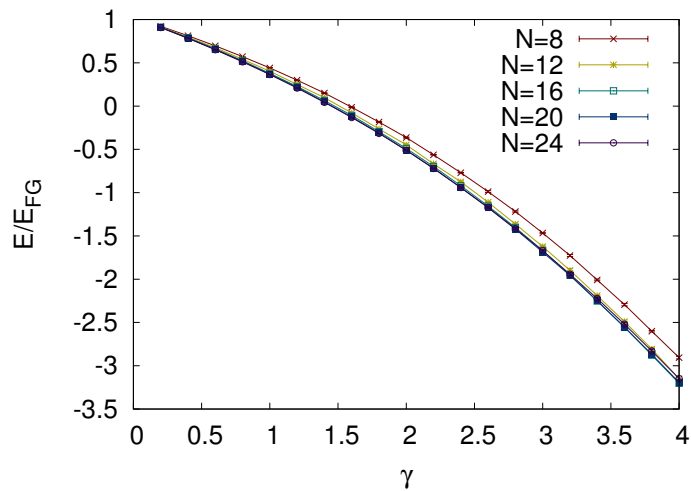


Figure 4.2: The ground-energy of  $N = 8, \dots, 24$  unpolarized fermions in a 1D segment (discretized using  $N_x = 80$  points), in units of its non-interacting counterpart  $E_{FG}$ , as a function of the dimensionless coupling  $\gamma$ .

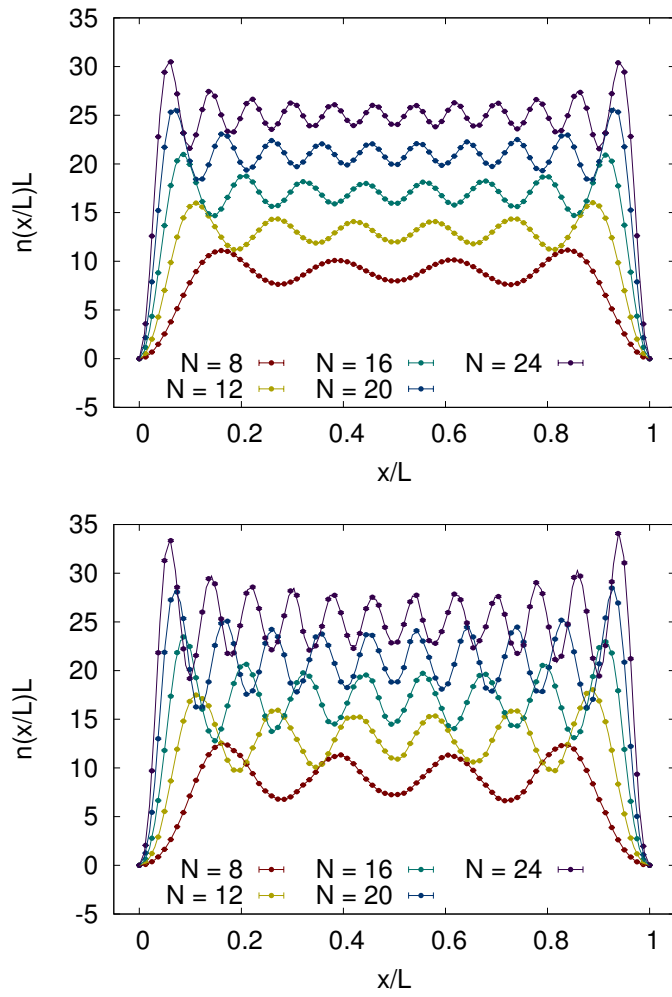


Figure 4.3: Density profiles versus the scaled position  $x/L$  for  $N_x = 80$  at weak coupling ( $\gamma = 0.2$ , top panel) and strong coupling ( $\gamma = 3.0$ , bottom panel), for particle numbers  $N = 8, 12, 16, 20, 24$  (from bottom to top).

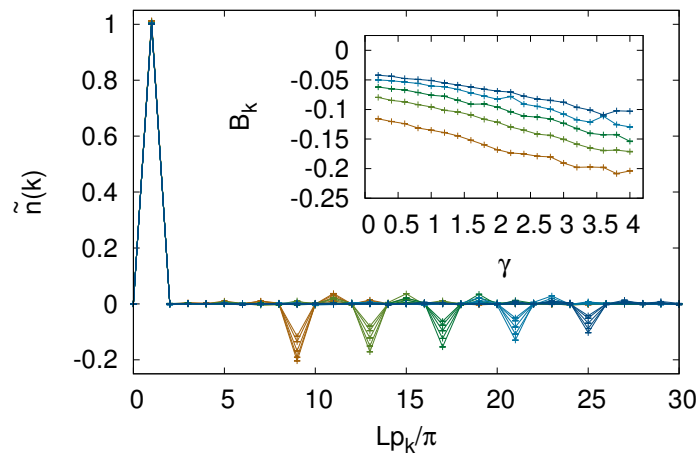


Figure 4.4: Hard-wall transform coefficients  $B_k$  of Eq. (4.34), as a function of  $Lp_k/\pi = k$ , for  $N_x = 80$  and several values of the coupling  $\gamma$  and particle number  $N$ . Note the maximum at  $k = 1$  is equal to unity to an accuracy better than 2% for all  $\gamma$  and  $N$ ; the minima, on the other hand, show clear variation with increasing  $N = 8, \dots, 24$  (left to right) as well as increasing  $\gamma$  (top to bottom; see inset). Inset: Value of the minimum as a function of the coupling  $\gamma$  for  $N = 8, \dots, 24$  (bottom to top).

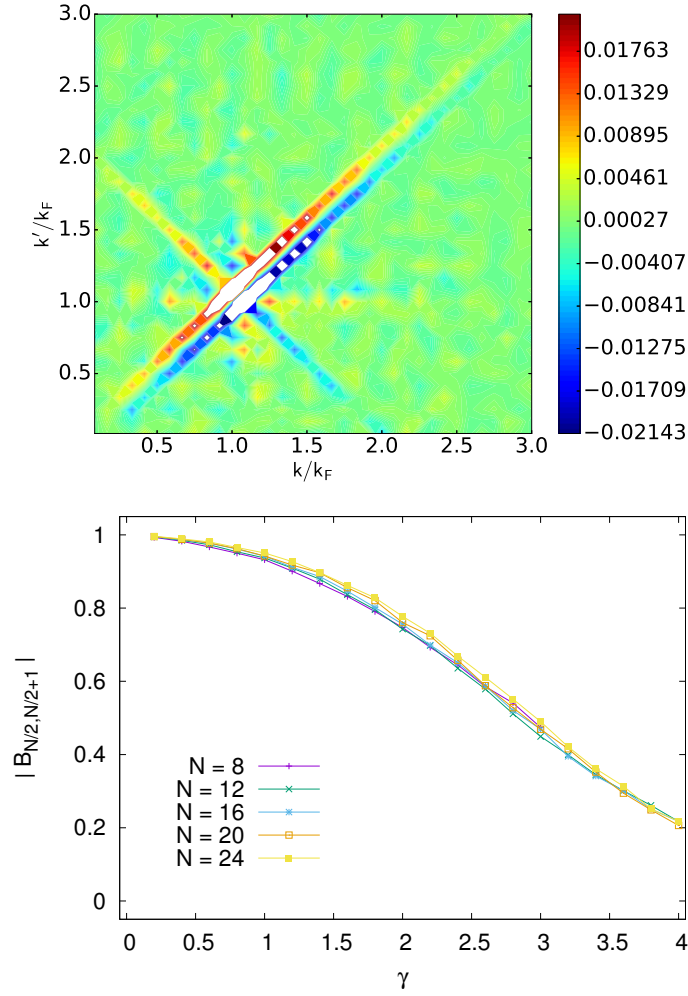


Figure 4.5: Top: Hard-wall transform coefficients  $B_{k,k'}$  of Eq. (4.36), as a function of  $k = Lp_k/\pi$  and  $k' = Lp_{k'}/\pi$ , for  $N_x = 80$ ,  $\gamma = 4.0$ , and  $N = 24$ . Bottom: Amplitude variation of the main peak  $B_{\frac{N}{2}, \frac{N}{2}+1}$  as a function of  $\gamma$  for several particle numbers.

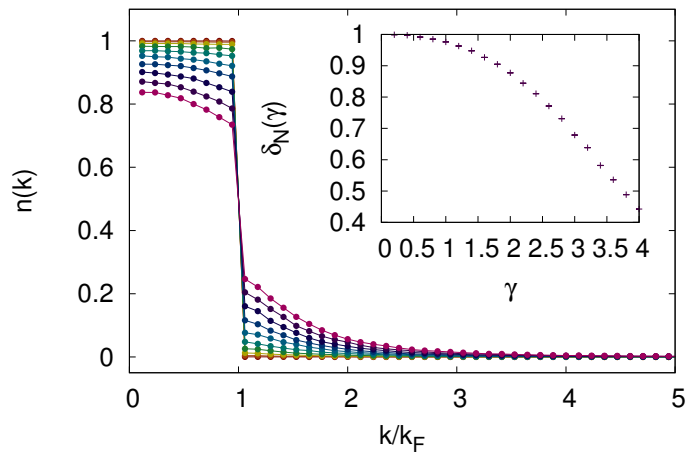


Figure 4.6: Quasi-momentum distribution  $n(k)$  for  $N = 16$  particles as a function of  $\gamma = 0.2, 0.6, 1.0, \dots, 3.8$  (top to bottom around  $k = 0$ ), for  $N_x = 80$ . Inset:  $\gamma$ -dependence of the discontinuity  $\delta_N$  in  $n(k)$  at the Fermi surface. While  $\delta_N$  could depend on  $N$ , our results for different  $N$  agree within our statistical and systematic uncertainties.

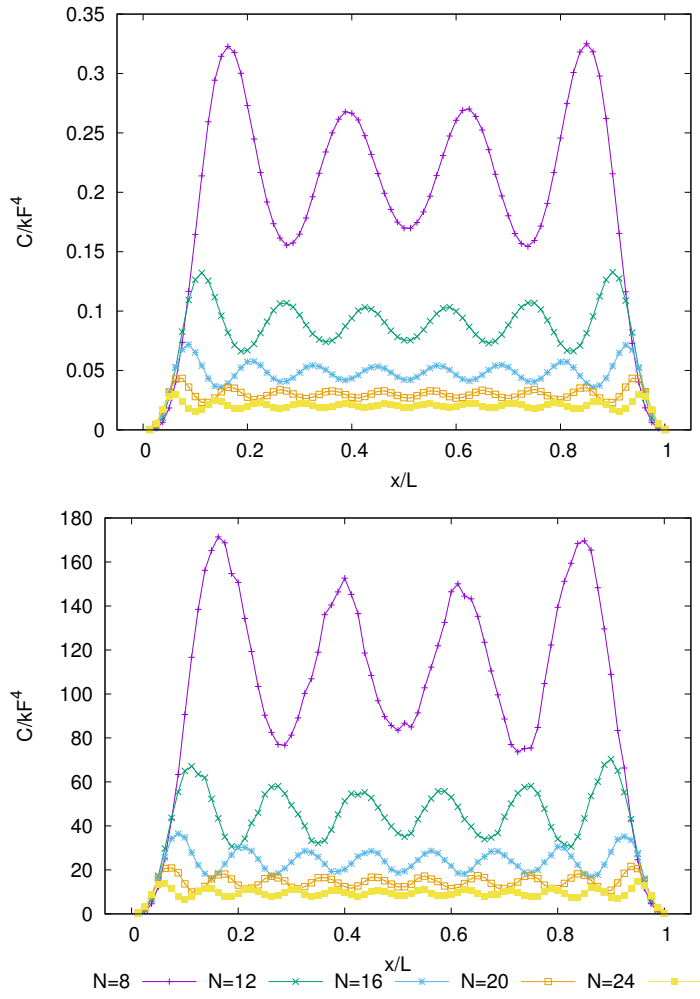


Figure 4.7: Contact density  $\mathcal{C}(x/L)$  as a function of the scaled position  $x/L$  for  $N_x = 80$  at weak coupling ( $\gamma = 0.2$ , top panel) and strong coupling ( $\gamma = 3.0$ , bottom panel), for particle numbers  $N = 8, 12, 16, 20, 24$  (top to bottom).

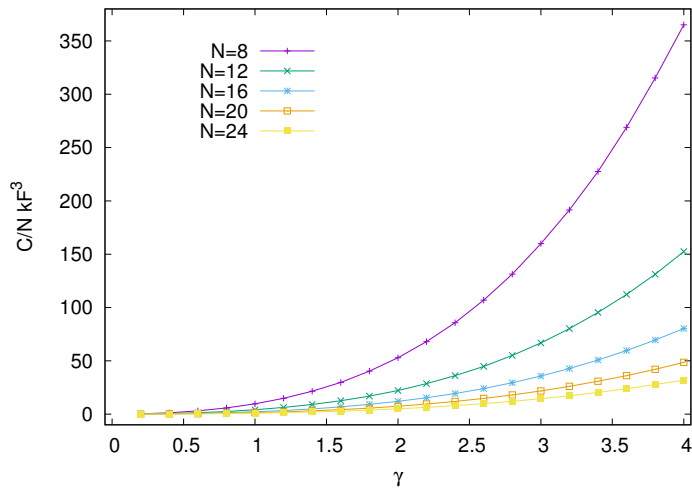


Figure 4.8: Tan's contact of  $N = 8, \dots, 24$  unpolarized fermions in a 1D segment (discretized using  $N_x = 80$  points), in units of its non-interacting counterpart  $E_{FG}$ , as a function of the dimensionless coupling  $\gamma$ .

## CHAPTER 5: Virial Projection in 1D and 2D

### Section 5.1: Introduction

The thermodynamics of strongly coupled matter is a topic of current interest in areas of physics that cover a wide range of scales, from quantum chromodynamics (QCD) (64) to ultracold atoms (65; 66; 67). The finite-temperature and density behavior of QCD is, in fact, one of the pressing challenges of that field, as QCD at finite baryon chemical potential is realized in relativistic heavy-ion collisions and deep inside neutron stars (64; 68). On the other hand, ultracold atoms have become an especially appealing laboratory to probe the properties of strongly coupled matter, due to their purity and malleability, and in particular due to the experimentalists' power to modify the interaction by dialing an external magnetic field across a Feshbach resonance (69). Naturally, this amount of control on the experimental side poses a challenge to theoretical approaches. Indeed, strongly coupled atoms can be routinely studied, but their precise quantitative analysis on the theory side usually requires ab initio non-perturbative tools such as quantum Monte Carlo methods.

An alternative way to characterize the thermodynamics of a many-body system has historically been given by the virial expansion (VE), which is non-perturbative and valid in the dilute limit. The VE is an expansion in powers of the fugacity  $z = e^{\beta\mu}$  (where  $\beta$  is the inverse temperature and  $\mu$  is the chemical potential), such that the grand-canonical partition function is written as

$$\mathcal{Z} = \sum_{n=0}^{\infty} Q_n z^n, \quad (5.1)$$

where  $Q_n$  are the  $n$ -particle canonical partition functions. We arrive at the most common form of the VE by expanding the pressure  $P$  in powers of  $z$ :

$$\beta PV = \ln \mathcal{Z} = Q_1 \sum_{n=1}^{\infty} b_n z^n, \quad (5.2)$$

where  $V$  is the ( $d$ -dimensional, spatial) volume and  $b_n$  are the virial coefficients. Other quantities of interest besides  $P$  can also be expanded in powers of  $z$  (see e.g. (70)). The appeal of the VE is that it encodes, at order  $n$ , how the 2- through  $n$ -body problems govern the physics of the many-body system. Using Eq. (5.1)

in Eq. (5.2) one sees this explicitly:

$$b_2 = \frac{Q_2}{Q_1} - \frac{Q_1}{2}, \quad (5.3)$$

$$b_3 = \frac{Q_3}{Q_1} - Q_2 + \frac{Q_1^2}{3}, \quad (5.4)$$

$$b_4 = \frac{Q_4}{Q_1} - Q_3 - \frac{Q_2^2}{2Q_1} + Q_2Q_1 - \frac{Q_1^3}{4}, \quad (5.5)$$

and so forth. The above equations are entirely based on thermodynamics and valid for arbitrary interaction and spatial dimension.

The task of calculating  $b_n$  has typically been equated with solving the  $n$ -body problem, constructing the  $Q_n$ , and inserting those in the above equations. It is therefore not surprising that second-order VEs are easily carried out, as all that is needed for  $b_2$  is the solution to the two-body problem. In fact, formulas exist for  $b_2$  for many cases, some of which we quote below, based on the celebrated Beth-Uhlenbeck result (71). Obtaining  $b_3$  and beyond, however, typically requires numerical methods (see e.g. (72; 73; 74)). Although the  $b_n$  are a proxy for other quantities, their calculation has become an attractive challenge per se, especially in cases such as the unitary limit (75) (the universal limit of zero interaction range and infinite scattering length), where the  $b_n$  represent universal constants of quantum many-body physics. For that reason, the calculation of the  $b_n$  has been vigorously pursued by several groups (76; 77; 78; 79; 80; 81; 74).

In this work we focus on the virial coefficients of the generic lattice Hamiltonian of two-species nonrelativistic fermions with zero-range interactions, i.e.

$$\hat{H} = \sum_{\mathbf{p}} \frac{\mathbf{p}^2}{2m} \hat{n}_{\mathbf{p}} - g \sum_{\mathbf{x}} \hat{n}_{\uparrow}(\mathbf{x}) \hat{n}_{\downarrow}(\mathbf{x}), \quad (5.6)$$

where the total density operator in momentum space is  $\hat{n}_{\mathbf{p}} = \hat{n}_{\uparrow, \mathbf{p}} + \hat{n}_{\downarrow, \mathbf{p}}$ , and  $\hat{n}_s(\mathbf{x})$  is the density for spin  $s$  at position  $x$ . We will use units such that  $\hbar = k_B = m = 1$ .

For the above Hamiltonian, we obtain the first six virial coefficients of the one-dimensional (1D) case, i.e. the Gaudin-Yang model (82), and the first four virial coefficients of the two-dimensional (2D) case. While the former is a classic problem that has been extensively studied (see e.g. (83) for a recent review of 1D Fermi gases), to our knowledge its virial coefficients beyond  $b_2$  have not been calculated. The 2D case, in contrast, has been under intense scrutiny in recent years, as it has been realized experimentally with ultracold atoms by several groups (84; 85; 86; 87; 88; 89; 90). Moreover, its thermal properties have been explored theoretically as well by various authors (see Ref. (91) for a review) and its virial coefficients  $b_2$  and  $b_3$  have been known for a few years.

To determine  $b_n$ , we developed two stochastic methods which bypass the direct solution of the  $n$ -body problem. One of our objectives is to show that it is possible to design methods that allow to calculate high-order virial coefficients without solving the  $n$ -body problem, at the price of reduced precision. The first method is based on the idea of Fourier particle-number projection of nuclear physics (92), as applied to the auxiliary field path-integral representation of  $\mathcal{Z}$ . That approach naturally yields a complex measure, and for that reason we implement the complex Langevin algorithm to sample the field (93). The resulting method is able to compute high-order virial coefficients at weak couplings and can also estimate the radius of convergence  $\alpha_0$  of the VE as a function of the coupling strength. The second method consists in the stochastic evaluation of the *change* in the virial coefficients due to interaction effects,  $\Delta b_n$ . This second method uses the definition of the  $b_n$  in their path-integral form derived from  $\mathcal{Z}$ , but it does not use  $\mathcal{Z}$  directly. Thus, it is able to evaluate  $b_n$  at stronger couplings than the projection method, but gives no information about the radius of convergence. Besides those two stochastic methods, we implement a semiclassical lattice approximation (SCLA) at leading order (LO). In all cases we use the known results for  $\Delta b_2$  as the renormalization condition that connects the bare lattice coupling to the physical coupling.

The generalization of our approaches to higher dimensions is straightforward. In fact, the generic system studied here (a nonrelativistic gas with zero-range interactions) has been under intense investigation both theoretically and experimentally in the last decade in 1D, 2D, and 3D, and analytic results exist for  $b_2$  in all dimensions based on the Beth-Uhlenbeck formula mentioned above (71; 94; 95; 96; 76).

## Section 5.2: Formalism

### 5.2.1: Stochastic Methods

Using Eq. (5.2), the  $b_n$  can be obtained by Fourier projection. Following that route, we define the function

$$b_n(\alpha) \equiv \frac{1}{Q_1} \int_0^{2\pi} \frac{d\phi}{2\pi} e^{i\phi n} \ln \mathcal{Z}[z \rightarrow \alpha e^{-i\phi}] = b_n \alpha^n. \quad (5.7)$$

To proceed, we write  $\mathcal{Z}$  as a path integral over a Hubbard-Stratonovich (HS) field  $\sigma$  (see e.g. (107; 98)),  $\mathcal{Z} = \int \mathcal{D}\sigma \det^2 M[\sigma, z]$ , where we focus on unpolarized systems, thus the power of 2. The matrix  $M[\sigma, z]$  encodes the dynamics and parameters of the system of interest; in particular, the  $z$  dependence appears as  $M[\sigma, z] = \mathbb{1} + zU[\sigma]$ , where  $U[\sigma]$  contains the kinetic energy and interaction information (see (107) for details on the specific form of  $M[\sigma, z]$  and  $U[\sigma]$ ). Setting  $z \rightarrow \alpha e^{-i\phi}$  and differentiating both sides with respect to  $\alpha$  yields

$$b_n = \frac{1}{n\alpha^{n-1}} \frac{1}{Q_1} \int_0^{2\pi} \frac{d\phi}{2\pi} e^{i\phi n} \langle \text{tr} [2M^{-1} \partial M / \partial \alpha] \rangle_{\phi, \alpha}, \quad (5.8)$$

where  $P[\sigma, z] \equiv \det^2 M[\sigma, z]/\mathcal{Z}[z]$ , and we have used angle brackets as a shorthand notation for the expectation value with  $P[\sigma, \alpha e^{i\phi}]$  as a weight. In practice, we use a discrete Fourier transform such that

$$\frac{\partial b_n(\alpha)}{\partial \alpha} = \frac{1}{Q_1} \frac{1}{N_k} \sum_{k=0}^{N_k-1} e^{i\phi_k n} \langle \text{tr} [2M^{-1} \partial M / \partial \alpha] \rangle_{\phi_k, \alpha}. \quad (5.9)$$

where  $\phi_k = 2\pi k/N_k$ ,  $k = 0, \dots, N_k-1$ , and  $N_k$  is the number of discretization points. This is the fundamental equation of the proposed approach. Calculating the expectation values inside the sum in Eq. (5.9) for  $N_k$  values of  $\phi_k$ , and carrying out the Fourier sum for different values of  $n$ , one obtains the desired  $b_n$ . In such a calculation, the results for  $b_n$  must be independent of  $\alpha$ , such that that variable can be used as a measure of the reliability of the method. In practice we plot

$$b_n = \frac{1}{n\alpha^{n-1}} \frac{\partial b_n(\alpha)}{\partial \alpha}, \quad (5.10)$$

as a function of  $\alpha$  and fit a constant. The  $\alpha^n$  dependence of the  $n$ -th order term is the main limiting factor in extracting high-order virial coefficients. To overcome that limitation, it is desirable to make  $\alpha$  as large as possible but less than unity to remain in the virial region. Thus, deviations in Eq. (5.10) from constant behavior as  $\alpha$  is *decreased* are indicative of uncertainties due to statistical noise or insufficient Fourier points. On the other hand, non-constant behavior as  $\alpha$  is *increased* indicates the appearance of roots of  $\mathcal{Z}$  in the complex- $z$  plane, which yield branch-cut singularities in  $\ln \mathcal{Z}$  and point to the radius of convergence of the VE (see Supplemental Materials).

Evaluating the expectation values in Eq. (5.9) involves calculations that suffer from a phase problem, as  $P[\sigma, \alpha e^{-i\phi}]$  will generally be a complex weight. To address that issue, we turn to complex stochastic quantization via the complex Langevin (CL) method, which has recently been applied to the characterization of other aspects of non-relativistic fermions (99; 100; 101; 102). We employ the CL method in the same way described in Ref. (99) (where it was applied to address repulsive interactions), setting the fugacity to  $z \rightarrow \alpha e^{-i\phi_k}$ . The quantity in the expectation value appearing in Eq. (5.9), namely  $\text{tr} [M^{-1} \partial M / \partial \alpha]$ , corresponds to the density of the system. Thus, the proposed approach effectively consists in the Fourier projection of the virial coefficients from the density equation of state, which is reminiscent of other approaches such as those of Refs. (79; 78; 81; 96).

Our second method calculates the interaction effects on  $b_n$  using their definition in terms of path integrals, derived analytically from the path integral form of  $\mathcal{Z}$ . In that formalism, the change in  $b_n$  due to interactions

is

$$\begin{aligned}\Delta b_2 &= \frac{\Delta Q_{1,1}}{Q_1}, & \Delta b_3 &= \frac{2\Delta Q_{2,1}}{Q_1} - Q_1 \Delta b_2, \\ \Delta b_4 &= \frac{2\Delta Q_{3,1} + \Delta Q_{2,2}}{Q_1} - \frac{Q_1^2}{2} \Delta b_2 - \frac{Q_1}{2} (\Delta b_2^2 + 2\Delta b_3),\end{aligned}$$

where  $Q_{m,n}$  is the partition function for  $m$  particles of one species and  $n$  of the other, and  $\Delta Q_{m,0} = 0$  because we only have contact interactions. The VE of the fermion determinant yields

$$\begin{aligned}Q_{1,1} &= \int \mathcal{D}\sigma \operatorname{tr}^2 U[\sigma], & (5.11) \\ 2Q_{2,1} &= \int \mathcal{D}\sigma \operatorname{tr}^3 U[\sigma] \left(1 - \frac{\operatorname{tr} U^2[\sigma]}{\operatorname{tr}^2 U[\sigma]}\right), \\ 2Q_{3,1} &= \frac{1}{3} \int \mathcal{D}\sigma \operatorname{tr}^4 U[\sigma] \left(1 - \frac{3 \operatorname{tr} U^2[\sigma]}{\operatorname{tr}^2 U[\sigma]} + \frac{2 \operatorname{tr} U^3[\sigma]}{\operatorname{tr}^3 U[\sigma]}\right), \\ Q_{2,2} &= \frac{1}{4} \int \mathcal{D}\sigma \operatorname{tr}^4 U[\sigma] \left(1 - \frac{\operatorname{tr} U^2[\sigma]}{\operatorname{tr}^2 U[\sigma]}\right)^2,\end{aligned}$$

and so on at higher orders. Inserting these expressions in Eq. (5.11) (and their noninteracting versions) yields stochastic formulas for  $\Delta b_n$ . To evaluate those, we use the usual two-species action  $S[\sigma, z] = -2 \ln \det M[\sigma, z]$  to sample  $\sigma$ , and extrapolate the results to the  $z = 0$  limit. This method is similar in spirit to that of Ref. (74), but employs a field integral representation instead of an integral over particle paths.

## 5.2.2: Semiclassical Lattice Approximation

Using the formulas of Eq. (5.11), it is possible to implement what we call the semiclassical lattice approximation, in which we neglect the commutator of the kinetic energy matrix  $T$  and the potential energy matrix  $V$  at leading order. Thus, the matrix  $U[\sigma]$  becomes simply  $U[\sigma] = e^{-\beta T} \mathcal{V}[\sigma]$ , where  $\mathcal{V}[\sigma]$  encodes the specific form of the HS transformation. Such an approximation amounts to a coarse discretization of the imaginary-time direction, which nevertheless becomes exact in two different limits:  $V \rightarrow 0$  and  $T \rightarrow 0$ . In between those limits, higher orders in the SCLA can be reached by using finer temporal meshes; we leave calculations beyond LO to future work. At LO, the path integrals can be carried out analytically:

$$\Delta b_3 = -2^{1-d/2} \Delta b_2, \quad (5.12)$$

$$\begin{aligned}\Delta b_4 &= 2(3^{-d/2} + 2^{-d-1}) \Delta b_2 \\ &\quad + 2^{1-d/2} (2^{-d-1} - 1) (\Delta b_2)^2,\end{aligned} \quad (5.13)$$

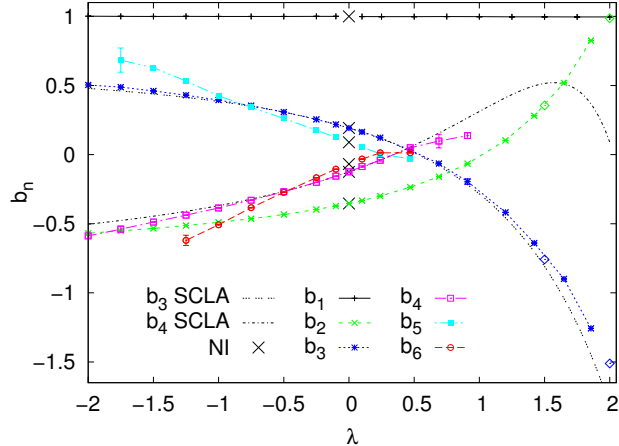


Figure 5.1: Virial coefficients  $b_n$  for  $n = 1 - 6$  for the 1D Fermi gas, as a function of the dimensionless coupling  $\lambda$ , as obtained with our projection method. Crosses on the  $y$  axis denote the non-interacting values  $b_n = (-1)^{n+1}n^{-3/2}$ . The leading order of the semiclassical lattice approximation (LO-SCLA) is shown with a dashed-dotted line for  $\Delta b_3$  and with a dashed line for  $\Delta b_4$ . Green and blue diamonds show the results obtained with our second stochastic method, for comparison.

where we present our results in terms of  $\Delta b_2$  because we will use the exact  $\Delta b_2$  as a renormalization condition.

## Section 5.3: Results

### 5.3.1: Virial coefficients in 1D

To analyze the 1D case, our calculations used a lattice of spatial size  $N_x = 30$  and temporal size  $N_\tau = 120 - 200$ . We otherwise used the same lattice parameters as those of Ref. (99). The number of Fourier points was set to  $N_k = 30$  for the main results, with explorations covering  $N_k = 20 - 100$  showing no significant variation. By definition,  $b_1 = 1$  and, for the 1D contact interaction studied here (see Ref. (94)),

$$b_2^{(1D)} = -\frac{1}{\sqrt{2}} + \frac{e^{\lambda^2/4}}{2\sqrt{2}}[1 + \text{erf}(\lambda/2)], \quad (5.14)$$

where  $\text{erf}$  is the error function and  $\lambda$  is the dimensionless coupling. The noninteracting limit is  $b_2^{(1D)} \rightarrow -\frac{1}{2\sqrt{2}}$ . We will use the analytic form of Eq. (5.14) as a renormalization condition, i.e. to *define* the coupling  $\lambda$  from our lattice determination of  $b_2$ . As a consequence, our plots of  $b_2$  below will be exact by definition. Our first result appears in Fig. 5.1, where we map out the  $\lambda$  dependence of the first six  $b_n$ . The smoothness of the results gives confidence that the method works as expected. Perhaps the most prominent feature in Fig. 5.1 is the monotonicity of the stochastic data for each  $b_n$ : besides the constant  $b_1 = 1$ , the even  $n$  coefficients increase as a function of  $\lambda$ , whereas the odd ones decrease. More specifically, toward the repulsive

side ( $\lambda < 0$ ), the  $b_n$  grow in magnitude and maintain their sign: the even ones which start out negative at  $\lambda = 0$  become more negative and the odd ones which start positive grow as well. Toward the attractive side, the monotonic behavior implies that in a wide region  $0 < \lambda < 1$  many of the coefficients cross the  $b_n = 0$  line, which suggests the VE may be useful up to  $z \simeq 0.5$  (see however our results below for the radius of convergence). Beyond that point, the coefficients grow in magnitude and eventually change sign relative to their noninteracting values. Using the second stochastic method (applied below in 2D), we checked the above results of Fig. 5.1 for  $b_2$  and  $b_3$ .

### 5.3.2: Radius of convergence via projection method

In the inset of Fig. 5.2 we show  $b_n$  as a function of  $\alpha$  (see main text). As anticipated, for each virial order  $n$  there is a region around  $\alpha = 0$  for which  $b_n$  does not vary, which allows us to extract the value of  $b_n$  itself. Beyond a  $\lambda$ -dependent value of  $\alpha$ , however, the calculation runs into the roots of  $\ln \mathcal{Z}$  in the complex plane and the constant behavior is lost. We stress that this is not due to systematic or statistical effects, but rather a feature of the calculation that represents the radius of convergence  $\alpha_0$  of the virial expansion. The main plot of Fig. 5.2 shows our results for  $\alpha_0$  as a function of  $\lambda$ , obtained by locating the point where the constant behavior as a function of  $\alpha$  is lost. Our results are consistent with the expected value  $\alpha_0 = 1$  for the noninteracting case, which is easily derived by noting that the noninteracting partition function has a root at  $z = -1$ . The dashed line in the main plot of Fig. 5.2 shows a fit  $\alpha_0(\lambda) = 1/(1 + C|\lambda|)$ , where  $C \simeq 3.05(5)$  on repulsive side ( $\lambda < 0$ ) and  $C \simeq 4.15(5)$  on attractive side ( $\lambda > 0$ ). While the fit is merely descriptive, it does point to a nontrivial feature, namely the non-analyticity of  $\alpha_0$  around the maximum at  $\lambda = 0$ : the data appears to display a cusp.

### 5.3.3: Virial coefficients in 2D

Besides the 1D case above, we applied the second method to the 2D analogue, which was studied up to second order in the VE in Refs. (95; 103; 96) and up to third order in Refs. (72; 73). The Hamiltonian is essentially identical to that of Eq. (5.6), generalized to 2D. In that case, the coupling  $g$  becomes simply a bare parameter and the physical coupling is given by  $\lambda_2 = \sqrt{\beta\varepsilon_B}$ , where  $\varepsilon_B$  is the binding energy of the two-body system. The second-order virial coefficient in 2D is known (95; 96; 104) and given by

$$b_2^{(2D)} = -\frac{1}{4} + e^{\lambda_2^2} - \int_0^\infty \frac{dy}{y} \frac{2e^{-\lambda_2^2 y^2}}{\pi^2 + 4 \ln^2 y}. \quad (5.15)$$

The noninteracting limit yields  $b_2^{(2D)} \rightarrow -\frac{1}{4}$ . As in our 1D calculations, we used Eq. (5.15) to define  $\lambda_2$  by calculating  $b_2$  on the lattice. In Fig. 5.3 we show our results for  $b_2$ ,  $b_3$ , and  $b_4$ . By definition,  $b_2$  is reproduced exactly, and the output of the calculation is  $b_3$  and  $b_4$ .

#### 5.3.4: Semiclassical lattice approximation

The predictions of the LO-SCLA are compared with those of our stochastic methods in Figs. 5.1 and 5.3. The LO-SCLA predicts in 1D:  $\Delta b_3 = -\sqrt{2}\Delta b_2$  and  $\Delta b_4 = (4\sqrt{3} + 3)/6 \Delta b_2 - 3\sqrt{2}/4 (\Delta b_2)^2$ ; and in 2D:  $\Delta b_3 = -\Delta b_2$  and  $\Delta b_4 = 11/12 \Delta b_2 - 7/8 (\Delta b_2)^2$ . As is clear in Figs. 5.1 and 5.3, there are differences between those predictions and the stochastic results. However, it is remarkable that at LO the SCLA predicts not only the correct sign of  $\Delta b_3$  but also a deviation smaller than 10% in 1D and close to 20% in 2D, at least for the regime of couplings that studied here. Such results encourage higher orders studies of the SCLA, which will be carried out elsewhere.

While we focus here on 1D and 2D, it is also interesting to test the predictions of the LO-SCLA for the 3D Fermi gas at unitarity. There, known results (see e.g. (77; 78; 79; 80; 81)) give  $\Delta b_2 = 1/\sqrt{2}$  and  $\Delta b_3 = -0.35505\dots$ , such that  $\Delta b_3/\Delta b_2 \simeq -0.50\dots$ , while the LO-SCLA yields  $\Delta b_3/\Delta b_2 = -1/\sqrt{2} \simeq -0.707$ , thus matching the correct sign of  $\Delta b_3$  but overshooting its magnitude by about 40%. Similarly, the most accurate result at unitarity (74) is  $b_4 = 0.078(18)$ , which yields  $\Delta b_4 = 0.109(18)$ , while the LO-SCLA yields  $\Delta b_4 = 0.029\dots$ , which matches the sign of the expected result but undershoots its magnitude by roughly a factor of 3. Nevertheless, these results are encouraging when considering that they come from a mere leading-order approximation. From the equations in main text it is easy to see that

$$\Delta b_2 = \frac{\Delta Q_{1,1}}{Q_1} = \frac{1}{Q_1} \int \mathcal{D}\sigma (\text{tr}^2 U[\sigma] - \text{tr}^2 U_0), \quad (5.16)$$

where  $U_0 = e^{-\beta T}$  is the noninteracting transfer matrix ( $T$  being the kinetic energy matrix), and  $U[\sigma] = e^{-\beta T} \mathcal{V}[\sigma]$  ( $\mathcal{V}$  being the chosen Hubbard-Stratonovich representation of the interaction). Carrying out the path integrals, it is straightforward to find

$$\Delta b_2 = (e^{\beta g} - 1) \frac{V}{Q_1} \left( \frac{\text{tr} U_0}{V} \right)^2 \quad (5.17)$$

where  $Q_1/V \rightarrow 2/\lambda_T^d$  in the continuum limit in  $d$  spatial dimensions and all lengths are in units of the lattice spacing  $\ell = 1$ . Moreover,  $\text{tr} U_0 = Q_1/2$ , such that, in the continuum limit,

$$\Delta b_2 = \frac{1}{\lambda_T^d} \frac{e^{\beta g} - 1}{2}. \quad (5.18)$$

The calculation of  $\Delta b_3$  is only slightly more tedious and yields

$$\Delta b_3 = \frac{2\Delta Q_{1,1}}{Q_1} - Q_1 \Delta b_2 = -\frac{1}{\lambda_T^d} \frac{e^{\beta g} - 1}{2^{d/2}}. \quad (5.19)$$

We thus obtain the result advertised in the main text, namely

$$\Delta b_3 = -2^{1-d/2} \Delta b_2. \quad (5.20)$$

The calculation of  $\Delta b_4$  follows the same steps but yields a contribution that is quadratic in  $\Delta b_2$ :

$$\Delta b_4 = 2(3^{-d/2} + 2^{-d-1})\Delta b_2 \quad (5.21)$$

$$+ 2^{1-d/2} (2^{-d-1} - 1) (\Delta b_2)^2. \quad (5.22)$$

### 5.3.5: Systematic effects

Because we chose a lattice regularization to carry out our calculations, there are a few systematic effects that need to be taken into account. First of all, we have put the system on a lattice and must describe how to take the continuum limit. That amounts to enlarging the window  $\ell \ll \lambda_T \ll L$ , where  $\ell = 1$ ,  $L = N_x \ell$ , and  $\lambda_T = \sqrt{2\pi\beta}$  is the thermal wavelength.

Our main results correspond to  $N_x = 30$  and  $\lambda_T \simeq 7$ , such that the above window is well satisfied. As an illustration of the size of the finite- $N_x$  effects, we show results for varying  $N_x$  in Fig. 5.4 (top). The variation is appreciable but small on the scale of the corresponding plot in the main text.

The second systematic effect to account for is the number of Fourier points  $N_k$  used for the projection. Relying on Nyquist's theorem, taking  $N_k$  at least twice as large as the highest desired virial coefficient  $n_{\max}$  should be sufficient. However, that lower bound turns out to be much too optimistic in practice. As a conservative choice, we set  $N_k = 30$  and find that it enables projections up to  $n = 6$  with up to two decimal places. Note that the computation time scales linearly with  $N_k$  and is perfectly parallelizable in that variable.

The third systematic effect is the dependence on the temporal lattice spacing  $\tau$ . We have tested  $\tau = 0.05$ , 0.25, and 0.5, as shown in Fig. 5.4 (bottom). Remarkably, the variation is small on the scale of the plot in the main figure (somewhat zoomed-in here).

## Section 5.4: Summary and Conclusions

We have calculated the first few virial coefficients  $b_n$  of two systems: fermions in 1D and 2D, both with a contact interaction. In 1D, we evaluated the first six  $b_n$  as a function of the coupling strength  $\lambda$  in both attractive and repulsive regimes. In the 2D case, we calculated  $\Delta b_3$ , and  $\Delta b_4$  for attractive interactions. To carry out our calculations, we implemented two different stochastic lattice methods. The first method relied on projecting the  $b_n$  out of the path integral form of the density equation of state. The second approach used a path-integral representation of the virial coefficients, as derived from the path integral form of  $\mathcal{Z}$ . The latter method enables calculations in a way that requires neither matrix inversion nor determinants, but which is sensitive to statistical noise as  $n$  is increased, due to the various volume-scaling cancelations required to resolve each  $b_n$  from the canonical partition functions. However, that noise can at least partially be addressed by obtaining more samples, a task that can be carried out in a perfectly scalable fashion. The stochastic approaches proposed here are not as precise as exact diagonalization, but provide a systematic way to high-order coefficients without solving the  $n$ -body problem. Finally, we used a semiclassical approximation which at leading order compares remarkably well with our stochastic results for the coupling strengths studied.

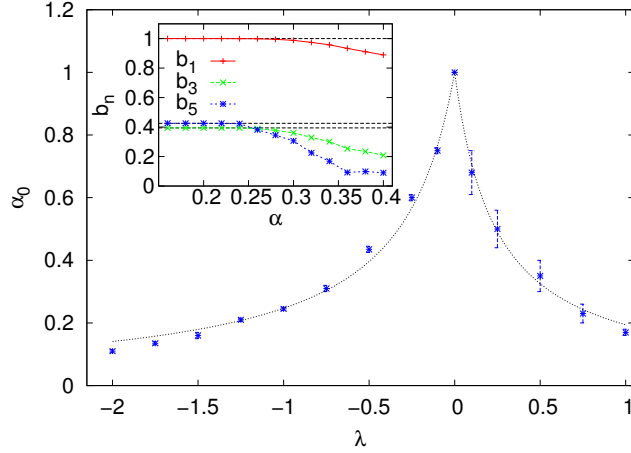


Figure 5.2: Estimate of the radius of convergence  $\alpha_0$  of the virial expansion as a function of the coupling  $\lambda$ . Inset:  $b_n$  for  $n = 1, 3, 5$  for  $\lambda = -1$ . Constant behavior as a function of  $\alpha$  is expected when the coefficient of the  $n$ -th power of  $z$  is extracted successfully. Deviation from such a constant as  $\alpha$  is increased shows the appearance of roots of  $\mathcal{Z}$  in the complex- $z$  plane, which yields the estimate  $\alpha_0$  for the radius of convergence shown in the main plot.

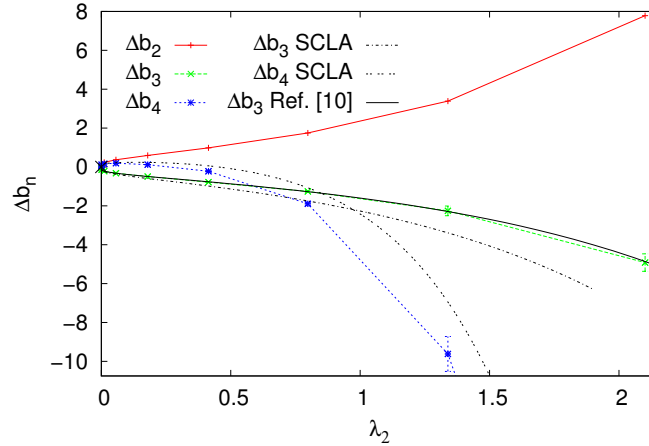


Figure 5.3: Interaction change of the virial coefficients  $\Delta b_n$  for  $n = 2 - 4$  for the 2D Fermi gas, as a function of the dimensionless coupling  $\lambda_2$ . The solid red line connects the data for  $\Delta b_2$ , the green shows  $\Delta b_3$ , and the blue shows  $\Delta b_4$ . The leading order of the semiclassical lattice approximation (LO-SCLA) is shown with a dashed-dotted line for  $\Delta b_3$  and with a dashed line for  $\Delta b_4$ . The solid black line shows the result for  $\Delta b_3$  of Ref. (73). Note that the data for  $\Delta b_2$  reproduces the exact result of Eq. (5.15) by virtue of the renormalization condition (see text).

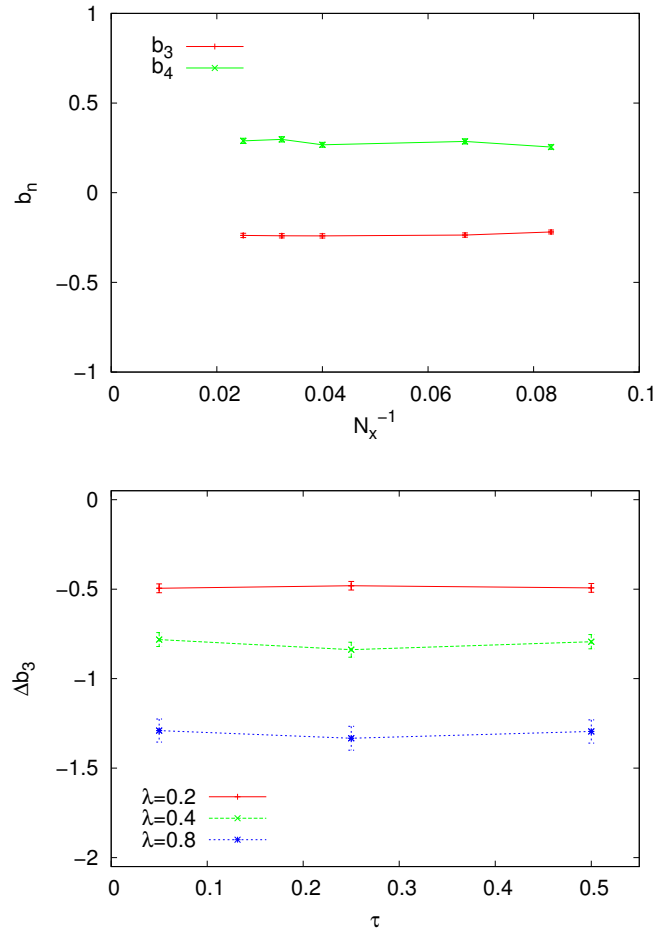


Figure 5.4: Top: Illustration of the size of the finite- $N_x$  effects on  $b_3$  and  $b_4$  in 1D at  $\lambda = 1$ . The errorbars show statistical effects. Bottom: Illustration of the size of the finite- $\tau$  effects on  $\Delta b_3$  in 2D for varying  $\lambda$ .

## CHAPTER 6: Systems with Three-Body Forces

In this chapter we describe the application of the semiclassical lattice approximation (SCLA) to the calculation of virial coefficients of systems with three-body interactions. We analyze such a case in the situation in which two-body interactions are completely turned off, in order to understand such a limiting case. As in a previous chapter, the SCLA allows us to obtain results for different spatial dimensions.

### Section 6.1: Introduction

Motivated by the recent interest in one-dimensional (1D) Fermi and Bose gases in the fine-tuned situation where only three-body interactions are present, we explore here the thermodynamics of that system in the limit of low fugacity, focusing on the fermionic case but going beyond 1D. As mentioned above, we implement the SCLA to calculate the virial coefficients  $b_n$ , and carry out their evaluation up to  $n = 5$  at leading order (LO) in that approximation. Not surprisingly, the approximation was seen in a previous chapter to work better at weak coupling, which makes sense as the radius of convergence of the virial expansion was found to be quickly reduced as a result of the interaction. In that regard, the implementation of  $\Delta b_2$  as a physical quantity (renormalization condition) in the case of two-body interactions proved to be an efficient way to approach the continuum limit. We repeat that approach here for the case of three-body forces by expressing our results entirely in terms of  $\Delta b_3$ , which is the lowest non-trivial virial coefficient that is affected by three-body forces.

### Section 6.2: Hamiltonian and virial expansion

To make contact with the extant literature on the quantum many-body problem, as well as with the rest of this thesis, we set up our formalism in the same way as for conventional Monte Carlo methods for fermions. We assume a non-relativistic kinetic energy and a two-body contact interaction, such that the Hamiltonian for two flavors  $\uparrow, \downarrow$  is  $\hat{H} = \hat{T} + \hat{V}$ , where

$$\hat{T} = \int d^d x \hat{\psi}_s^\dagger(\mathbf{x}) \left( -\frac{\hbar^2 \nabla^2}{2m} \right) \hat{\psi}_s(\mathbf{x}) \quad (6.1)$$

and

$$\hat{V} = -g_{dD} \int d^d x \hat{n}_1(\mathbf{x}) \hat{n}_2(\mathbf{x}) \hat{n}_3(\mathbf{x}), \quad (6.2)$$

where the field operators  $\hat{\psi}_s, \hat{\psi}_s^\dagger$  are fermionic fields for particles of type 1, 2, 3 (summed over  $s$  above), and  $\hat{n}_s(\mathbf{x})$  are the coordinate-space densities. In the remainder of this work, we will take  $\hbar = k_B = m = 1$ .

As mentioned in a previous chapter, the virial expansion is an expansion around the dilute limit  $z \rightarrow 0$ , where  $z = e^{\beta\mu}$  is the fugacity, i.e. it is a low-fugacity expansion. The corresponding coefficients accompanying the powers of  $z$  in the expansion of the grand-canonical potential  $\Omega$  are the virial coefficients; specifically,

$$-\beta\Omega = \ln \mathcal{Z} = Q_1 \sum_{n=1}^{\infty} b_n z^n \quad (6.3)$$

where

$$\mathcal{Z} = \text{tr} \left[ e^{-\beta(\hat{H} - \mu\hat{N})} \right] = \sum_{N=0}^{\infty} z^N Q_N \quad (6.4)$$

is the grand-canonical partition function,  $Q_1$  is the one-body partition function,  $b_1 = 1$ , and the higher-order coefficients require solving the corresponding few-body problems:

$$Q_1 b_2 = Q_2 - \frac{Q_1^2}{2!}, \quad (6.5)$$

$$Q_1 b_3 = Q_3 - b_2 Q_1^2 - \frac{Q_1^3}{3!}, \quad (6.6)$$

$$Q_1 b_4 = Q_4 - \left( b_3 + \frac{b_2^2}{2} \right) Q_1^2 - b_2 \frac{Q_1^3}{2!} - \frac{Q_1^4}{4!}, \quad (6.7)$$

$$\begin{aligned} Q_1 b_5 &= Q_5 - (b_4 + b_2 b_3) Q_1^2 - (b_2^2 + b_3) \frac{Q_1^3}{2} \\ &\quad - b_2 \frac{Q_1^4}{3!} - \frac{Q_1^5}{5!}, \end{aligned} \quad (6.8)$$

and so forth.

Since  $Q_1 \propto V$ , the above expressions display precisely how the volume dependence cancels out in each  $b_n$ . In particular, the highest power of  $Q_1$  will always involve single-particle (i.e. noninteracting) physics

and will therefore cancel in  $\Delta b_n$ :

$$Q_1 \Delta b_2 = \Delta Q_2 \quad (6.9)$$

$$Q_1 \Delta b_3 = \Delta Q_3 - \Delta b_2 Q_1^2, \quad (6.10)$$

$$Q_1 \Delta b_4 = \Delta Q_4 - \Delta \left( b_3 + \frac{b_2^2}{2} \right) Q_1^2 - \frac{\Delta b_2}{2} Q_1^3, \quad (6.11)$$

$$\begin{aligned} Q_1 \Delta b_5 &= \Delta Q_5 - \Delta(b_4 + b_2 b_3) Q_1^2 \\ &\quad - \frac{1}{2} \Delta(b_2^2 + b_3) Q_1^3 - \frac{\Delta b_2}{3!} Q_1^4, \end{aligned} \quad (6.12)$$

and so on. Note that, when only three-body interactions are present, as is the case we consider here, there is no change in the two-body spectrum, i.e.  $\Delta b_2 = 0$ . Therefore, the above expressions simplify to

$$Q_1 \Delta b_3 = \Delta Q_3, \quad (6.13)$$

$$Q_1 \Delta b_4 = \Delta Q_4 - \Delta b_3 Q_1^2, \quad (6.14)$$

$$Q_1 \Delta b_5 = \Delta Q_5 - (\Delta b_4 + b_2 \Delta b_3) Q_1^2 - \frac{\Delta b_3}{2} Q_1^3. \quad (6.15)$$

In terms of the partition functions  $Q_{MNL}$  of  $M$  particles of type 1,  $N$  of type 2, and  $L$  of type 3, we have

$$\Delta Q_3 = \Delta Q_{111}, \quad (6.16)$$

$$\Delta Q_4 = 3\Delta Q_{211}, \quad (6.17)$$

$$\Delta Q_5 = 3\Delta Q_{311} + 3\Delta Q_{221}. \quad (6.18)$$

From this last set of equations, we see that the number of non-trivial contributions to each virial coefficient is actually small. The main task is in calculating each of these terms and for that purpose we implement a semiclassical approximation, as explained below.

### Section 6.3: The semiclassical approximation at leading order

In a wide range of many-body methods, the grand-canonical partition function  $\mathcal{Z}$  is expressed as a path integral over an auxiliary Hubbard-Stratonovich (HS) field. Here we use a different route, but with the same first step: we introduce a Trotter-Suzuki (TS) factorization of the Boltzmann weight. Here, we will use the lowest-order TS factorization, however, as the proposed approximation consists in keeping only the leading

term in the following formula (105):

$$e^{-\beta(\hat{T}+\hat{V})} = e^{-\beta\hat{T}}e^{-\beta\hat{V}} \times e^{-\frac{\beta^2}{2}[\hat{T},\hat{V}]} \times \dots, \quad (6.19)$$

where the higher orders involve exponentials of nested commutators of  $\hat{T}$  with  $\hat{V}$ . Thus, the LO in this expansion consists in setting  $[\hat{T}, \hat{V}] = 0$ , which becomes exact in the limit where either  $\hat{T}$  or  $\hat{V}$  can be ignored (i.e. respectively the strong- and weak-coupling limits). Although we will not pursue orders beyond LO here, it is noteworthy that such orders can effectively be reached using a TS factorization. Indeed, the leading order can simply be viewed as the most coarse possible TS factorization, i.e. with time step  $\tau = \beta$ ; thus, higher orders  $n$  can be defined by using progressively finer discretizations, e.g.  $\tau = \beta/n$ . We leave such explorations to future work.

As the simplest example, we consider  $Q_{111}$ .

$$Q_{111} = \sum_{\mathbf{P}_j} \langle \mathbf{P} | e^{-\beta\hat{T}} e^{-\beta\hat{V}} | \mathbf{P} \rangle \quad (6.20)$$

$$= \sum_{\mathbf{P}_j} e^{-\beta(p_1^2+p_2^2+p_3^2)/2m} \langle \mathbf{P} | e^{-\beta\hat{V}} | \mathbf{P} \rangle, \quad (6.21)$$

where we have used a collective momentum index  $\mathbf{P} = (\mathbf{p}_1, \mathbf{p}_2, \mathbf{p}_3)$ . Inserting a coordinate-space completeness relation to evaluate the potential energy factor, we obtain

$$\begin{aligned} e^{-\beta\hat{V}}|\mathbf{X}\rangle &= \prod_{\mathbf{z}} (1 + C\hat{n}_1(\mathbf{z})\hat{n}_2(\mathbf{z}))|\mathbf{X}\rangle \\ &= |\mathbf{X}\rangle + C \sum_{\mathbf{z}} \delta(\mathbf{x}_1 - \mathbf{z})\delta(\mathbf{x}_2 - \mathbf{z})\delta(\mathbf{x}_3 - \mathbf{z})|\mathbf{X}\rangle \\ &= [1 + C\delta(\mathbf{x}_1 - \mathbf{x}_3)\delta(\mathbf{x}_2 - \mathbf{x}_3)]|\mathbf{X}\rangle, \end{aligned} \quad (6.22)$$

where  $C = e^{\beta g_{dD}} - 1$ , we used the fermionic relation  $\hat{n}_s^2 = \hat{n}_s$ , and again we introduced a collective index  $\mathbf{X} = (\mathbf{x}_1, \mathbf{x}_2, \mathbf{x}_3)$ . The  $C$ -independent term yields the noninteracting result, such that we may write

$$\begin{aligned} \Delta Q_{111} &= C \sum_{\mathbf{P}_j, \mathbf{x}_k} e^{-\beta(p_1^2+p_2^2+p_3^2)/2m} \\ &\quad \times \delta(\mathbf{x}_1 - \mathbf{x}_3)\delta(\mathbf{x}_2 - \mathbf{x}_3) |\langle \mathbf{X} | \mathbf{P} \rangle|^2, \end{aligned} \quad (6.23)$$

which simplifies substantially when using a plane wave basis since  $|\langle \mathbf{X} | \mathbf{P} \rangle|^2 = 1/V^3$ . We then find

$$\Delta Q_{111} = C \frac{Q_{100}^3}{V^2} \quad (6.24)$$

where

$$Q_{100} = \sum_{\mathbf{p}_1} e^{-\beta p_1^2/2m}. \quad (6.25)$$

Thus,

$$\Delta b_3 = C \frac{Q_{100}^3}{V^2 Q_1} = C \frac{Q_1^2}{27V^2}, \quad (6.26)$$

where we used  $Q_1 = 3Q_{100}$ . We will use this result, together with the exact solution of Ref. (), to define  $C$  at finite temperature, i.e. to renormalize the problem. Thus,  $\Delta b_3$  will play the role of the renormalized dimensionless coupling constant.

The general form of the change  $\Delta Q_{MNL}$  in the partition function for  $M$  spin-up particles and  $N$  spin-down particles, with a contact interaction, is given by

$$\Delta Q_{MNL} = \sum_{\mathbf{P}, \bar{\mathbf{X}}} e^{-\beta \bar{\mathbf{P}}^2/2m} |\langle \bar{\mathbf{X}} | \bar{\mathbf{P}} \rangle|^2 (C f_a(\bar{\mathbf{X}}) + C^2 f_b(\bar{\mathbf{X}}) + \dots). \quad (6.27)$$

where  $\bar{\mathbf{P}}, \bar{\mathbf{X}}$  represent all momenta and positions of the  $M + N + L$  particles, and the functions  $f_a, f_b, \dots$ , which encode the matrix element of  $e^{-\beta \hat{V}}$ , depend on the specific  $MNL$  case being considered. The wavefunction  $\langle \bar{\mathbf{X}} | \bar{\mathbf{P}} \rangle$  is a product of three Slater determinants which, if using a plane-wave single-particle basis, leads to Gaussian integrals over the momenta  $\bar{\mathbf{P}}$ .

## Section 6.4: Results

### 6.4.1: Virial coefficients

Using the steps outlined above, we have calculated  $\Delta b_4$  and  $\Delta b_5$ , which take the following form on the lattice:

$$\Delta b_4 = -C \frac{Q_1 Q_1(2\beta)}{18V^2} = -\frac{3}{2} \frac{Q_1(2\beta)}{Q_1} \Delta b_3, \quad (6.28)$$

$$\begin{aligned} \Delta b_5 &= C \left( \frac{Q_1(2\beta)^2}{9V^2} + \frac{Q_1 Q_1(3\beta)}{27V^2} \right) \\ &= \left( \frac{3Q_1(2\beta)^2}{Q_1^2} + \frac{Q_1(3\beta)}{Q_1} \right) \Delta b_3, \end{aligned} \quad (6.29)$$

for the fermionic three-species system with a contact interaction, in  $d$  spatial dimensions. In the last equation, the first term on the right-hand side represents the contribution of  $Q_{221}$ , and the second term that of  $Q_{311}$ .

Taking the continuum limit, it is easy to perform the resulting Gaussian integrals to obtain

$$\Delta b_4 = -\frac{3}{2^{d/2+1}} \Delta b_3, \quad (6.30)$$

$$\Delta b_5 = \left( \frac{3}{2^d} + \frac{1}{3^{d/2}} \right) \Delta b_3. \quad (6.31)$$

Using these results, one may calculate the pressure, density, compressibility and even Tan's contact (with knowledge of  $\Delta b_3$  as a function of the interaction strength, e.g.  $\beta\epsilon_B$  in 1D, where  $\epsilon_B$  is the trimer binding energy). In order to provide a description of the thermodynamics that is as universal as possible across spatial dimensions, we will use here  $\Delta b_3$  as the measure of the interaction strength and display our results in terms of that parameter. Furthermore, we will identify the (dimensionless) contact density as

$$\mathcal{C} = \frac{\lambda_T^d}{V} \frac{\partial \ln \mathcal{Z}}{\partial \Delta b_3}, \quad (6.32)$$

which differs from the conventional definition by a chain-rule factor  $\partial \Delta b_3 / \partial \lambda$  (to be determined by solving the 3-body scattering problem), where  $\lambda$  is the  $d$ -dimensional coupling constant. To make the expression dimensionless, we have used the thermal wavelength  $\lambda_T = \sqrt{2\pi\beta}$ .

#### 6.4.2: Thermodynamics and contact across dimensions

The interaction change in the pressure  $\Delta P$  can be written in dimensionless form in arbitrary dimension as

$$\left( \frac{\beta V}{Q_1} \right) \Delta P = \sum_{k=1}^{\infty} \Delta b_k z^k. \quad (6.33)$$

Similarly, the interaction change in the density can be written as

$$\left( \frac{V}{Q_1} \right) \Delta n = \sum_{k=1}^{\infty} k \Delta b_k z^k, \quad (6.34)$$

and, using our definition of the contact in Eq. (6.32),

$$\Delta \mathcal{C} = \frac{\lambda_T^d Q_1}{V} \sum_{k=1}^{\infty} \frac{\partial \Delta b_k}{\partial \Delta b_3} z^k. \quad (6.35)$$

Implementing our LO-SCLA results, we obtain

$$\left(\frac{\beta V}{Q_1}\right) \Delta P \simeq \Delta b_3 z^3 \left[ 1 - \frac{3}{2^{d/2+1}} z + \left( \frac{3}{2^d} + \frac{1}{3^{d/2}} \right) z^2 \right], \quad (6.36)$$

$$\left(\frac{V}{Q_1}\right) \Delta n \simeq 3 \Delta b_3 z^3 \left[ 1 - \frac{4}{2^{d/2+1}} z + \frac{5}{3} \left( \frac{3}{2^d} + \frac{1}{3^{d/2}} \right) z^2 \right], \quad (6.37)$$

$$\Delta \mathcal{C} \simeq \frac{\lambda_T^d Q_1}{V} z^3 \left[ 1 - \frac{3}{2^{d/2+1}} z + \left( \frac{3}{2^d} + \frac{1}{3^{d/2}} \right) z^2 \right]. \quad (6.38)$$

Again, the above expressions are the representations of the interaction dependence of the pressure, eq. 6.36, density, eq. 6.37, and contact, eq. 6.38, to order  $b_5$  in the virial expansion. Since we are dealing with three-body interactions, to this order in the virial expansion we expect these quantities to be directly proportional to  $\Delta b_3$ , which again is the measure of the three-body interaction strength. Using the SCLA to leading order we do indeed see this scaling in these results. Likewise, we would expect that if we took these results to order six in the virial expansion, then there would be a  $(\Delta b_3)^2$  term. This is true as there would be two sets of three particles available to interact.

Notice that for each of these expressions we expect a positive definite value across all dimensions, and across all values of  $\ln z = \beta\mu$ . We can see an example of this in figure 6.1, which shows the interaction dependence of the pressure and density plotted against  $\ln z = \beta\mu$  for a single value of  $\Delta b_3$ . This will hold for the contact as well because the dominant orders at positive and negative value of  $\beta\mu$  are indeed positive. We need only represent one value of  $\Delta b_3$  in these plots as the pressure and density are directly proportional to this value. Finally, we do see a crossing of the pressure plot of dimensions one, two, and three at a value of  $\beta\mu = -1.12$ . We also see a similar crossing in the density plot at a value of  $\beta\mu = -1.39$ .

## Section 6.5: Summary and Conclusions

In this chapter we have calculated the high-temperature thermodynamics of three-flavored Fermi gases with a contact three-body interaction in  $d$  spatial dimensions. To that end, we have implemented the LO-SCLA to the virial coefficients and in that context established a relation between the first few non-trivial virial coefficients, namely  $\Delta b_4$ ,  $\Delta b_5$ , as functions of  $\Delta b_3$ . Using that LO-SCLA, we calculated the pressure, density, and Tan's contact as functions of the fugacity  $z$ , interaction strength (as determined by  $\Delta b_3$ ), and the number of spatial dimensions. To the best of our knowledge, this is the first time that the thermodynamics of these classic (and simple!) systems has been examined. In that regard, our results constitute predictions for upcoming ultracold atom experiments.

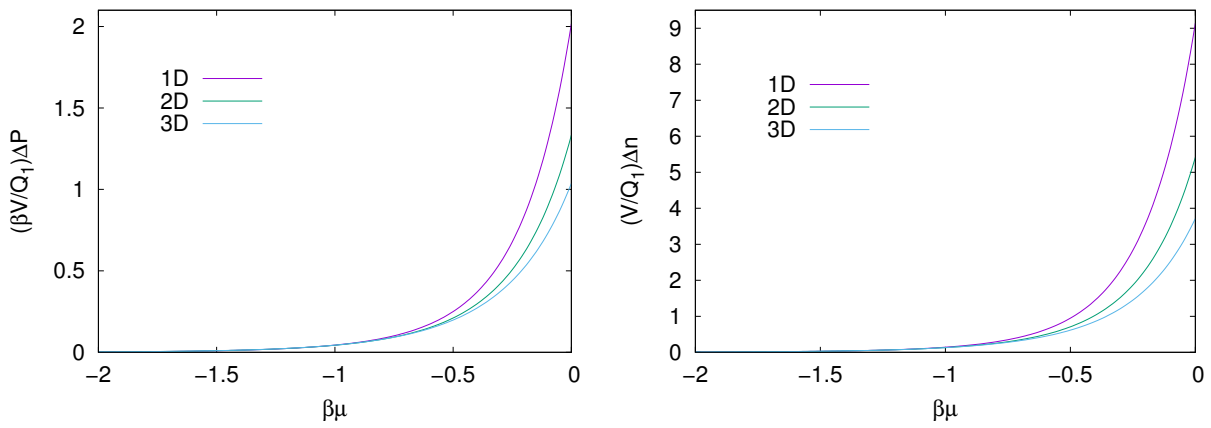


Figure 6.1: Above are plots of the three body pressure (left) and density (right) equations of state to order five in the virial expansion in their dimensionless form in one two and three dimensions plotted against the log of the fugacity,  $\ln z = \beta\mu$ . We have represented only one value of  $\Delta b_3$  here as the values are directly proportional to this value.

## BIBLIOGRAPHY

- [1] J.R. McKenney, C.R. Shill, W.J. Porter, J.E. Drut, *Journal of Phys. B* **49**, 225001 (2016)
- [2] C.R. Shill, J.E. Drut, *EPJ Web of Conferences* **175**, 03003 (2018)
- [3] C.R. Shill, J.E. Drut, *Phys. Rev. A* **98**, 053615 (2018)
- [4] T.C. Stoof, B. Gubbels, B.M. Dickerscheid, *Ultracold Quantum Fields*; Springer, 2009.
- [5] P. Kapitza, *Nature* **141**, 74 (1938).
- [6] N.S. Bose, *Z. Phys.* **26**, 178 (1924).
- [7] H.K. Onnes, *Comm. Phys. Lab. Univ. Leiden*, Nos. 119, 120, 122 (1911).
- [8] J. Bardeen, L.N. Cooper, J.R. Schrieffer, *Phys. Rev.* **108**, 1175 (1957).
- [9] M.H. Anderson, J.R. Ensher, M.R. Matthews, C.E. Wieman, E.A. Cornell, *Science* **269**, 198 (1995).
- [10] C.C. Bradley, C.A. Sackett, J.J. Tollett, R.G. Hulet, *Phys. Rev. Lett.* **75**, 1687 (1995).
- [11] K.B. Davis, M.O. Mewes, M.R. Andrews, N.J. vanDruten, D.S. Durfee, D.M. Kurn, W. Ketterle, *Phys. Rev. Lett.* **75**, 3969 (1995)
- [12] E. Tiesinga, B.J. Verhaar, H.T.C. Stoof, *Phys. Rev. A* **47**, 4114 (1993).
- [13] W. Ketterle, et al. IOS Press, 2006.
- [14] M.W. Zwierlein, C.A. Stan, C.H. Schunck, S.M.F. Raupach, A.J. Kerman, W. Ketterle, *Phys. Rev. Lett.* **92**, 120403 (2004)
- [15] J. Kinast, S.L. Hemmer, M.E. Gehm, A. Turlapov, J.E. Thomas, *Phys. Rev. Lett.* **92**, 150402 (2004)
- [16] R.K. Pathria, *Statistical Mechanics*; 2nd ed. **9780080167473**. Elsevier Science & Technology Books, 1972.
- [17] W. Dickhoff, D. Van Neck, *Many-Body Theory Exposed*; 2nd ed. World Scientific Publishing Co. 2008.
- [18] M.E. Peskin, D.V. Schroeder, *An Introduction to Quantum Field Theory*; Perseus Books, 1995.
- [19] H. Fehske, R. Schneider and A. Weie, *Computational Many-Particle Physics*; *Lect. Notes Phys.* 739 Springer, Berlin Heidelberg 2008, DOI 10.1007/ 978-3-540- 74686-7
- [20] M. Suzuki, *Fractal decomposition of exponential operators with applications to many-body theories and Monte Carlo simulations*; *Phys. Lett. A* 146, 319(1990)
- [21] C.P. Robert, *The Metropolis-Hastings Algorithm*. U. Paris-Dauphine PSL & U. Warwick, **arXiv:1504.01896v3**.
- [22] Metropolis, N., Rosenbluth, A., Rosenbluth, M., Teller, A., and Teller, E. (1953). *Equations of state calculations by fast computing machines*. *J. Chem. Phys.*, **21(6)**: 1087-1092.
- [23] R.M. Neal, *MCMC using Hamiltonian dynamics*. U. Toronto. Handbook of Markov Chain Monte Carlo, (2012).
- [24] I. Bloch, J. Dalibard, and W. Zwerger, *Rev. Mod. Phys.* **80**, 885 (2008); S. Giorgini, L. P. Pitaevskii, and S. Stringari, *Rev. Mod. Phys.* **80**, 1215 (2008); J. Levinsen, M. M. Parish, *Annu. Rev. Cold Atoms Mol.* **3**, 1 (2015); *Ultracold Fermi Gases*, Proceedings of the International School of Physics “Enrico Fermi”, Course CLXIV, Varenna, June 20 – 30, 2006, M. Inguscio, W. Ketterle, C. Salomon (Eds.) (IOS Press, Amsterdam, 2008).
- [25] N.T. Zinner and A. S. Jensen, *J. Phys. G: Nucl. Part. Phys.* **40**, 053101 (2015).

- [26] I. Bloch, J. Phys. B: At. Mol. Opt. Phys. **38** S629 (2005); M. A. Cazalilla, A. M. Rey, Rep. Progr. Phys. **77**, 124401 (2014).
- [27] M. Mancini, G. Pagano, G. Cappellini, L. Livi, M. Rider, J. Catani, C. Sias, P. Zoller, M. Inguscio, M. Dalmonte, L. Fallani, Science **349**, 1510 (2015); B. K. Stuhl, H.-I. Lu, L. M. Ayccock, D. Genkina, and I. B. Spielman, Science **349**, 1514 (2015).
- [28] A. L. Gaunt, T. F. Schmidutz, I. Gotlibovych, R. P. Smith, Z. Hadzibabic, Phys. Rev. Lett. **110**, 200406 (2013).
- [29] J. Friedel, Philos. Mag. **43** 153 (1952); Nuovo Cim. Suppl. **7**, 287 (1958).
- [30] I. Tütto and A. Zawadowski Phys. Rev. B **32**, 2449 (1985).
- [31] V. I. Fernández and C. M. Naón Phys. Rev. B **64**, 033402 (2001).
- [32] B. Chatterjee and K. Byczuk, J. Phys.: Conference Series **592**, 012059 (2015).
- [33] E. G. Dalla Torre, D. Benjamin, Y. He, D. Dentelski, and E. Demler, arXiv:1507.04345.
- [34] R. F. Zhang, A. S. Argon, and S. Veprek, Phys. Rev. Lett. **102**, 015503 (2009).
- [35] K. W. Clark, X.-G. Zhang, G. Gu, J. Park, G. He, R. M. Feenstra, and A.-P. Li, Phys. Rev. X **4**, 011021 (2014).
- [36] M. Bouhassoune, B. Zimmermann, P. Mavropoulos, D. Wortmann, P. H. Dederichs, S. Blügel, and S. Lounis, Nature Comm. **5**, 5558 (2014).
- [37] M. Fabrizio and A. O. Gogolin, Phys. Rev. B **51**, 17827 (1995).
- [38] R. Egger and H. Grabert, Phys. Rev. Lett. **75**, 3505 (1995).
- [39] G. Bedürftig, B. Brendel, H. Frahm, R. M. Noack, Phys. Rev. B, **58**, 10225 (1998).
- [40] D. Vieira, H. J. P. Freire, V. L. Campo Jr., and K. Capelle J. Magn. Magn. Mater. **320**, e418 (2008).
- [41] G. Xianlong Phys. Rev. A **86**, 023616 (2012).
- [42] Z. Xu, L. Li, G. Xianlong and S. Chen, J. Phys.: Condens. Matter, **25** 055601 (2013).
- [43] A. Angelone, M. Campostrini, and E. Vicari, Phys. Rev. A **89**, 023635 (2014).
- [44] S. A. Soeffing, M. Bortz, I. Schneider, A. Struck, M. Fleischhauer, S. Eggert, Phys. Rev. B **79**, 195114 (2009).
- [45] S. Tan, Ann. Phys. **323**, 2952 (2008); *ibid.* **323**, 2971 (2008); *ibid.* **323**, 2987 (2008); S. Zhang, A. J. Leggett, Phys. Rev. A **77**, 033614 (2008); F. Werner, Phys. Rev. A **78**, 025601 (2008); E. Braaten, L. Platter, Phys. Rev. Lett. **100**, 205301 (2008); E. Braaten, D. Kang, L. Platter, *ibid.* **104**, 223004 (2010).
- [46] X.J. Liu, Phys. Rep. **524**, 37 (2013).
- [47] C. E. Berger, E. R. Anderson, J. E. Drut, Phys. Rev. A **91**, 053618 (2015).
- [48] T. Grining, M. Tomza, M. Lesiuk, M. Przybytek, M. Musiał, P. Massignan, M. Lewenstein, R. Moszynski New J. Phys. **17**, 115001 (2015).
- [49] C. E. Berger, J. E. Drut, W. J. Porter, Comput. Phys. Commun. (2016)
- [50] T. Giamarchi, *Quantum Physics in One Dimension*, (Oxford University Press, Oxford, 2004).
- [51] X.-W. Guan, M. T. Batchelor, and C. Lee, Rev. Mod. Phys. **85**, 1633 (2013).

- [52] T. Deguchi and R. Yue, arXiv:cond-mat/9704138
- [53] A. Imambekov, T. L. Schmidt, and L. I. Glazman, *Rev. Mod. Phys.* **84**, 1253 (2012).
- [54] A. Imambekov and L. Glazman, *Phys. Rev. Lett.* **102**, 126405 (2009); *Science* **323**, 228 (2009);
- [55] P. D'Amico and M. Rontani, *Phys. Rev. A* **91**, 043610 (2015).
- [56] E. J. Lindgren, J. Rotureau, C. Forssén, A. G. Volosniev, N. T. Zinner *New J. Phys.* **16**, 063003 (2014);
- [57] T. Sowiński, M. Gajda, K. Rzażewski, *EPL* **109**, 26005 (2015).
- [58] T. Sowiński, *Few-Body Syst.* **56**, 659 (2015).
- [59] L. Rammelmüller, W. J. Porter, A. C. Loheac, J. E. Drut *Phys. Rev. A* **92**, 013631 (2015).
- [60] F. F. Assaad and H. G. Evertz, *Worldline and Determinantal Quantum Monte Carlo Methods for Spins, Phonons and Electrons*, in *Computational Many-Particle Physics*, H. Fehske, R. Shmiedler, and A. Weise Eds., Springer, Berlin (2008);
- [61] J. E. Drut and A. N. Nicholson, *J. Phys. G: Nucl. Part. Phys.* **40**, 043101 (2013);
- [62] S. Duane, A. D. Kennedy, B. J. Pendleton, D. Roweth, *Phys. Lett. B* **195**, 216 (1987); S. A. Gottlieb, W. Liu, D. Toussaint, R. L. Renken, *Phys. Rev. D* **35**, 2531 (1987).
- [63] A. G. Volosniev, D. V. Fedorov, A. S. Jensen, M. Valiente, and N. T. Zinner, *Nat. Commun.* **5**, 5300 (2014).
- [64] G. Aarts, *Introductory lectures on lattice QCD at nonzero baryon number*, *J. Phys. Conf. Ser.* **706**, 022004 (2016).
- [65] S. Giorgini, L.P. Pitaevskii, S. Stringari, *Theory of ultracold Fermi gases*, *Rev. Mod. Phys.* **80**, 1215 (2008).
- [66] I. Bloch, J. Dalibard, W. Zwerger *Many-Body Physics with Ultracold Gases*, *Rev. Mod. Phys.* **80**, 885 (2008).
- [67] M. Lewenstein, A. Sanpera, V. Ahufinger, *Ultracold Atoms in Optical Lattices: Simulating Quantum Many-body Systems*, (Oxford University Press, New York, 2012)
- [68] G. Baym et al., *From hadrons to quarks in neutron stars: a review*, *Rept. Prog. Phys.* **81**, 056902 (2018).
- [69] C. Chin, R. Grimm, P. Julienne, and E. Tiesinga, *Feshbach resonances in ultracold gases*, *Rev. Mod. Phys.* **82**, 1225 (2010).
- [70] X.-J. Liu, *Virial expansion for a strongly correlated Fermi system and its application to ultracold atomic Fermi gases*, *Phys. Rep.* **524**, 37 (2013).
- [71] E. Beth and G. E. Uhlenbeck, *The quantum theory of the non-ideal gas. II. Behaviour at low temperatures*, *Physica (Utrecht)* **4**, 915 (1937).
- [72] X.-J. Liu, H. Hu, and P. D. Drummond, *Exact few-body results for strongly correlated quantum gases in two dimensions*, *Phys. Rev. B* **82**, 054524 (2010)
- [73] V. Ngampruetikorn, J. Levinsen, and M. M. Parish, *Pair correlations in the two-dimensional Fermi gas*, *Phys. Rev. Lett.* **111**, 265301 (2013).
- [74] Y. Yan, D. Blume, *Path integral Monte Carlo determination of the fourth-order virial coefficient for unitary two-component Fermi gas with zero-range interactions*, *Phys. Rev. Lett.* **116**, 230401 (2016).
- [75] *The BCS-BEC Crossover and the Unitary Fermi Gas*, edited by W. Zwerger (Springer-Verlag, Berlin, 2012).

- [76] D. Lee and T. Schäfer, *Cold dilute neutron matter on the lattice. I. Lattice virial coefficients and large scattering lengths* Phys. Rev. C **73**, 015201 (2006).
- [77] X.-J. Liu, H. Hu, and P. D. Drummond, *Virial expansion for a strongly correlated Fermi gas*, Phys. Rev. Lett. **102**, 160401 (2009).
- [78] X. Leyronas, *Virial expansion with Feynman diagrams*, Phys. Rev. A **84**, 053633 (2011).
- [79] D. B. Kaplan, S. Sun, *A new field theoretic method for the virial expansion*, Phys. Rev. Lett. **107**, 030601 (2011).
- [80] D. Rakshit, K. M. Daily, and D. Blume, *Natural and unnatural parity states of small trapped equal-mass two-component Fermi gases at unitarity and fourth-order virial coefficient*, Phys. Rev. A **85**, 033634 (2012).
- [81] V. Ngampruetikorn, M. M. Parish, and J. Levinsen, *High-temperature limit of the resonant Fermi gas*, Phys. Rev. A **91**, 013606 (2015).
- [82] M. Gaudin, *Un système à une dimension de fermions en interaction*, Phys. Lett. **24A**, 55 (1967).
- [83] X.-W. Guan, M. T. Batchelor, and C. Lee, *Fermi gases in one dimension: From Bethe ansatz to experiments*, Rev. Mod. Phys. **85**, 1633 (2013).
- [84] K. Martiyanov, V. Makhalov, and A. Turlapov, Phys. Rev. Lett. **105**, 030404 (2010).
- [85] M. Feld, B. Fröhlich, E. Vogt, M. Koschorreck, and M. Köhl, Nature (London) **480**, 75 (2011); B. Fröhlich, M. Feld, E. Vogt, M. Koschorreck, W. Zwerger, and M. Köhl, Phys. Rev. Lett. **106**, 105301 (2011); P. Dyke, E.D. Kuhnle, S. Whitlock, H. Hu, M. Mark, S. Hoinka, M. Lingham, P. Hannaford, and C. J. Vale, Phys. Rev. Lett. **106**, 105304 (2011); A. A. Orel, P. Dyke, M. Delahaye, C. J. Vale, and H. Hu, New J. Phys. **13**, 113032 (2011).
- [86] A. T. Sommer, L. W. Cheuk, M. J. H. Ku, W. S. Bakr, and M. W. Zwierlein, Phys. Rev. Lett. **108**, 045302 (2012); Y. Zhang, W. Ong, I. Arakelyan, and J. E. Thomas, Phys. Rev. Lett. **108**, 235302 (2012); S.K. Baur, B. Fröhlich, M. Feld, E. Vogt, D. Pertot, M. Koschorreck, and M. Köhl, Phys. Rev. A **85**, 061604 (2012); M. Koschorreck, D. Pertot, E. Vogt, B. Fröhlich, M. Feld, and M. Köhl, Nature (London) **485**, 619 (2012); E. Vogt, M. Feld, B. Fröhlich, D. Pertot, M. Koschorreck, M. Köhl, Phys. Rev. Lett. **108**, 070404 (2012).
- [87] B. Fröhlich, M. Feld, E. Vogt, M. Koschorreck, M. Köhl, C. Berthod, and T. Giamarchi, Phys. Rev. Lett. **109**, 130403 (2012).
- [88] M. Randeria, Physics **5**, 10 (2012).
- [89] V. Makhalov, K. Martiyanov, A. Turlapov, Phys. Rev. Lett. **112**, 045301 (2014).
- [90] P. Dyke, K. Fenech, T. Pepler, M. G. Lingham, S. Hoinka, W. Zhang, B. Mulkerin, H. Hu, X.-J. Liu, C. J. Vale, arXiv:1411.4703.
- [91] J. Levinsen, M. M. Parish, *Strongly interacting two-dimensional Fermi gases*, Annual Review of Cold Atoms and Molecules. May 2015, 1-75.
- [92] W. E. Ormand, D. J. Dean, C. W. Johnson, G. H. Lang, and S. E. Koonin, *Demonstration of the auxiliary-field Monte Carlo approach for sd-shell nuclei*, Phys. Rev. C **49**, 1422 (1994).
- [93] G. Aarts and I.-O. Stamatescu, *Stochastic quantization at finite chemical potential*, J. High Energy Phys. **09** (2008) 018.
- [94] M. D. Hoffman, P. D. Javernick, A. C. Loheac, W. J. Porter, E. R. Anderson, and J. E. Drut, *Universality in one-dimensional fermions at finite temperature: Density, compressibility, and contact*, Phys. Rev. A **91**, 033618 (2015).

- [95] C. Chaffin and T. Schäfer, *Scale breaking and fluid dynamics in a dilute two-dimensional Fermi gas*, Phys. Rev. A **88**, 043636 (2013).
- [96] W. S. Daza, J. E. Drut, C. L. Lin, and C. R. Ordóñez, *Virial expansion for the Tan contact and Beth-Uhlenbeck formula from two-dimensional  $SO(2,1)$  anomalies* Phys. Rev. A **97**, 033630 (2018).
- [97] J. E. Drut and A. N. Nicholson, *Lattice methods for strongly interacting many-body systems*, J. Phys. G: Nucl. Part. Phys. **40**, 043101 (2013).
- [98] D. Lee, *Lattice simulations for few- and many-body systems*, Prog. Part. Nucl. Phys. **63**, 117 (2009).
- [99] A. C. Loheac and J. E. Drut, *Third-order perturbative lattice and complex Langevin analyses of the finite-temperature equation of state of nonrelativistic fermions in one dimension*, Phys. Rev. D **95**, 094502 (2017).
- [100] L. Rammelmüller, W. J. Porter, J. E. Drut, J. Braun *Surmounting the sign problem in non-relativistic calculations: a case study with mass-imbalanced fermions*, Phys. Rev. D **96**, 094506 (2017).
- [101] A. C. Loheac, J. Braun, J. E. Drut, *Polarized fermions in one dimension: density and polarization from complex Langevin calculations, perturbation theory, and the virial expansion*, Phys. Rev. D **98**, 054507 (2018).
- [102] L. Rammelmüller, A. C. Loheac, J. E. Drut, J. Braun, *Finite-temperature equation of state of polarized fermions at unitarity*. Phys. Rev. Lett. in print.
- [103] C. R. Ordóñez, *Path-integral Fujikawas approach to anomalous virial theorems and equations of state for systems with  $SO(2,1)$  symmetry*, Physica, **446**, 64 (2016).
- [104] E. R. Anderson, J. E. Drut, *Pressure, compressibility, and contact of the two-dimensional attractive Fermi gas*, Phys. Rev. Lett. **115**, 115301 (2015).
- [105] S. Blanes, F. Casas, J. A. Oteo, J. Ros, *The Magnus expansion and some of its applications*, Physics Reports, **470**, 5-6 (2009)
- [106] *The BCS-BEC Crossover and the Unitary Fermi Gas*, edited by W. Zwerger (Springer-Verlag, Berlin, 2012).
- [107] J. E. Drut and A. N. Nicholson, *Lattice methods for strongly interacting many-body systems*, J. Phys. G: Nucl. Part. Phys. **40**, 043101 (2013).
- [108] M. D. Hoffman, A. C. Loheac, W. J. Porter, J. E. Drut *Thermodynamics of one-dimensional  $SU(4)$  and  $SU(6)$  fermions with attractive interactions* Phys. Rev. A **95**, 033602 (2017).